LIBRARY

JET PROPULSION

A publication of the
AMERICAN ROCKET SOCIETY
Research and Development

BIND

VOLUME 28 MARCH 1958 SCIENCE & TECHNOLOGY NUMBER 3

INVITED ARTICLE

Recent Advances in Real Gas Effects in Hypersonic Flow . . *Wayland C. Griffith* 157

CONTRIBUTED ARTICLES

Some Effects of Oxidizer Concentration and Particle Size on Resonance Burning of Composite Solid Propellants . . . . . *Leon Green Jr.* 159
A Generalized Optimization Procedure for N-Staged Missiles . *Leon Weisbord* 164
Escape From a Circular Orbit Using Tangential Thrust . . . . *D. J. Benney* 167
The Optimization of Nozzle Area Ratio for Rockets Operating in a Vacuum . . . . . *M. Goldsmith* 170
An Analysis of Fuel-Oxidant Mixing in Screaming Combustors . . . . . *William R. Mickelsen* 172
Heat Transfer in Laminar Pipe Flow With Uniform Coolant Injection . . . . . *S. W. Yuan and A. B. Finkelstein* 178
Influence of Pressure on the Combustion of Liquid Spheres . . . . . *George A. Agoston, Bernard J. Wood and Henry Wise* 181

TECHNICAL NOTES

Solar Sailing—A Practical Method of Propulsion Within the Solar System . . *Richard L. Garwin* 188
Combustion Instability in Solid Propellant Rocket Motors . . . . *E. W. Price and J. W. Sofferis* 190
A Preliminary Study of Vortex-Boiling Burnout Heat Fluxes . . *W. R. Gambill and N. D. Greene* 192
Burning Rate Studies. III. Correlation of Experimental Results With the Thermal Model . . . . *D. L. Hildenbrand and W. P. Reid* 194

TECHNICAL COMMENTS

Terminology in Rocket Combustion Instability . . . . . *E. W. Price* 197
A Remark on the Free Vibration of a Variable Mass . . . . . *George Leitmann* 197
On the Free Vibration of a Variable Mass . . . . . *J. J. Marcinek* 198

DEPARTMENTS

New Patents 199 Book Reviews 202 Technical Literature Digest 205

Ever hear of a thirty-five header?

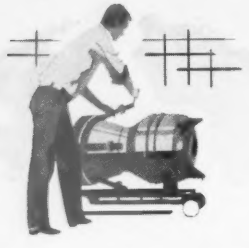

Tandem locomotives, teamed to pull a train up a grade, are often called a double header. It would take a "35 header" to equal the power of the RMI rocket engine shown here.

RMI propulsion systems are now being perfected for use in ballistic and guided missiles as well as in the manned aircraft of the future. These advanced propulsion systems incorporate the principle which has guided RMI since 1941 . . . *reliability in application.*

Another reason why RMI's program of advanced research and engineering continues to be a good investment for taxpayers, government and industry!

RMI **REACTION MOTORS, INC.**

DENVILLE, NEW JERSEY

TRONA* is basic in the chemistry of high energy fuels and solid propellant oxidants.

Wherever men make ready for outer space... from barren arctic IGY laboratories to tropical ballistic missile blast-offs... Trona chemicals are putting the punch into high energy fuels and other propulsion systems. As the only basic producer of these three important raw materials used in high energy fuels and as solid propellant oxidizers—**BORON, LITHIUM and AMMONIUM PERCHLORATE**—American Potash & Chemical Corporation has a vital stake in the space age. Recipient of the 14th Annual Chemical Engineering Achievement Award for pioneering work in the atomic age metals, Trona continues in the forefront of basic research and technical development of these vital chemicals and their compounds for high energy and missile applications.

TRONA **American Potash & Chemical Corporation**

3000 West Sixth Street, Los Angeles 54, California
99 Park Avenue, New York 16, New York

Offices: LOS ANGELES, NEW YORK, CHICAGO, SAN FRANCISCO, PORTLAND (Ore.), ATLANTA, COLUMBUS (O.), SHREVEPORT

Plants: LOS ANGELES AND TRONA, CALIFORNIA; HENDERSON, NEVADA; SAN ANTONIO, TEXAS (American Lithium Chemicals, Inc. & San Antonio Chemicals, Inc.); WEST HANOVER, MASSACHUSETTS

*TRADENAME AND TRADEMARK OF AP&CC

Recipient of 14th Annual Award for Chemical Engineering Achievement in BORON and LITHIUM

Other Trona chemicals for high energy propulsion: POTASSIUM PERCHLORATE • LITHIUM NITRATE • LITHIUM PERCHLORATE • LITHIUM METAL RUBIDIUM & CESIUM • TRIMETHYL BORATE • TRIMETHOXYBOROXINE • DECABORANE • ELEMENTAL BORON • BORON TRICHLORIDE • BORON TRIBROMIDE

JET PROPULSION

A publication of the

AMERICAN ROCKET SOCIETY

Research and Development

IRWIN HERSEY—DIRECTOR OF PUBLICATIONS

EDITOR MARTIN SUMMERFIELD

ASSISTANT EDITOR LARKIN JOYNER

ART EDITOR JOHN CULIN

ASSOCIATE EDITORS

ALI BULENT CAMBEL, *Northwestern University*
IRVIN GLASSMAN, *Princeton University*
M. H. SMITH, *Princeton University*

CONTRIBUTORS

MARSHAL FISHER, *Princeton University*
GEORGE F. McLAUGHLIN

ADVERTISING PRODUCTION MANAGER

WALTER BRUNKE

ADVERTISING & PROMOTION MANAGER

WILLIAM CHENOWETH

ADVERTISING REPRESENTATIVES

D. C. Emery & Associates
155 East 42 St., New York, N. Y.
Telephone: Yukon 6-6855

James C. Galloway & Co.
6535 Wilshire Blvd., Los Angeles, Calif.
Telephone: Olive 3-3223

Jim Summers & Associates
35 E. Wacker Dr., Chicago, Ill.
Telephone: Andover 3-1154

R. F. and Larry Pickrell
318 Stephenson Bldg., Detroit, Mich.
Telephone: Trinity 1-0790

Louis J. Bresnick
304 Washington Ave., Chelsea 50, Mass., Telephone: Chelsea 3-3335

AMERICAN ROCKET SOCIETY

Founded 1930

OFFICERS

President	George P. Sutton
Vice-President	John P. Stapp
Executive Secretary	James J. Harford
Secretary	A. C. Slade
Treasurer	Robert M. Lawrence
General Counsel	Andrew G. Haley

BOARD OF DIRECTORS

Terms expiring on dates indicated

Krafft Ehricke, 1959	H. S. Seifert, 1958
S. K. Hoffman, 1958	K. R. Stehling, 1958
Simon Ramo, 1960	Martin Summerfield, 1959
H. W. Ritchey, 1959	Wernher von Braun, 1960

Maurice J. Zucrow, 1960

TECHNICAL DIVISION CHAIRMEN

David G. Simons, Human Factors	John F. Tormey, Propellants and Combustion
Lawrence S. Brown, Instrumentation and Guidance	Brooks T. Morris, Ramjet
Edward N. Hall, Liquid Rocket	William L. Rogers, Solid Rocket

Krafft A. Ehricke, Space Flight

Scope of JET PROPULSION

This Journal is a publication of the American Rocket Society devoted to the advancement of the field of jet propulsion through the dissemination of original papers disclosing new knowledge or new developments. As used herein, the term "jet propulsion" embraces all engines that develop thrust by rearward discharge of a jet through a nozzle or duct; and thus it includes air-consuming engines and underwater systems as well as rockets. JET PROPULSION is open to contributions dealing not only with propulsion but with other aspects of jet-propelled flight, such as flight mechanics, guidance, telemetering, and research instrumentation. Increasing emphasis will be given to the scientific problems of extraterrestrial flight.

Information for Authors

Manuscripts must be as brief as the proper presentation of the ideas will allow. Exclusion of dispensable material and conciseness of expression will influence the Editors' acceptance of a manuscript. In terms of standard-size double-spaced typed pages, a typical maximum length is 22 pages of text (including equations), 1 page of references, 1 page of abstract, and 12 illustrations. Fewer illustrations permit more text, and vice versa. Greater length will be acceptable only in exceptional cases.

Short manuscripts, not more than one quarter of the maximum length stated for full articles, may qualify for publication as Technical Notes or Technical Comments. They may be devoted to new developments requiring prompt disclosure or to comments on previously published papers. Such manuscripts are usually published within two months of the date of receipt.

Sponsored manuscripts are published occasionally as an ARS service to the industry. A manuscript that does not qualify for publication according to the above-stated requirements as to subject scope or length, but which nevertheless deserves widespread distribution among jet propulsion engineers, may be printed as an extra part of the Journal or as a special supplement, if the author or his sponsor will reimburse the Society for actual publication costs. Estimates are available on request. Acknowledgment of such financial sponsorship appears as a footnote on the first page of the article. Publication is prompt since such papers are not in the ordinary backlog.

Manuscripts must be double spaced on one side of paper only with wide margins to allow for instructions to printer. Include a 100 to 200 word abstract. State the authors' positions and affiliations in a footnote on the first page. Do not type equations; write them in ink. Identify unusual symbols or Greek letters for the printer. References are to be grouped at the end of the manuscript and are to be given as follows: for journal articles: authors first, then title, journal, volume, year, page numbers; for books: authors first, then title, publisher, city, edition, and page or chapter numbers. Line drawings must be clear and sharp to make clear engravings. Use black ink on white paper or tracing cloth. Lettering should be large enough to be legible after reduction. Photographs should be glossy prints, not matte or semi-matte. Each illustration must have a legend; legends should be listed in order on a separate sheet.

Manuscripts must be accomplished by written assurance as to security clearance in the event the subject matter lies in a classified area or if the paper originates under government sponsorship. Full responsibility rests with the author.

Submit manuscripts in duplicate (original plus first carbon, with two sets of illustrations) to the Editor, Martin Summerfield, Professor of Aeronautical Engineering, Princeton University, Princeton, N. J. Preprints of papers presented at ARS national meetings are automatically considered for publication.

JET PROPULSION is published monthly by the American Rocket Society, Inc., and the American Interplanetary Society at 20th & Northampton Sts., Easton, Pa., U. S. A. Editorial offices: 500 Fifth Ave., New York 36, N. Y. Price: $12.50 per year, $2.00 per single copy. Second-class mail privileges authorized at Easton, Pa. Notice of change of address should be sent to the Secretary, ARS, at least 30 days prio to publication. Opinions expressed herein are the authors' and do not necessarily reflect the views of the Editors or of the Society.

© Copyright 1958 by the American Rocket Society, Inc.

Recent Advances in Real Gas Effects in Hypersonic Flow

WAYLAND C. GRIFFITH

Lockheed Missile Systems Division, Palo Alto, Calif.

The author studied engineering science at Harvard University where he received an A.B. in 1946 and a Ph.D. in 1949. His thesis was on an experimental measurement of vibrational relaxation times in gases. In 1950 he joined the shock wave laboratory of the Physics Department at Princeton University where he continued his research on physical problems in gas dynamics. In 1951 he was appointed assistant professor of physics; later, associate professor. The subjects on which he has worked extensively include transonic flow, thermal boundary layers, shock structure, chemical kinetics, diffraction of blast waves, and supersonic flow. As one of the editors of the *Journal of Fluid Mechanics*, he has an intimate and up-to-date knowledge of the problem on which he writes. Dr. Griffith is currently manager of the Flight Sciences Division in the Missile Systems Division of Lockheed Aircraft Corp.

OF THE many problems confronting the aerodynamicist engaged in the development of satellites and ballistic missiles, two arise through departures in the behavior of air from the ideal gas relations. At high altitudes the atmosphere is so rarefied that the equations of continuum mechanics no longer hold, while the temperature produced by hypersonic flight through the lower atmosphere is sufficient to dissociate and ionize air molecules. This article describes recent progress in our understanding of these effects. The bibliography is not intended to be at all complete, but is selected to serve as a guide to literature on the subject.

The nearly exponential decrease of atmospheric density with altitude results in a rapidly increasing molecular mean free path so that, at about 200,000 ft, the average distance between molecular collisions becomes comparable with the diameter of a missile. Under such conditions new aerodynamic phenomena arise. "Slip-flow" is used to designate this regime since the average velocity of the molecules near a surface has a finite value and the air appears to be slipping over the body. At higher altitudes free molecule flow occurs in which molecules striking the missile are not deflected back to it by further intermolecular encounters.

The air densities, and hence the altitudes, at which these various flow regimes exist are somewhat difficult to specify. Knudsen's number K, the ratio of the molecular mean free path to some pertinent body dimension, is usually used as a criterion. From the kinetic theory of gases it is easy to show that K is approximately equal to the ratio of Mach number to Reynolds number. Classically, the limits of slip flow have been chosen as $0.1 < K < 1.0$ (see, for example, Estermann (5)[1]) but some care must be used in selecting an appropriate "typical" body dimension in any given problem. Tsien (24) discusses the problem in some detail, and more recently the group working on low density flows at Berkeley has reported experimental results on the onset of slip flow over flat plates and around spheres (see, for example, Laurmann (11)). In an excellent review of recent developments in hypersonic flow in this journal Lees (13) points out that the *local* air density in the boundary layer near a stagnation point is so much higher than the ambient density that any criterion for the onset of slip flow based only on free stream conditions is of doubtful validity. The slip flow regime is postponed to much lower densities than has previously been supposed. A theoretical problem of some interest arises in trying to fit the boundary conditions at a surface into either a kinetic theory of the flow or into the Navier-Stokes equations. Several articles on this problem have appeared, for example, Wang Chang and Uhlenbeck (25) and Yang and Lees (26). Much of the work has dealt with concentric rotating cylinders with comparatively small differences in speed and temperature. Extrapolation to missile conditions is clearly risky until the theory is more firmly established than at present.

The gas dynamic problem in free molecule flow becomes one of finding out how various atoms and ions reflect from solid surfaces. In its details the process must be a very complex one involving the binding force between particle and surface atoms as well as the geometry of scattering from a microscopically rough surface. In practice, the custom has been to assume that some fraction of the particles reflect specularly and that the rest are momentarily absorbed and then emitted isotropically. The mean energy of the emitted molecules is specified by a parameter called the "accommodation coefficient" which measures the extent to which these molecules reach thermal equilibrium with the wall. Much new data is becoming available on various gas and solid combinations (Merlic (17)) but progress on fundamentals seems to be temporarily at a standstill. This is unfortunate if for no other reason than that a similar concept of partial specular and diffuse reflection is being used quite widely in studying the intermediate regime mentioned above.

Since a ballistic missile spends most of its flight time in the outer atmosphere one might at first suppose that even the small amount of air encountered there would have some effect on the missile's trajectory. This is not the case, however, and the missile actually does "re-enter" the lower atmosphere before aerodynamic and thermal problems become significant. Satellites, on the other hand, because of their prolonged travel through the outer atmosphere, are gradually affected by the rarefied air and eventually fall back to earth. Thus the problems of free molecule and slip flow are associated primarily with satellites, while high temperature gas effects are predominantly the concern of ballistic missile designers.

Aerodynamic and heating problems arising in hypersonic flight through the atmosphere are complicated by a number of molecular and atomic processes not encountered previously. Among these are vibrational and electronic excitation, dissociation, chemical reaction and ionization. New mechanisms for heat transfer are provided by radiation and by atomic recombination on the surface of a missile. Other problems arise from the generation of an ionized wake.

The equilibrium properties of any gas can be computed from statistical mechanics once all of the quantum mechanical energy levels are known. Fortunately nearly all of the necessary data have been accumulated in three decades of physical research. Tables giving thermodynamic properties of many pure gases have been prepared by the National Bureau of Standards (19) and of air by Feldman (6), Logan (15), and

Received Jan. 24, 1958.

[1] Numbers in parentheses indicate References at end of paper.

Hochstim and Arave (8). Normal and oblique shock relations are also available over a wide range of conditions.

One notable exception to the fund of physical data mentioned above is the dissociation energy of nitrogen. Spectroscopic evidence indicated a value of either 7.38 or 9.76 ev. An unambiguous choice was made possible by a purely gas dynamic measurement. The velocity of a plane shock wave depends upon the state of the gas behind it so that the degree of dissociation, which in turn depends upon the dissociation energy, can be determined from a velocity measurement. Toennies and Greene (22) measured the velocity of incident and reflected shocks in a shock tube and found that their data led to the higher value of 9.76 ev.

In discussing the properties of a gas, it is customary to refer to the ratio pV/RT as the "compressibility factor." Two independent effects cause departures from the ideal gas value of 1: intermolecular forces leading to the van der Waals coefficients, and a change in the number of particles by dissociation and ionization. The first effect is quite negligible at the densities encountered in flight, although it may make a detectable contribution in hypersonic wind tunnel work. The second effect is important in flight and in shock tube work, while it is absent in hypersonic tunnel experiments because of the low operating temperature.

Because the excitation of the internal degrees of freedom of oxygen and nitrogen, as well as chemical reactions between them, proceeds at rates which are comparable to the rates of change in the flow about a hypersonic missile, knowledge of these rates is required for a complete solution of the gas dynamic problem.

Vibrational excitation proceeds according to a linear relaxation equation; that is, the rate of change of vibrational energy is proportional to the amount that vibrational energy is out of equilibrium with the mean translational temperature. Vibrational relaxation times have been measured in the shock tube by Blackman (1) for pure oxygen and nitrogen, and the effectiveness of oxygen-nitrogen collisions in exciting oxygen has been determined. At 3000 K and 1 atm the pure gas relaxation times are 2 μsec and 30 μsec, respectively. A collision between nitrogen and oxygen molecules is about 40 per cent as effective in exciting vibration in oxygen as an oxygen-oxygen collision. The effectiveness of oxygen in exciting nitrogen has not been measured but may be expected to have a lower value as well. Vibrational relaxation requires many collisions, not so much because the quantum level spacing is large compared to kT, but because the probability of excitation in a collision which is sufficiently energetic is extremely small. Since the total energy per molecule which can be involved in vibration is only kT at best, vibrational relaxation is not particularly important to hypersonic flow in itself. As a stage in the mechanism of dissociation however, it plays an important role.

Lighthill (14) points out that dissociation is complete in any gas at a temperature far below D/k (where D is the dissociation energy) because of the very large volume of phase space available to two atoms as compared with one molecule. Thus oxygen and nitrogen are completely dissociated at 6000 K and 10,000 K, respectively, even though the values of D/k are 59,400 K and 113,300 K. Dissociation proceeds relatively slowly because only a few molecules in the tail of the Maxwellian distribution function have enough energy to break the molecular bond.

The rate of dissociation is given by the fraction of collisions which are sufficiently energetic, $(D/kT)^s e^{-D/kT}$, multiplied by an efficiency factor which is less than unity. The parameter s must also be determined by experiment. Measurements by Matthews (16), Eckermann (4), Camac (3), and Treanor (23) indicate that the efficiency factor is between $\frac{1}{3}$ and $\frac{1}{10}$ for oxygen and nitrogen and that s has a value between 2 and 3. Unfortunately none of the data thus far available is accurate enough to establish these values with precision. The rates are highly dependent on temperature, having both a power of T and the Boltzmann factor in the expression. Thus no part of the process is correctly describable by a dissociation relaxation time, contrary to statements by some authors. It is preferable to state either the instantaneous rate itself or the time to reach, say, 90 per cent of the equilibrium value.

Because the binding energies of oxygen and nitrogen differ by nearly a factor of two, it is clear that both the dissociation rates and equilibrium degree of dissociation are quite different at any given temperature. In air this means that the order of equilibration is: oxygen vibration, oxygen dissociation or nitrogen vibration, nitrogen dissociation. The cross-over of rates just mentioned may account for an apparent overdissociation of oxygen behind a plane shock wave in air that was observed by Resler (21). More experimental work will be needed before a clear picture of these fundamental processes is available.

Although the very large energies absorbed in dissociation and the change in number of particles may be expected to have a strong influence on hypersonic flow patterns, as shown by Lighthill (14) and Eckermann (4), boundary layer heat transfer is not so strongly effected. Lees (12) investigated the role of atomic recombination in heat transfer through a hypersonic boundary layer and found that the rate depends mainly on the difference between the total stream enthalpy and the surface enthalpy. The rate for a boundary layer in complete thermodynamic equilibrium differs by only about 30 per cent from that for the case where atoms recombine only on the surface. The diffusion of atoms is limited by collisions with molecules to such an extent that little increase in heating occurs even though the energy of recombination may be delivered right at the surface.

Compounds of nitrogen and oxygen, principally NO, NO_2 and NO^+, appear in equilibrium in trace amounts at elevated temperatures. These are probably not important in themselves but do serve as catalysts for the very important production of electrons and ions. The transient existence of similar compounds might also be of significance but at present too little is known to offer much concrete evidence. The reaction with the lowest energy barrier for electron production is $N + O \rightarrow NO^+ + e$. So little is known about the cross section, however, that one cannot be sure that this is actually an important source of electrons. Bond (2) and Petschek (20) have studied the ionization of argon behind strong shock waves and conclude that the rate of approach to equilibrium ionization is controlled by the electron population. If the same is true for air, then knowledge of the first source of electrons is extremely important.

The energy radiated from an electronically excited and ionized gas can be computed from the particle wave functions and the Einstein radiation coefficients. Such computations are often very laborious with the result that few have been carried out. Failing a purely theoretical attack it is possible to make some intelligent guesses on the strength of a whole electronic band from a knowledge of other band systems. Hindmarsh (7) discusses this problem in some detail. Meyerott (18) makes use of the recent experimental data of Keck et al. (9) and Kivel et al. (10) on the emissivity of hot air to to show that the radiant heat transfer to a ballistic missile is only about 10 per cent of the convective heat transfer. Thus the radiation problem seems to be of primary importance only to recovery of a satellite vehicle, for example a translunar rocket. For an excellent summary of the radiant heat transfer problem the reader is referred to the paper by Meyerott (18).

References

1 Blackman, V., "Vibrational Relaxation in Oxygen and Nitrogen," *Journal of Fluid Mechanics*, vol. 1, 1956, p. 61.

2 Bond, J. W., Jr., "Structure of a Shock Front in Argon,"

Physical Review, vol. 105, 1957, p. 1683.

3 Camac, M., and Petty, C., "The Vibration and Dissociation Relaxation Rates of Molecular Oxygen in Argon-Oxygen Mixtures," Tenth Anniversary Meeting of the Division of Fluid Dynamics, American Physical Society, Lehigh University, Nov. 25, 1957.

4 Eckermann, J., "A Study of the Relaxation Time of Thermal Dissociation of Nitrogen Using Free-flight Techniques," 1957, unpublished.

5 Estermann, I., "Gases at Low Densities," Thermodynamics and Physics of Matter, Princeton University Press, 1955.

6 Feldman, S., "Hypersonic Gas Dynamic Charts for Equilibrium Air," AVCO Research Laboratory, 1957.

7 Hindmarsh, W. R., "Radiation from Gases," A.E.R.E., GP/R 2028.

8 Hochstim, A. R., and Arave, R. J., "Gas Properties Behind Shocks at Hypersonic Velocities," Convair Report Zph-004, 1957.

9 Keck, J., Kivel, B., and Wintink, T., Jr., "Emissivity of High-temperature Air," AVCO Research Laboratory Report 8, 1957.

10 Kivel, B., Mayer, H., and Bethe, H., "Radiation from Hot Air," *Annals of Physics*, vol. 2, 1957, p. 57.

11 Laurmann, J., and Ipsen, D. C., "Use of a Free Molecule Probe in High Speed Rarefied Gas Flow Studies," University of California, Berkeley, Report HE-150-146, 1957.

12 Lees, L., "Laminar Heat Transfer Over Blunt-nosed Bodies at Hypersonic Flight Speeds," JET PROPULSION, vol. 26, 1956, p. 259.

13 Lees, L., "Recent Developments in Hypersonic Flow," JET PROPULSION, vol. 27, 1957, p. 1162.

14 Lighthill, M. J., "Dynamics of a Dissociating Gas," *Journal of Fluid Mechanics*, vol. 2, 1957, p. 1.

15 Logan, J. G., Jr., "Thermodynamic Charts for High Temperature Air Calculations," Cornell Aeronautical Laboratory, 1956.

16 Matthews, D. L., "The Dissociation Rate of Oxgyen," Tenth Anniversary Meeting of the Division of Fluid Dynamics, American Physical Society, Lehigh University, Nov. 25, 1957.

17 Merlic, E., "An Experimental Determination of Reflection Coefficients for Air on Aluminum," University of California, Institute of Engineering Research, Tech. Rep., 1956.

18 Meyerott, R., "Radiation Heat Transfer to Hypersonic Vehicles," Lockheed Missile Systems Division Report 2264, 1957.

19 National Bureau of Standards, Tables of Thermal Properties of Gases, Circular 564, 1955.

20 Petschek, H., Thesis, Cornell University, 1955 (to be published).

21 Resler, E. L., Jr., private communication, 1956.

22 Toennies, J. P., and Greene, E. F., "Dissociation of N_2 in Shock Waves," *Journal of Chemical Physics*, vol. 23, 1955, p. 1366.

23 Treanor, C. E., "Non-equilibrium High Temperature Phenomena," U. S. Navy Bureau of Ordnance Symposium, Washington, D. C., Nov. 12–14, 1957.

24 Tsien, H. S., "Superaerodynamics, Mechanics of Rarefied Gases," *Journal of the Aeronautical Sciences*, vol. 13, 1946, p. 653.

25 Wang Chang, C. S., and Uhlenbeck, G. E., "The Couette Flow Between Two Parallel Plates as a Function of Knudsen Number," University of Michigan, Research Institute Tech. Rep., 1954.

26 Yang, H.-T., and Lees, L., "Plane Couette Flow at Low Mach Number According to the Kinetic Theory of Gases," Guggenheim Aeronautical Laboratory, California Institute of Technology, Tech. Rep., 1957.

Some Effects of Oxidizer Concentration and Particle Size on Resonance Burning of Composite Solid Propellants[1]

LEON GREEN Jr.[2]

Aerojet-General Corp., Azusa, Calif.

A comparison of four experimental, composite propellant formulations with nominally constant burning rates, tested at 170 F in internal-burning tubular charges partially supported the widely held belief that the tendency toward irregular reaction increases as the energy content of the propellant is raised. However, the highest energy formulation showed a smooth reaction, apparently as a result of a burning rate lower than anticipated on the basis of Crawford bomb measurements. The results suggest that the rate of energy release (the product of burning rate, propellant density and heat of explosion) affords a better measure of the relative stability behavior of various formulations than does either burning rate or energy content alone. A subsequent brief comparison at 170 F of three other composite propellants with constant energy content, but with varying burning rates (obtained by varying the oxidizer particle-size distribution), indicated that the tendency toward irregular reaction increased as the burning rate increased or as the particle size became finer. Owing to propellant processing difficulties, efforts to study the influence of burning rate alone while controlling both oxidizer concentration and particle-size distribution were not successful. It is recommended that the apparent influence of a coarse oxidizer particle-size distribution in suppressing resonance burning be investigated further.

Introduction

THE tendency of solid propellant charges to exhibit resonance burning is obviously a function of propellant composition, since some propellants never show this behavior, while others almost always do, at least in tests of internal-burning charges conducted at extreme conditioning temperature. On the basis of development experience, a qualitative proposition has been advanced; namely, resonant burning is encountered only in motors employing high energy propellants, i.e., propellants with a high heat of explosion or a high specific impulse. Examples of such propellants are the double-base compositions using nitrocellulose of high nitration

Presented at the ARS 12th Annual Meeting, New York, N. Y., Dec. 2–5, 1957.

[1] This research was supported by the U. S. Air Force through the Air Force Office of Scientific Research of the Air Research and Development Command.

[2] Principal Engineer, Nuclear Projects Department. Mem. ARS.

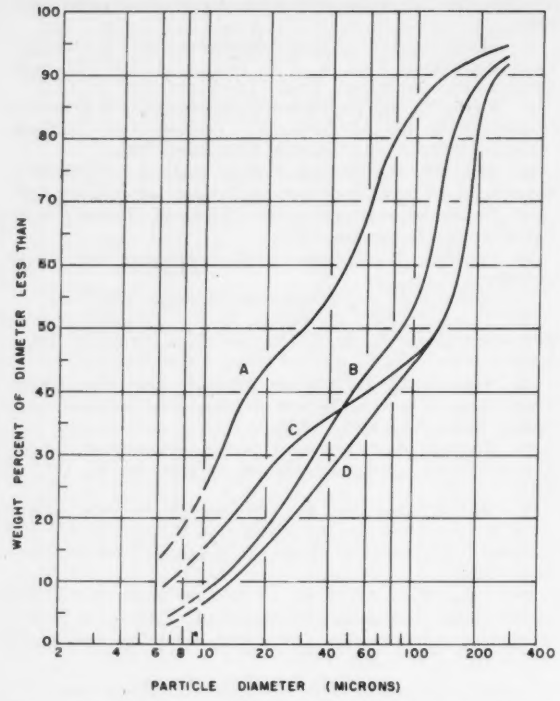

Fig. 1 Particle-size distribution of ammonium perchlorate employed in propellants A, B, C and D

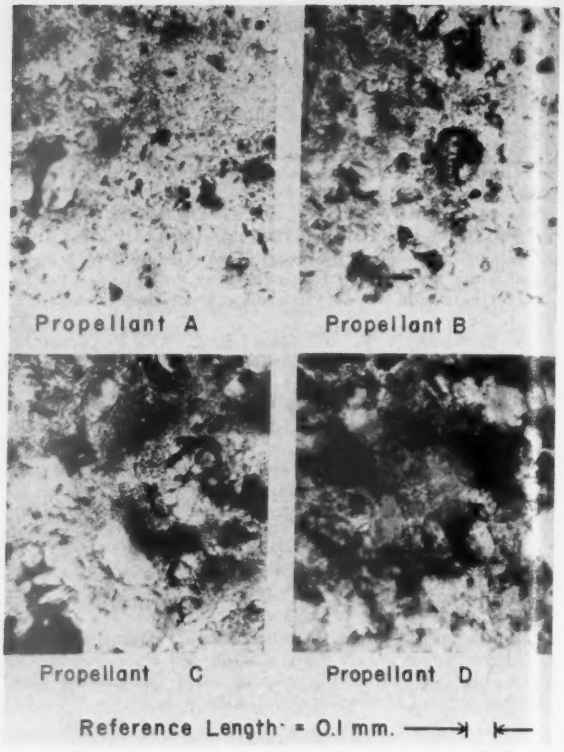

Fig. 2 Photomicrographs of samples of propellants A, B, C and D (taken by transmitted light)

(such as JPN ballistite) and composite propellants employing ammonium perchlorate as oxidizer. The lower energy propellants that have not reportedly manifested unstable combustion include the slow-burning, double-base formulations, such as Russian cordite, and the German and Japanese propellants described by Wimpress (1),[3] as well as the composite propellants using potassium perchlorate, ammonium picrate, sodium nitrate, potassium nitrate and ammonium nitrate. A general description of these various types of propellant is given in (2). Wimpress states that the trend toward resonance increases with increasing burning rate, but this observation does not apply to the fast-burning potassium perchlorate formulations. Although the correlation with energy content has been observed in homogeneous double-base propellants as well as in composite ammonium perchlorate and organic fuel systems, the burning rates of both propellants systems also generally increase with energy content, and it was not possible to state whether the observed trend in reaction stability was attributable to either energy content or burning rate alone. In the composite systems, moreover, the burning rate increases with decreasing oxidizer particle size. The objective of the present investigation was to distinguish the effects of these variables.

Experimental Propellants

It was desired to study the effect of (i) varying energy content (determined by oxidizer concentration) in propellants of approximately equal burning rates but with particle-size distribution not controlled, (ii) varying burning rate in propellants of equal energy content and constant particle-size distribution and (iii) varying particle-size distribution in propellants of equal energy content but with burning rate not controlled. This choice of experiments was determined by the fact that the effectiveness of burning-rate accelerators (added in amount of a few weight per cent or less) in compensating for the effect of oxidizer concentration and particle size is limited; i.e., it was not considered possible to control both burning rate and particle size while varying the oxidizer concentration significantly, or to control both burning rate and concentration while varying the particle size.

The first objective was achieved with a moderate amount of laboratory development. Four experimental propellants, identified as A, B, C and D, were formulated using different concentrations and oxidizer grinds. Particle-size distributions of the ammonium perchlorate grinds employed and photomicrographs of propellant samples are presented in Figs. 1 and 2, respectively. The comparison of interior ballistic properties presented in Table 1 shows that the strand burning rates at standard conditions (60 F and 1000 psia) in a Crawford bomb (3) were approximately equal. Subsequently, however, a test temperature of 170 F was selected (as discussed later), and at this temperature a greater divergence of burning rates was manifested, with propellant D exhibiting a markedly lower temperature sensitivity than did the other formulations. This divergence was accepted, since the development of another set of propellants would have required an effort exceeding the authorized scope of the program.

The second objective was not achieved. Three experimental propellants (designated E, F and G) were formulated using a conventional (medium) oxidizer grind, but having the burning-rate accelerators present in zero, medium and relatively high concentrations. Unfortunately, it was found that these propellants would cure satisfactorily only when the burning-rate accelerator (which also apparently was required to accelerate the curing process) was present in the relatively high concentration. After considerable effort to obtain satisfactory curing properties proved unsuccessful, the development of propellants E, F and G was discontinued.

The third objective mentioned above was accomplished by the formulation of propellants H, I and J with constant (fairly high) concentration of burning-rate accelerators, but

[3] Numbers in parentheses indicate References at end of paper.

Table 1 Comparative ballistic properties of experimental composite propellants with varying energy content but approximately constant burning rate under standard conditions

Propellant	A	B	C	D
Total oxidizer content, per cent	70	75	80	85
Density, lbm/in.^{3}	0.0580	0.0595	0.0616	0.0636
Strand burning rate rate at 1000 psi and 60 F, in./sec.	0.35	0.37	0.34	0.34
Heat of explosion,[1] cal/g	698	864	1010	1050
Heat of explosion/-unit vol., Btu/in.^{3}	72.9	92.5	112	120.8
Nominal rate of heat release at 60 F and 1000 psi, Btu/in.^{2} sec	25.5	34.2	38.1	41.1
Flame temperature, °R	3570	4320	5030	5330
Specific impulse,[2] lbf-sec/lbm	211	226	239	251
Impulse density, lbf-sec/in.^{3}	12.8	13.5	14.7	16.0
Average specific heat ratio, γ	1.22	1.24	1.22	1.17
Molecular weight of gases in combustion chamber	21.9	23.6	25.5	27.2
Characteristic gas velocity, c, fps	4350	4600	4800	4860

[1] Enthalpy change between propellant at 25 C and reaction products (in relative concentration corresponding to equilibrium composition of flame temperature) at 25 C, with water and hydrogen chloride in liquid state.

[2] Assuming mobile equilibrium of products during expansion from 1000 psi.

with the three different oxidizer particle-size distributions shown in Fig. 3. Photomicrographs of propellant samples are shown in Fig. 4, and the interior-ballistic properties of these propellants are given in Table 2. It may be noted that even the coarsest-grained propellant showed a higher burning rate than any of those described in Table 1.

Test Procedure

Internal-burning, tubular charges of each of the experimental propellants were statically tested at 170 F and at various nominal pressure levels, as determined by the ratio, K, of burning surface area to nozzle throat area. The test temperature was selected on the basis of preliminary firings which indicated that irregular reaction of propellants of the general class involved was most likely to be exhibited at high temperatures. The internal charge diameter was 3.0 in., the web thickness 0.5 in. and the length 16.5 in. This short grain length was selected in order to minimize any effects due to high aft-end gas velocity (4).

In the tests of propellants A, B, C and D, the conventional pressure measurements were supplemented by high frequency response instrumentation, in order to check the possible modes of acoustical oscillation associated with any rough burning. The detailed results of these measurements are available elsewhere (5) and will not be discussed here. In summary, it will suffice to say that oscillations of frequencies corresponding to both longitudinal and transverse modes were detected, but the amplitudes generally did not exceed a few psi, even in the tests exhibiting irregular low frequency pressure vs. time histories. This behavior is consistent with the

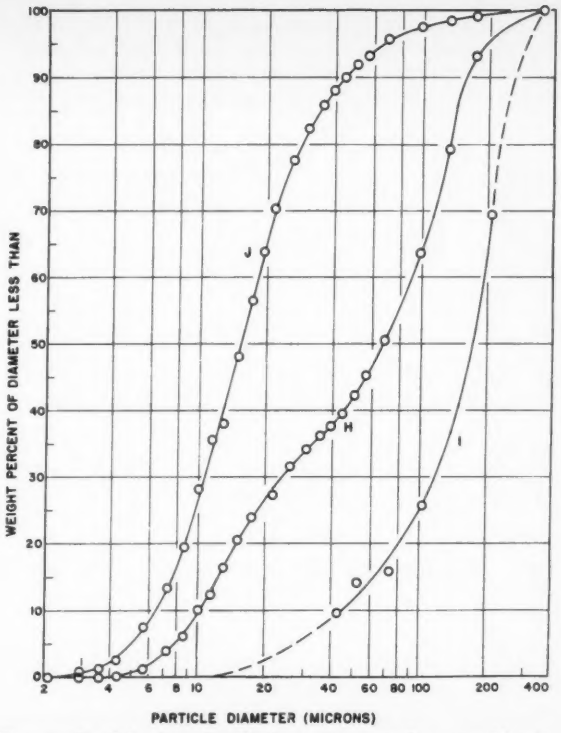

Fig. 3 Particle-size distribution of ammonium perchlorate employed in propellants H, I and J

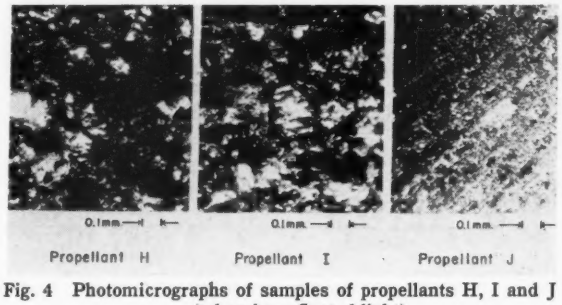

Fig. 4 Photomicrographs of samples of propellants H, I and J (taken by reflected light)

Table 2 Comparative ballistic properties of experimental composite propellants with varying burning rate but with constant energy content

Propellant	H	I	J
Total oxidizer content, not including burning-rate accelerators, per cent	76	76	76
Density, lbm/in.^{3}	0.0623	0.0601	0.0625
Strand burning rate at 1000 psia and 60 F, in./sec	0.70	0.48	1.24
Heat of explosion, cal/gm	932	932	932
Heat of explosion/unit volume, Btu/in.^{3}	104	101	105
Nominal rate of heat release at 60 F and 1000 psia, Btu/in.^{2} sec	73.0	48.3	130
Flame temperature, °R	4830	4830	4830
Specific impulse, lbf sec/lbm	233	233	233
Average specific heat ratio	1.20	1.20	1.20
Molecular weight of gases in combustion chamber	26.2	26.2	26.2

observation that the amplitude of acoustical oscillation in the cavity ("sonant" burning, the existence of which is a necessary but not sufficient condition for the occurrence of gross irregularities in the mean pressure-time history, or "resonant" burning) does not necessarily determine the magnitude of the gross irregularities (6, 7). In the tests of propellants H, I and J, no high frequency measurements were made.

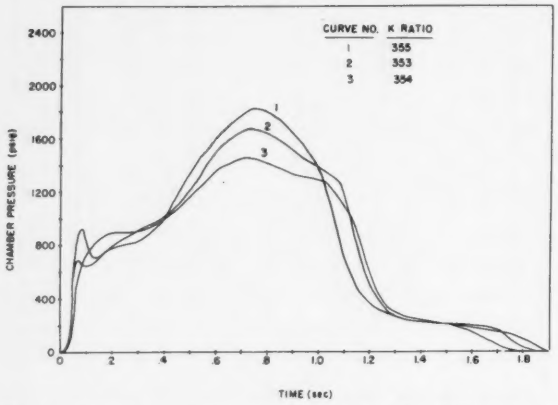

Fig. 5 Pressure-vs.-time curves obtained in the static tests of propellant A

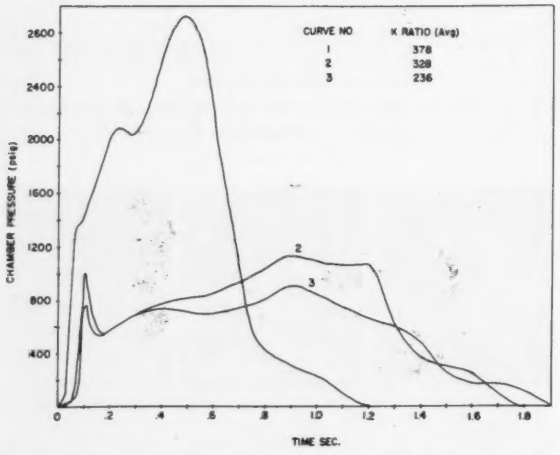

Fig. 6 Pressure-vs.-time curves obtained in the static tests of propellant B

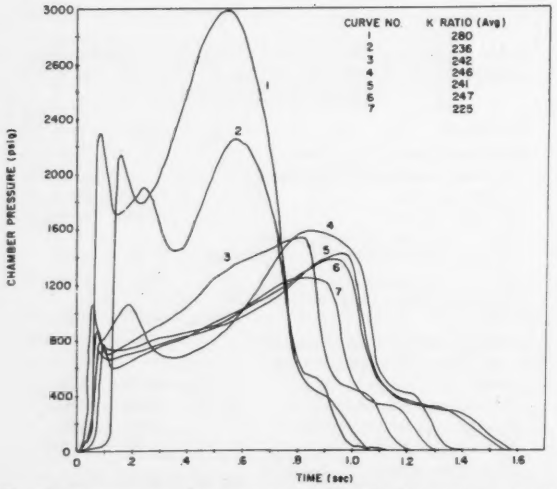

Fig. 7 Pressure-vs.-time curves obtained in the static tests of propellant C

Experimental Results

The pressure-time curves obtained from the tests of propellants A, B, C and D are presented in Figs. 5, 6, 7 and 8, respectively, and the interior ballistic data are summarized in Table 3. These results generally confirm the belief stated earlier that irregular reaction tends to be more pronounced in high energy propellants than in low energy ones. The firing curves obtained with propellant A (which show a sensitivity of pressure to K ratio so high that the measured K values were not sufficiently accurate) are uniformly smooth, while those obtained with propellants B and C show an increasing degree of irregularity manifesting resonant burning. The extended "tail-off" observed in the tests of propellants A and B is attributable to a nonuniform distribution of oxidizer along the length of the grain, because of the settling of the particles when cast in low concentration in a fuel of low viscosity; the high concentration end of the grain burns out before the low concentration end does. This effect becomes less pronounced as the nominal concentration level is increased, but some tail-off is always observed with grains of constant web thickness because of erosive-burning effects. The presence of tail-off in many of the tests required a compensation of this effect in reduction of the firing curve data. The mean pressures and mean burning rates reported herein were computed by extrapolating the principal portion of the pressure-time decline to the zero-pressure ordinate. The point of intersection was used to define the effective duration of reaction at the nominal mean pressure level, thus disregarding the effects of tail-off.

In the case of propellant C, pronounced "secondary pressure peaks" (as distinguished from the initial "ignition peak") occur early in the tests corresponding to curves 2 and 4. The secondary pressure peaks observed with propellants B and C must be distinguished from the smooth, broad "hump" which is observed at the midpoint of the pressure-time histories obtained with propellant A. This burning anomaly is a property of the particular class of composite propellants employed. These often show a nonuniform distribution of burning rate across the grain web, with the maximum value occurring at the center of the web. This effect is most pronounced in the formulations employing relatively low oxidizer concentrations and becomes negligible in formulations with high oxidizer concentration. In composite propellants, this effect may be attributable to a nonuniform distribution of oxidizer, but a similar burning-rate nonuniformity has also been observed in extruded, double-base propellants (1). Surprisingly, the highest energy charges (propellant D) showed uniformly smooth curves. This result is attributed to two factors: First, the coarse particle size employed in this

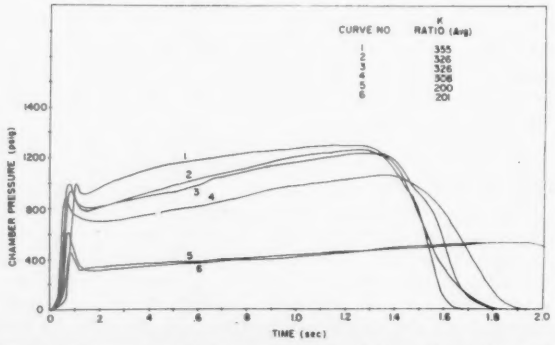

Fig. 8 Pressure-vs.-time curves obtained in the static tests of propellant D

Table 3 Summary of data obtained from the static testing of internal-burning, tubular charges of experimental propellants A, B, C and D

Curve No.	Avg. K	Nozzle throat area, in.²	Avg. pressure, psia	Avg. burning rate, in./sec	Nominal heat release rate, Btu/in.²/sec
PROPELLANT A (Fig. 5)					
1	355	0.482	1154	0.412	30.1
2	353	0.483	1152	0.411	30.0
3	354	0.482	1030	0.382	27.9
PROPELLANT B (Fig. 6)					
1	378	0.450	1900	0.662	61.2
2	328	0.522	804	0.324	30.0
3	236	0.728	663	0.299	27.7
PROPELLANT C (Fig. 7)					
1	280	0.617	1939	0.643	72.0
2	281	0.615	1439	0.534	59.8
3	242	0.703	966	0.425	47.6
4	246	0.703	1054	0.494	55.3
5	241	0.694	953	0.460	51.5
6	247	0.694	969	0.460	51.5
7	225	0.770	898	0.470	52.6
PROPELLANT D (Fig. 8)					
1	355	0.484	1105	0.331	40.0
2	326	0.523	996	0.319	38.5
3	326	0.524	992	0.314	37.9
4	308	0.557	824	0.268	34.5
5	200	0.850	425	0.223	26.9
6	201	0.848	424	0.220	26.6

formulation apparently tends to promote stable combustion (as has been suggested by development experience) and thus may counteract the effect of the increased energy content. Second, the burning rates of the propellant D charges were found to be considerably lower than the values indicated by strand burning measurements using the Crawford bomb, an effect which is not readily explainable. Accordingly, the rates of energy release (here taken as the product of heat of explosion, the propellant mass density and the linear burning rate) experimentally observed with the propellant D charges are actually lower than the corresponding rates observed with propellant C, as is shown in Table 3. These results suggest that the rate of energy release may possibly afford a measure of the relative reaction stability.

The pressure-vs.-time curves obtained in the static tests of propellants H, I and J are grouped in Figs. 9, 10 and 11, respectively. The results shown herein followed the anticipated trend; the finest grained, fastest burning propellant, J, showed the most irregular behavior. In general, however, the irregularities were observed in the tests at low pressure levels, with the charges fired at low K ratios. The inconsistent relation between average pressure and K ratio for curves 4 and 5 of Fig. 11 is attributed to grain fracture during resonance. It is not known whether the nozzle separation indicated in Fig. 11 was attributable to a high initial resonant-burning peak or to the presence of undetected, internal fissures within the propellant.

The charges of propellant H, with the intermediate distribution of oxidizer particle size, showed a smoother reaction, with only mild irregularities being observed. The extended regression (tail-off) observed in curve 5 of Fig. 9 indicates that some fracturing or fissuring of the grain occurred during the run. The tests of the slower burning propellant I showed the least tendency toward resonance, but the results were

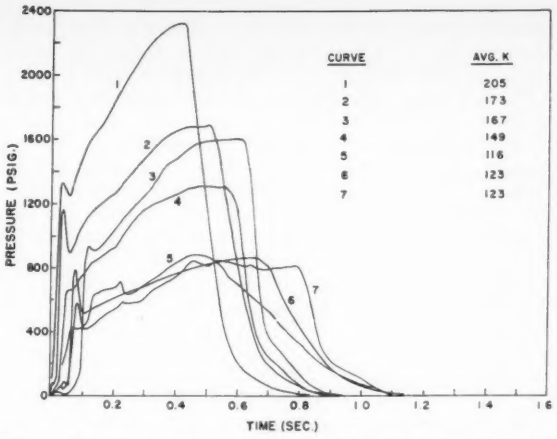

Fig. 9 Pressure-vs.-time curves obtained in the static tests of propellant H

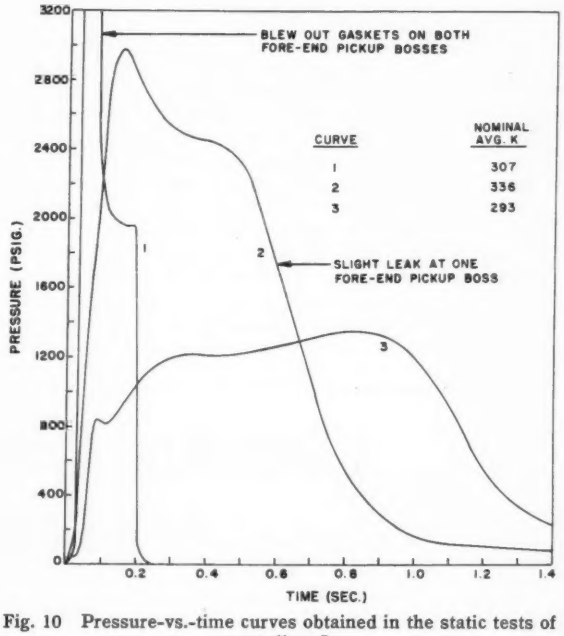

Fig. 10 Pressure-vs.-time curves obtained in the static tests of propellant I

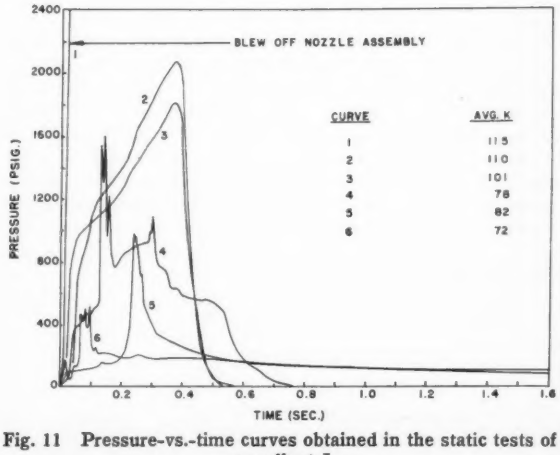

Fig. 11 Pressure-vs.-time curves obtained in the static tests of propellant J

partially obscured by the difficulty in fabricating satisfactory charges of this propellant, owing to the poor castability which is characteristic of a very coarsely ground oxidizer fraction.

Of the five tests performed with this propellant, three yielded pressure-time histories which, although smooth, showed initial pressures excessive enough to blow the gaskets sealing the two plugged fore-end bosses for the unused high frequency response pressure pickups, and thus exhibited an extremely regressive character. For comparison, the results of one such test are included as curve 1 of Fig. 10. Also, curve 2 of this figure represents a test in which the pressure was just high enough to cause a leak at one fore-end pickup location, thus producing a moderately regressive pressure-time characteristic. Only one test of propellant I (curve 3 of Fig. 10) was completely satisfactory. Nevertheless, it is emphasized that the erratic pressure-vs.-time curves obtained with propellant I are not characteristic of resonant burning, but are attributed to poor propellant consolidation. The low pressure-time integral shown by curve 1, for instance, manifests a significant loss of unburned propellant through the nozzle.

Conclusion

The study described above consituted an effort to investigate systematically certain trends in relative reaction stability with propellant composition which had been suggested by the experience accumulated in various rocket development programs. The study was hampered by a limited scope and by difficulties in processing experimental propellants of widely varying compositions which did not conform to conventional manufacturing practice. Nevertheless, the results permit the conclusion that the tendency of a propellant to exhibit resonance burning may not be judged on the basis of either energy content or burning rate alone, but that a nominal rate of energy release involving the product of the two quantities affords a better measure for estimating relative reaction stability. The apparent effectiveness of a coarsely ground oxidizer fraction in suppressing resonance was not investigated thoroughly enough to permit any judgment as to whether this beneficial effect is due to the coarse particle size per se, or to its influence in lowering the burning rate. Further efforts to distinguish particle-size and burning-rate effects are recommended.

Acknowledgments

The author wishes to thank the many individuals in the Aerojet-General organization who contributed to the investigation, particularly, K. L. Nall, who coordinated much of the experimental work. Propellant development was conducted by C. O. Brown and R. L. Parrette; thermochemical calculations were made by D. M. Meehan and G. Haynes; static testing and data reduction were supervised by R. Reichard and R. R. Stephens, respectively.

References

1 Wimpress, R. N., "Internal Ballistics of Solid-Fuel Rockets," McGraw-Hill, New York, 1950.

2 Galcit Staff (H. S. Tsien, Editor), "Jet Propulsion," California Institute of Technology, 1946.

3 Crawford, B. L., Jr., Huggett, C., Daniels, F., and Wilfong, R. E., "Direct Determination of Burning Rates of Propellant Powders," *Anal. Chem.*, vol. 19, 1947, pp. 630–633.

4 Smith, R. P., and Sprenger, D. F., "Combustion Instability in Solid-Propellant Rockets," Fourth Symposium (International) on Combustion, Williams and Wilkins, Baltimore, 1953, pp. 893–906.

5 Green, L., Jr., "Studies on the Reaction Stability of Solid Propellant Charges," Aerojet-Genral Report 1077 (AFOSR-TR-56-10, ASTIA AD 86012), March 9, 1956.

6 Green, L., Jr., "Observations on the Irregular Reaction of Solid Propellant Charges," JET PROPULSION, vol. 26, 1956, pp. 655–659.

7 Green, L., Jr., "Some Properties of a Simplified Model of Solid Propellant Burning," ARS Preprint 339-56, Nov. 1956.

A Generalized Optimization Procedure for N-Staged Missiles

LEON WEISBORD[1]

Wright Aeronautical Division, Curtiss-Wright Corp., Wood-Ridge, N. J.

This report is an extension of the Goldsmith report (Reference 2) and outlines a simple method for determining the optimum weight distribution for a staged rocket with different structural factors and propellant specific impulses in each stage. It is applicable for a rocket of any number of stages, and is not limited to either a horizontal or vertical trajectory. The report can be used in a first design estimate to determine the weight distribution among the various stages and the weight breakdown within each stage. A sample problem is included to illustrate the method of application.

Nomenclature

C = propellant exhaust velocity

$G = V + \int_0^{t_p} g \sin \theta dt$

K = structural factor

$\bar{M}$ = payload

M_g = gross weight

M_m = miscellaneous weight (structures, engines, controls, etc.)

M_0 = burnout weight

M_p = propellant weight

T = thrust

t_p = burning time

V = velocity

θ = angle between velocity vector and horizontal

Subscripts

1, 2, 3 = number of stage

N = last stage

$N - 1$ = next to last stage, etc.

Received Sept. 20, 1957.

[1] Senior Engineer, Advanced Engines Department.

Introduction

IT IS necessary for the rocket designer to know the best method of apportioning the weight of a staged rocket. It is possible to distribute the weight in an infinite variety of

ways to achieve the same final performance; however, there is only one minimum weight distribution. Knowledge of this theoretical minimum weight distribution is obviously an important bit of information in the preliminary design of the staged rocket.

The problem has been treated by Malina and Summerfield (1).[2] Their analysis held for a rocket of an arbitrary number of stages which used the same impulse and structural factor in each stage. Under these conditions the following relation holds for minimum take-off weight

$$\frac{\bar{M}}{M_{0_N}} = \frac{M_{0_N}}{M_{0_{N-1}}} = \frac{M_{0_{N-1}}}{M_{0_{N-2}}} = \ldots = \frac{M_{0_2}}{M_{0_1}} \quad \ldots\ldots [1]$$

However, the problem of optimum staging when structural factors and propellant specific impulses differed remained unsolved. Goldsmith (2) realized this lack and devised a method for the optimization of two-stage rockets under conditions of different impulses and structural factors. This pointed up the need for a general method of optimization for rockets of any number of stages.

Such a method is presented in this report. It is valuable as a first design weight breakdown and is quick and easy to apply

Analysis

The rocket velocity is given by Equation [2] which is the relation for drag-free flight with constant exhaust velocities

$$G = V + \int_0^{t_p} g \sin\theta dt = C_1 \ln \frac{M_{0_1}}{M_{0_1}} + C_2 \ln \frac{M_{0_2}}{M_{0_2}} + \ldots + C_N \ln \frac{M_{0_N}}{M_{0_N}} \ldots [2]$$

It can be seen that G in Equation [2] is equal to the velocity that would be attained if the rocket were fired horizontally. If the rocket were fired vertically, $\int_0^{t_p} g \sin\theta dt = gt_p$. An evaluation of the term $\int_0^{t_p} g \sin\theta dt$ is difficult since it depends on the particular trajectory and the engines used. In using this optimization procedure, $\int_0^{t_p} g \sin\theta dt$ must be approximated, but it will be between 0 and gt_p depending upon the trajectory followed.

Each stage of the rocket consists of propellant, payload and miscellaneous additional hardware consisting of tanks, structure, guidance, engines, etc. The miscellaneous weight will be lumped together and included in the calculation by defining a structural factor K as

$$\text{miscellaneous weight} = K(M_0 - \text{payload}) \quad \ldots\ldots [3]$$

This analysis will first derive expressions for a three-stage rocket, and follow with the general case.

The empty weight M_0 is defined as the payload plus the miscellaneous weight.

Expressions will now be written for the burnout weight at the end of each stage.

$$\left.\begin{aligned} M_{0_3} &= \bar{M} + K_3(M_{0_3} - \bar{M}) = K_3 M_{0_3} + (1 - K_3)\bar{M} \\ M_{0_2} &= K_2 M_{0_2} + (1 - K_2) M_{0_3} \\ M_{0_1} &= K_1 M_{0_1} + (1 - K_1) M_{0_2} \end{aligned}\right\} \ldots [4]$$

Equation [2] can be rewritten as

$$G = C_1 \ln \frac{M_{0_1}}{K_1 M_{0_1} + (1 - K_1) M_{0_2}} + C_2 \ln \frac{M_{0_2}}{K_2 M_{0_2} + (1 - K_2) M_{0_3}} + C_3 \ln \frac{M_{0_3}}{K_3 M_{0_3} + (1 - K_3)\bar{M}} \quad \ldots\ldots [5]$$

[2] Numbers in parentheses indicate References at end of paper.

or

$$C_1 \ln M_{0_1} - C_1 \ln [K_1 M_{0_1} + (1 - K_1) M_{0_2}] + C_2 \ln M_{0_2} - C_2 \ln [K_2 M_{0_2} + (1 - K_2) M_{0_3}] + C_3 \ln M_{0_3} - C_3 \ln [K_3 + (1 - K_3)\bar{M}] - G = 0 \quad \ldots\ldots [5a]$$

It is desired to minimize M_{0_1} for a given velocity. Therefore, in Equation [5 or 5a], M_{0_2} and M_{0_3} become the variables and the following must be satisfied for minimum take-off weight

$$\frac{\partial M_{0_1}}{\partial M_{0_2}} = 0 \qquad \frac{\partial M_{0_1}}{\partial M_{0_3}} = 0 \quad \ldots\ldots [6]$$

It is extremely difficult to write [5] in the form $M_{0_1} = f(M_{0_2}, M_{0_3})$ so that the partial derivatives can be found explicitly. However, it will be recognized that [5a] is of the form

$$f(x, y, z) = 0 \quad \ldots\ldots [7]$$

where G is a constant for any particular mission.

This function can be differentiated implicitly quite easily. The necessary partials (Equation [6]) can be obtained from the following relations holding for Equation [7]

$$\frac{\partial z}{\partial x} = -\frac{\dfrac{\partial f}{\partial x}}{\dfrac{\partial f}{\partial z}} \qquad \frac{\partial z}{\partial y} = -\frac{\dfrac{\partial f}{\partial y}}{\dfrac{\partial f}{\partial z}} \quad \ldots\ldots [8]$$

In our problem, Equation [5a] can be expressed as

$$f(M_{0_2}, M_{0_3}, M_{0_1}) = 0 \quad \ldots\ldots [9]$$

and we will find

$$\frac{\partial M_{0_1}}{\partial M_{0_2}} = -\frac{\dfrac{\partial f}{\partial M_{0_2}}}{\dfrac{\partial f}{\partial M_{0_1}}} \qquad \frac{\partial M_{0_1}}{\partial M_{0_3}} = -\frac{\dfrac{\partial f}{\partial M_{0_3}}}{\dfrac{\partial f}{\partial M_{0_1}}} \quad \ldots\ldots [10]$$

The above partials will be set equal to zero or

$$\frac{\partial M_{0_1}}{\partial M_{0_2}} = 0 = \frac{\partial f}{\partial M_{0_2}} \qquad \frac{\partial M_{0_1}}{\partial M_{0_3}} = 0 = \frac{\partial f}{\partial M_{0_3}} \quad \ldots [11]$$

The differentiation gives

$$\left.\begin{aligned} \frac{\partial f}{\partial M_{0_2}} &= -\frac{C_1(1 - K_1)}{K_1 M_{0_1} + (1 - K_1) M_{0_2}} + \frac{C_2}{M_{0_3}} - \frac{C_2 K_2}{K_2 M_{0_2} + (1 - K_2) M_{0_3}} \\ \frac{\partial f}{\partial M_{0_3}} &= -\frac{C_2(1 - K_2)}{K_2 M_{0_2} + (1 - K_2) M_{0_3}} + \frac{C_3}{M_{0_3}} - \frac{C_3 K_3}{K_3 M_{0_3} + (1 - K_3)\bar{M}} \end{aligned}\right\} \ldots [12]$$

Setting Equations [12] equal to zero as indicated by Equations [11] for minimization, obtain after algebraic manipulation

$$\frac{M_{0_2}}{M_{0_2}} = \frac{C_1 K_2 (1 - K_1)}{(1 - K_1)(1 - K_2)(C_2 - C_1) + C_2 K_1 (1 - K_2) \dfrac{M_{0_1}}{M_{0_2}}} \quad \ldots [12a]$$

and

$$\frac{\bar{M}}{M_{0_3}} = \frac{C_2 K_3 (1 - K_2)}{(1 - K_2)(1 - K_3)(C_3 - C_2) + C_3 K_2 (1 - K_3) \dfrac{M_{0_2}}{M_{0_3}}} \quad \ldots [12b]$$

Rewriting Equation [5] as

$$G = C_1 \ln \frac{1}{K_1 + (1 - K_1)\dfrac{M_{g_2}}{M_{g_1}}} + C_2 \ln \frac{1}{K_2 + (1 - K_2)\dfrac{M_{g_3}}{M_{g_2}}} + C_3 \ln \frac{1}{K_3 + (1 - K_3)\dfrac{\bar{M}}{M_{g_3}}} \quad \text{..[5b]}$$

we can now determine the necessary take-off weight and individual stage weights.

For any given problem it is necessary to establish C_1, C_2, C_3, K_1, K_2, K_3 and G. The steps in the solution are:

(a) Solve [12b] for

$$\frac{\bar{M}}{M_{g_3}} = f\left(\frac{M_{g_3}}{M_{g_2}}\right)$$

(b) Solve [12a] for

$$\frac{M_{g_3}}{M_{g_2}} = f\left(\frac{M_{g_2}}{M_{g_1}}\right)$$

(c) A short trial and error procedure follows. Select a numerical value for M_{g_2}/M_{g_1} and obtain numerical answers from Equations [12a and 12b]. Using the values found for M_{g_3}/M_{g_2}, M_{g_3}/M_{g_2} and $\bar{M}/M_{g_3}$, solve [5b] for G. If the value of G thus found is not the value desired, repeat the process using a different value of M_{g_2}/M_{g_1}.

The method outlined is, in actual practice, quite fast. The trial and error process takes five to ten minutes to reach a solution.

(d) Finally, obtain a maximum value of

$$\frac{\bar{M}}{M_{g_1}} = \frac{M_{g_2}}{M_{g_1}} \times \frac{M_{g_3}}{M_{g_2}} \times \frac{\bar{M}}{M_{g_3}}$$

This value of $\bar{M}/M_{g_1}$ is the optimum theoretical value for the conditions prescribed.

It will be immediately noted that when

$$C_1 = C_2 = C_3 \qquad K_1 = K_2 = K_3$$

the Malina-Summerfield conditions are encountered. Under these conditions Equations [12a and 12b] break down and become simply

$$\frac{\bar{M}}{M_{g_3}} = \frac{M_{g_3}}{M_{g_2}} = \frac{M_{g_2}}{M_{g_1}}$$

which is recognized as Equation [1], the Malina-Summerfield optimization criterion.

The analysis can now be easily extended to cover any number of stages.[3] If N represents the number of stages, N being the last stage to fire, Equations [12a and 12b] can be extended to give the $N - 1$ relations necessary for an N stage problem solution. That is

$$\left.\begin{aligned} \frac{\bar{M}}{M_{g_N}} &= \frac{C_{N-1}K_N(1 - K_{N-1})}{(1 - K_{N-1})(1 - K_N)(C_N - C_{N-1}) + C_N K_{N-1}(1 - K_N)\dfrac{M_{gN-1}}{M_{gN}}} \\ \frac{M_{gN}}{M_{gN-1}} &= \frac{C_{N-2}K_{N-1}(1 - K_{N-2})}{(1 - K_{N-2})(1 - K_{N-1})(C_{N-1} - C_{N-2}) + C_{N-1}K_{N-2}(1 - K_{N-1})\dfrac{M_{gN-2}}{M_{gN-1}}} \end{aligned}\right\} \text{..[13]}$$

etc. The Nth equation necessary for solution is, of course, Equation [2], written in the form of Equation [5b].

Sample Calculation and Check for Minimization

In order to illustrate the use of the method, a sample problem will be performed. This sample problem is not intended to illustrate any particular missile application. Rather, a group of widely differing structural factors and exhaust velocities will be selected. Let us use

$C_1 = 9{,}000$	$K_1 = 0.2$	$G = 30{,}000$
$C_2 = 15{,}000$	$K_2 = 0.25$	
$C_3 = 25{,}000$	$K_3 = 0.40$	

Substitute the appropriate numerical values into Equations [12a and 12b]. Then, perform the trial and error process mentioned before by first selecting a value of M_{g_2}/M_{g_1} and then solving Equation [5b] for G using the values determined from Equations [12a and 12b].

This procedure yields $M_{g_3}/M_{g_2} = 0.678$, $M_{g_3}/M_{g_2} = 0.260$ and $\bar{M}/M_{g_3} = 0.238$. Therefore, $M_{g_1}/\bar{M} = 23.8$, or for every pound of payload, 23.8 lb of take-off weight are needed. In addition, the size and weight of propellant for each stage can be determined easily by using the structural factors as indicated in [4]. Table 1 gives the complete weight breakdown for a payload of 1000 lb and approximate engine sizes and burning times. The engine thrusts were arbitrarily made equal to twice the gross weight.

Actually, it was never shown whether the procedure leads to a minimum or a maximum gross weight. It is easiest to decide this question by checking any other combination of stage weights. Since the procedure outlined describes either a maximum or a minimum, if any other combination of weights gives a higher ratio of gross weight to payload than 23.8, then the procedure is one of minimization of the gross take-off weight as desired.

Selecting $M_{g_2}/M_{g_1} = 0.600$ and $M_{g_3}/M_{g_2} = 0.400$, obtain by solution of Equation [5b] $\bar{M}/M_{g_3} = 0.1585$ Then $M_{g_1}/\bar{M}$

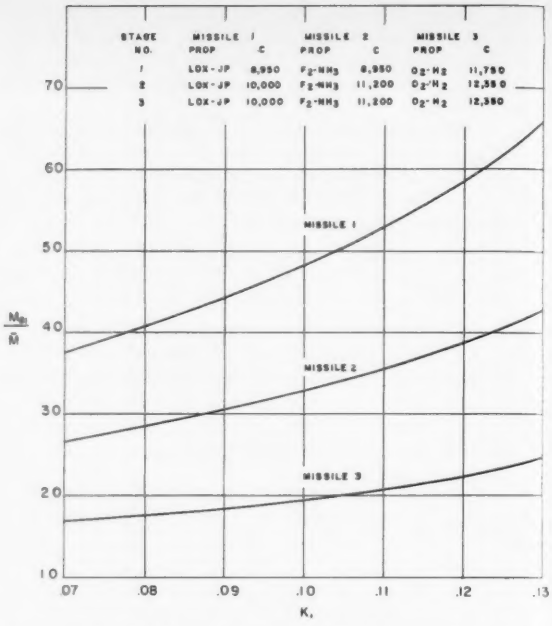

Fig. 1 Optimized three-stage missiles for the case $K_2 = K_1 + 0.01$, $K_3 = K_1 + 0.02$, $G = 30{,}000$ fps

[3] Vertregt (3) analyzed the problem through the use of Lagrangian multipliers. His analysis presents an implicit solution for the general case and a formal solution for the case of equal exhaust velocities.

= 26.3, which shows that this procedure is indeed one of minimization.

Table 1 Weight breakdown for 1000-lb payload

Stage	Misc. weight	Prop weight	Gross weight	Burnout weight	Thrust, 2 mg	Burning time
1	1540	6160	23,800	17,640	47,600	37
2	3065	9195	16,100	6,905	32,200	133
3	1136	1704	3,840	2,136	7,680	172

Fig. 1 shows optimized sizes for several propellant combinations vs. structural factors for a three-stage rocket when the structural factors are such that $K_2 = K_1 + 0.01$ and $K_3 = K_2 + 0.01$. It will be noted that the missile gross weight is not as sensitive at low structural factors as at higher values, and the higher the specific impulse the less the effect of structural factor for a value of $G = 30{,}000$.

Another conclusion may be drawn by an examination of Equation [2]. It will be seen that the burning times can be distributed among the stages in any fashion and not change the final velocity. In the sample problem the thrust was arbitrarily made equal to twice the stage gross weight which resulted in unequal burning times. The reverse procedure could have been taken. That is, the total burning time could have been divided equally between the various stages. This would then set the engine thrusts by the familiar relation

$$T = \frac{M_p}{t_p}\frac{C}{g} \qquad [14]$$

Of course, the entire procedure is based upon an accurate guess for the value of $\int_0^{t_p} g \sin\theta dt$. The value of the integral can usually be evaluated with some accuracy by a study of the planned trajectory. As pointed out previously, it will lie between 0 and gt_p. In familiar trajectories the value can be guessed with fairly good accuracy.

In addition, the value of G can be increased slightly, if desired, to take into account an estimated drag loss. Thus, it can be seen that the inclusion of the integral, while troublesome, still permits a degree of flexibility in the use of the optimization procedure.

References

1 Malina, F. J., and Summerfield, M., "The Problem of Escape from the Earth by Rocket," *Journal of the Aeronautical Sciences*, vol. 14, Aug. 1947, pp. 476–478.

2 Goldsmith, M., "On the Optimization of Two-Stage Rockets," JET PROPULSION, vol. 27, April 1957, pp. 415, 416.

3 Vertregt, M., "A Method of Calculating the Mass Ratios of Step Rockets," *Journal of the British Interplanetary Society*, vol. 15, March-April 1956, p. 95.

Escape From a Circular Orbit Using Tangential Thrust

D. J. BENNEY[1]

Canterbury University College, Christchurch, New Zealand

In this article we consider the problem of escape of a rocket from the gravitational field of a planet. Initially the space ship is taken to be in a circular orbit about the planet. The motors are then switched on and the thrust is taken as tangential to the direction of motion at each instant. Clearly the motion will remain in the plane of the circular orbit. It has been shown that a tangential thrust should be a close approximation to the optimal escape program.[2] In calculating the mass ratio it has been found convenient to use the *r-s* equation of the orbit, where *r* is the radius vector and *s* the length of path. This is most useful because the escape condition is very simply expressed in terms of *s*. We conclude by comparing the results we obtain for tangential thrust with those for circumferential thrust, which were found by Tsien.[3] We will find that a tangential thrust program leads to a slightly smaller value for the mass ratio. In particular, two cases are considered in some detail, namely, those of a large thrust and of a small or micro thrust.

Received Aug. 16, 1957.

[1] Mathematics Department. Present address: Massachusetts Institute of Technology, Cambridge, Mass.

[2] Lawden, D. F., "Optimal Programming of Rocket Thrust Direction," *Astronautica Acta*, vol. 1, 1955, pp. 41–56.

[3] Tsien, H. S., "Take-Off From Satellite Orbit," JET PROPULSION, vol. 23, July–Aug. 1953, pp. 233–236.

Nomenclature

f = constant rocket thrust per unit mass
r = distance from the center of attraction to the rocket
s = distance traversed by the rocket
θ = polar angle, measured from the initial line
ϕ = angle between the radius vector and the tangent to the orbit
ψ = angle between the initial line and the tangent to the orbit
v = velocity of the rocket
t = time measured from take-off
$\frac{\mu}{r^2}$ = gravitational force per unit mass
ρ = radius of curvature
a = radius of the initial circular orbit

THE initial conditions at $t = 0$ are $r = \rho = a$, $s = \theta = 0$, $\phi = \psi = \pi/2$. We shall require the following results of elementary calculus

$$\cos\phi = \frac{dr}{ds} \qquad \sin\phi = r\frac{d\theta}{ds} \qquad \rho = \frac{ds}{d\psi} \qquad \psi = \theta + \phi$$

Equations of Motion

During its flight the space ship is under the action of two forces, namely, the gravitational attraction and the tangential thrust, as indicated in Fig. 1.

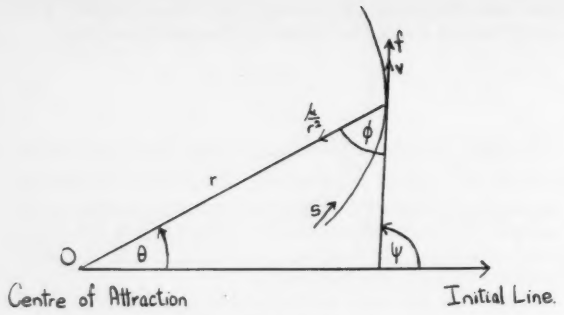

Fig. 1 Diagram showing the variables used in the problem

Resolution along the tangent and normal leads to the equations

$$v\frac{dv}{ds} = f - \frac{\mu}{r^2}\cos\phi = f - \frac{\mu}{r^2}\frac{dr}{ds}$$

$$\frac{v^2}{\rho} = \frac{\mu}{r^2}\sin\phi = \frac{\mu}{r}\frac{d\theta}{ds}$$

For convenience we introduce the corresponding dimensionless quantities by replacing r by r/a, s by s/a, and writing $f = \lambda g$ where $g = \mu/a^2$, so that g is the acceleration due to gravity at the point of projection. Distances are now in units of the initial radius a, velocity is in units of initial circular velocity v_i, time is in units of a/v_i and λ represents the ratio of thrust to local weight. The above equations then become

$$v\frac{dv}{ds} = \lambda - \frac{1}{r^2}\frac{dr}{ds} \quad \ldots\ldots [1]$$

$$\frac{v^2}{\rho} = \frac{1}{r}\frac{d\theta}{ds} \quad \ldots\ldots [2]$$

The initial conditions now at $t = 0$ are $r = v = 1$, $s = \theta = 0$, $\phi = \psi = \pi/2$.

Equation [1] may be integrated immediately and using the initial conditions yields

$$v^2 = \frac{2}{r} + 2\lambda s - 1 \quad \ldots\ldots [3]$$

At the escape position the orbit will be parabolic, and so if we use the subscript E to denote escape values we have

$$v_E^2 = \frac{2}{r_E} \quad \ldots\ldots [4]$$

and therefore

$$s_E = \frac{1}{2\lambda} \quad \ldots\ldots [5]$$

We now solve Equation [2] for v^2 in terms of r and the derivatives of r with respect to s. We have

$$v^2 = \frac{1}{r}\frac{d\theta}{ds}\frac{ds}{d\psi} = \frac{1}{r}\left(\frac{d(\theta+\phi)}{d\theta}\right)^{-1} = \frac{1}{r}\left(1 + \frac{d}{ds}\left(\cos^{-1}\frac{dr}{ds}\right)\frac{ds}{d\theta}\right)^{-1}$$

Therefore

$$v^2 = \frac{1 - \left(\frac{dr}{ds}\right)^2}{r\left(1 - \left(\frac{dr}{ds}\right)^2 - r\frac{d^2r}{ds^2}\right)} \quad \ldots\ldots [6]$$

Equating values of v^2 from Equations [3 and 6], and letting a prime denote differentiation with respect to s, we obtain the differential equation of the orbit

$$\frac{2}{r} + 2\lambda s - 1 = \frac{1 - r'^2}{r(1 - r'^2 - rr'')}$$

i.e.

$$[(2\lambda s - 1)r + 1][1 - r'^2] = [(2\lambda s - 1)r + 2]rr'' \ldots [7]$$

This differential equation has to be solved subject to the initial conditions that when $s = 0$, $r = 1$ and $r' = 0$.

The General Solution

We attempt to find a series solution for r in powers of the parameter λ by assuming the expansion

$$r = 1 + \sum_{n=1}^{\infty} \lambda^n r_n$$

where each r_i is a function of s, and where the boundary conditions require that when $s = 0$, $r_i = r_i' = 0$. Substituting this series into Equation [7] and equating the coefficients of λ and λ^2 we obtain

$$r_1'' + r_1 = 2s$$

$$r_2'' + r_2 = 4s(r_1 - s)$$

The solutions of these differential equations are

$$r_1 = 2(s - \sin s)$$

$$r_2 = 4\left(s^2 + \frac{1}{2}s^2\cos s - \frac{1}{2}s\sin s + 2\cos s - 2\right)$$

It is readily seen that each r_i is the solution of a differential equation of the type

$$r_i'' + r_i = F(s, r_1, \ldots r_{i-1}, r_1', \ldots r_{i-1}')$$

where $r_i(0) = r_i'(0) = 0$. These equations can be solved in turn by elementary means; but clearly the solution obtained will be of doubtful convergence at escape where $s = 1/2\lambda$.

Therefore, we consider two special cases according to whether λ is large or small.

Approximation for Large λ

Let $x = 2\lambda s$. Then initially where $s = 0$, $x = 0$; and at escape where $s = 1/2\lambda$, $x = 1$. On making x the independent variable in Equation [7] we obtain

$$[(x-1)r + 1]\left[1 - 4\lambda^2\left(\frac{dr}{dx}\right)^2\right] = [(x-1)r + 2]4\lambda^2 r\frac{d^2r}{dx^2} \quad \ldots\ldots [8]$$

We assume a series solution for r in inverse powers of λ^2, namely

$$r = 1 + \sum_{n=1}^{\infty} \lambda^{-2n} r_n$$

with the initial conditions $r_i = dr_i/dx = 0$, when $x = 0$. Substituting this series into Equation [8] and equating the coefficients of the constant and of λ^{-2} we obtain

$$x = 4(1 + x)\frac{d^2r_1}{dx^2} \quad \ldots\ldots [9]$$

$$(x-1)r_1 - 4x\left(\frac{dr_1}{dx}\right)^2 = 4\left[(1+x)\frac{d^2r_2}{dx^2} + 2xr_1\frac{d^2r_1}{dx^2}\right] \quad \ldots\ldots [10]$$

On integrating these equations we obtain the solutions

$r_1 = \frac{1}{8}[e^{2u} - 2ue^u - 1]$

$$r_2 = -\frac{15}{128} - \frac{1}{64}e^u + \frac{1}{32}\left[-\frac{1}{4}e^{4u} + e^{2u}\left(u + \frac{1}{2}\right) + e^{2u}(-u^2 - 3u + 2) + e^u\left(\frac{2}{3}u^3 + 2u^2 - 4u + 4\right) - 2(u + 1)\right]$$

where $u = \log(1 + x)$.

A similar procedure could be used to calculate r_3, r_4, etc. To calculate the mass ratio we use Equation [3], i.e.

$$\left(\frac{ds}{dt}\right)^2 = \frac{2}{r} + x - 1$$

Putting $T = \lambda t$ this becomes

$$\frac{1}{4}\left(\frac{dx}{dT}\right)^2 = x - 1 + \frac{2}{1 + \frac{1}{\lambda^2}r_1 + \frac{1}{\lambda^4}r_2 + \ldots}$$

Therefore

$$T_E = \frac{1}{2}\int_0^1 \frac{dx}{(1+x)^{1/2}}\left[1 + \frac{1}{\lambda^2}\frac{r_1}{1+x} + \frac{1}{\lambda^4}\times\left(\frac{r_2 - r_1^2}{1+x} + \frac{3r_1^2}{2(1+x)^2}\right) + 0\left(\frac{1}{\lambda^6}\right)\right] \quad [11]$$

Let

$$T_E = a_0 + \frac{a_1}{\lambda^2} + \frac{a_2}{\lambda^4} + 0\left(\frac{1}{\lambda^6}\right) \quad [12]$$

On substituting for r_1 and r_2 a somewhat lengthy calculation yields

$$a_0 = \sqrt{2} - 1 = 0.414212$$

$$a_1 = \frac{31}{48}\sqrt{2} - \frac{2}{3} - \frac{\sqrt{2}}{4}\log 2 = 0.001615$$

$$a_2 = \left[-104 + \frac{3}{7} - \frac{1}{25} - \frac{52}{9}\right] + \sqrt{2}\left[-\frac{1}{4} - \frac{24}{7} + \frac{4}{5} + \frac{104}{9} + 88 + \frac{17}{2}\right] + \sqrt{2}\left[\frac{8}{3}(\log 2)^3 - 4(\log 2)^2 + \left(\frac{48}{5} - \frac{16}{3} - 42\right)\log 2\right]$$

i.e. $$a_2 = -0.000064$$

Therefore

$$T_E = 0.414212 + \frac{0.001615}{\lambda^2} - \frac{0.000064}{\lambda^4} + 0\left(\frac{1}{\lambda^6}\right) \quad [13]$$

If M_0 is the initial mass of the rocket and fuel, then

$$\log\left(\frac{M_0}{M_E}\right) = \frac{\sqrt{ga}}{c}T_E$$

where c is the exhaust velocity. We compare this result with that for circumferential thrust obtained by Tsien,[3] where for λ large

$$T_E = 0.414212 + \frac{0.002349}{\lambda^2} - \frac{0.000048}{\lambda^4} + 0\left(\frac{1}{\lambda^6}\right)$$

This shows that a somewhat smaller mass ratio is required for escape when a tangential thrust is employed.

Approximation for Small λ

Perhaps of more practical interest is the problem of escape from a circular orbit by means of a microthrust. We now obtain a rather crude approximation for this case, i.e., when λ is small. Intuitively r' and r'' will both be small for the first part of the orbit. We simplify our equation by assuming that $r'' = 0$ throughout the motion. The approximate solution of Equation [7] is

$$r \doteqdot \frac{1}{1 - 2\lambda s} \quad [14]$$

This satisfies the boundary conditions to order λ. Using Equations [5 and 7] we see that at escape, $1 - r'^2 = 2rr''$. The approximation given by [14] then yields

$$r_E \doteqdot \frac{1}{(20)^{1/3}\lambda^{1/2}} \qquad s_E \doteqdot \frac{1}{2\lambda}\left[1 - (20)^{1/3}\lambda^{1/2}\right]$$

As $ds^2 = dr^2 + r^2 d\theta^2$, we have

$$\theta_E \doteqdot \int_0^{s_E}(1 - 2\lambda s)ds$$

Therefore

$$\theta_E \doteqdot \frac{1}{4\lambda}$$

So the approximate number of revolutions to escape n_E is given by

$$n_E = \frac{\theta_E}{2\pi} \doteqdot \frac{1}{8\pi\lambda}$$

Further as

$$\left(\frac{ds}{dt}\right)^2 = 2\lambda s + \frac{2}{r} - 1$$

we find that

$$T_E = \lambda t_E \doteqdot 1 - (20)^{1/3}\lambda^{1/4} \quad [15]$$

Thus, the mass ratio for escape when λ is small is given by

$$\log\left(\frac{M_0}{M_E}\right) \qquad \frac{\sqrt{ga}}{c}\left(1 - (20)^{1/3}\lambda^{1/4}\right)$$

Tsien found that $T_E \doteqdot 1 - 2^{1/4}\lambda^{1/4}$ for circumferential thrust; so that again we obtain a somewhat smaller mass ratio for escape.

The Optimization of Nozzle Area Ratio for Rockets Operating in a Vacuum

M. GOLDSMITH[1]

The Rand Corporation, Santa Monica, Calif.

The correct choice of nozzle area ratio should be considered in rocket-powered missiles even when intended to operate at high altitudes, where ambient pressure may be neglected. Under such conditions, specific impulse of the propellant increases monotonically with increasing area ratio (exit area/throat area), but the increased weight of larger nozzles degrades performance. Hence an optimum area ratio can be sought which will provide maximum performance for the stage in question. Gains in stage velocity increment due to correct choice of area ratio are usually only a few per cent, which may be of importance in some applications. The present investigation results in a linearized analytic approach to the problem of calculating the the optimum area ratio. Design charts are presented.

Nomenclature

A_e = nozzle exit area
A_0 = nozzle area at start of exit cone
A_t = nozzle throat area
C_F = nozzle thrust coefficient
c^* = propellant characteristic velocity
I_{sp} = specific impulse
g = sea-level acceleration of gravity
k = $A_t l\rho/\sin\alpha$
m_I = weight of inert parts (total burnout weight)
m_n = weight of exit cone
m_p = weight of propellant
m_s = inert (burnout) weight of vehicle (without nozzle exit cone)
m_s' = $m_s - k\epsilon_0$
l = nozzle wall thickness
α = nozzle exit half-angle
γ = ratio of specific heats
ΔV = stage velocity increment
ϵ = A_e/A_t
ϵ_0 = A_0/A_t
ν = $m_p/(m_I + m_p)$
ν_0 = $m_p/(m_s' + m_p)$
ρ = nozzle wall weight density

Subscript

opt = optimum

Introduction

IN STUDIES of missile systems in which one or more rocket-powered stages operate at very high altitude, the question of correct choice for nozzle area ratio always arises. Where the ambient pressure is sufficiently small that it can be neglected, elementary rocket theory shows that specific impulse of the propellant increases monotonically with increasing area ratio (exit area/throat area). However, the larger nozzles impose a weight penalty on the missile, which will degrade over-all performance. Therefore, an optimum area ratio can be sought which will provide maximum performance for the stage in question.

Received July 15, 1957.

[1] Engineer, Aeronautics Department. Mem. ARS.

Analysis

The velocity increment for the stage is a useful criterion of performance. For a rocket with constant effective exhaust velocity (constant specific impulse) during burning, the following well-known equation may be written for the stage velocity increment

$$\Delta V = gI_{sp} \ln \frac{1}{1-\nu} \quad \ldots\ldots\ldots\ldots\ldots [1]$$

where I_{sp} is specific impulse, g is sea-level accleration of gravity, and ν is the ratio of propellant weight to gross weight of the stage. The effects of gravity and drag are ignored in Equation [1].

For increasing values of ϵ, the nozzle area ratio, the value of I_{sp} will increase; likewise, the value of ν will be decreased, owing to the increased weight of the nozzle. Examination of Equation [1] then reveals that some optimum value of ϵ should be chosen to obtain a maximum velocity increment. The purpose of this note is to develop a systematic method of determining this optimum area ratio.

To find the maximum velocity increment, using Equation [1], we differentiate with respect to ϵ, all other variables being considered as constant, and set the differential equal to zero.

$$\frac{d\Delta V}{d\epsilon} = \frac{\partial \Delta V}{\partial I_{sp}} \frac{dI_{sp}}{d\epsilon} + \frac{\partial \Delta V}{\partial \nu} \frac{d\nu}{d\epsilon} = 0$$

Therefore, for best performance

$$\ln(1-\nu)\left(\frac{dI_{sp}}{d\epsilon}\right) = I_{sp}\frac{1}{1-\nu}\left(\frac{d\nu}{d\epsilon}\right) \quad \ldots\ldots\ldots [2]$$

From rocket theory, it is shown that

$$I_{sp} = \frac{c^*}{g} C_F$$

where c^* is a characteristic constant of a propellant system, and C_F is the over-all thrust coefficient. Therefore, Equation [2] may be rewritten as

$$\frac{d \ln C_F}{d\epsilon} = \frac{d\nu/d\epsilon}{(1-\nu)\ln(1-\nu)} \quad \ldots\ldots\ldots\ldots [3]$$

Unfortunately, it is not possible to obtain an analytic expression for $\ln C_F$ in terms of the area ratio. Hence, the function $d \ln C_F/d\epsilon$ must be computed numerically.

Now, an analytic representation for ν may be found. Consider a rocket nozzle with a conical exit section of half-angle α, and constant wall thickness t. The parameter ν is defined as

$$\nu = \frac{m_p}{m_p + m_I}$$

where m_p is the weight of propellant carried, and m_I is the weight of inert parts (structure, payload, guidance, etc.). Let us break m_I into two parts, the weight m_n of the nozzle exit cone aft of section A_0, where the conical exit begins, and

m_n, the weight of all the rest of the inert parts.

It is easily shown that m_n is accurately expressed by

$$m_n = (A_e - A_0)t\rho \frac{1}{\sin \alpha} \quad \ldots\ldots\ldots\ldots\ldots [4]$$

where t is the thickness of the nozzle wall, ρ is the density of the material, and α is the exit cone half-angle. Then write

$$m_n = (\epsilon - \epsilon_0)\frac{A_t t\rho}{\sin \alpha}$$

where A_t is the throat area. Therefore

$$\nu = \frac{m_p}{m_s + m_p + \dfrac{A_t t\rho}{\sin \alpha}(\epsilon - \epsilon_0)} \quad \ldots\ldots\ldots\ldots [5]$$

For convenience, the following quantities are defined

$$k = \frac{A_t t\rho}{\sin \alpha} \qquad m_s' = m_s - k\epsilon_0 \qquad \nu_0 = \frac{m_p}{m_s' + m_p}$$

Introducing the expression for ν given in Equation [5] into Equation [3], the following relation is obtained

$$\frac{d \ln C_F}{d\epsilon} = \frac{\dfrac{-m_p k}{(m_s' + m_p + k\epsilon)^2}}{\left[(1 - \nu_0)\dfrac{1 + (k/m_s')\epsilon}{[1 + [k/(m_s' + m_p)]\epsilon}\right]\left\{\ln\left[\dfrac{1 + (k/m_s')\epsilon}{1 + [k/(m_s' + m_p)]\epsilon}\right]\right\}} \quad \ldots\ldots\ldots\ldots [6]$$

Now, if the quantity $\epsilon k/m_s' \ll 1$, i.e., if the weight of the nozzle exit cone is much less than the remainder of the inert weight, the following approximate expression, better suited for computation, can be obtained from Equation [6]

$$\frac{d \ln C_F}{d\epsilon} \approx -\frac{\nu_0 k}{[\ln (1 - \nu_0)]m_s'} \times \left[1 - \left(\frac{2}{m_s' + m_p} + \frac{[1 + \ln(1 - \nu_0)]\nu_0}{m_s' \ln (1 - \nu_0)}\right)k\epsilon\right] \quad \ldots\ldots [7]$$

If the function $d \ln C_F/d\epsilon$ could be represented with sufficient accuracy by a polynomial of only order two, then an explicit expression could be obtained for the optimum value of area ratio. Unfortunately, it is necessary to use a higher order polynomial to represent this function with sufficient accuracy, and the solution of Equation [7] is best found by graphical means.

The functions of C_F vs. ϵ have the ratio of specific heats, γ, of the combustion gas as a parameter. Fortunately, many rocket propellants have an effective γ ranging from 1.20 to 1.25, and using a value of $\gamma = 1.23$ will give a sufficiently accurate representation of C_F for most examples. Fig. 1 shows a curve of $d \ln C_F/d\epsilon$ vs. ϵ prepared for this value of γ.

Curves showing the right-hand side of Equation [7] are best parameterized by the value of ν_0, which is close to ν, the ratio of propellant weight to gross weight, and k/m_s', which relates nozzle exit cone weight to the weight of the rest of the inert parts of the rocket. If Equation [7] is rewritten, the utility of these parameters can be seen

$$\frac{d \ln C_F}{d\epsilon} = \frac{\nu_0}{\ln [1/(1 - \nu_0)]}\left(\frac{k}{m_s'}\right)\left\{1 - \left(\frac{k}{m_s'}\right)\times \left[2(1 - \nu_0) + \left(\nu_0 - \frac{\nu_0}{\ln [1/(1 - \nu_0)]}\right)\right]\epsilon\right\} \quad \ldots\ldots [7a]$$

Equation [1] can also be rewritten in terms of these parameters

$$\Delta V = c^* C_F \ln\left\{1 + \frac{\nu_0}{(1 - \nu_0)[1 + (k/m_s')\epsilon]}\right\} \quad \ldots\ldots [1a]$$

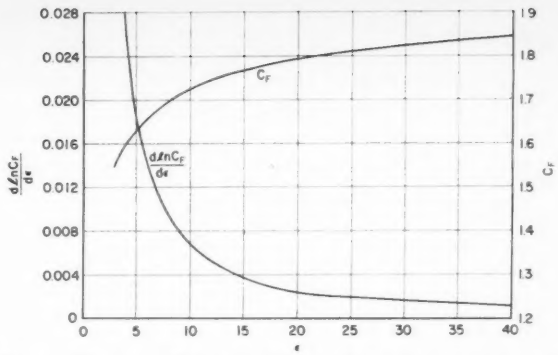

Fig. 1 Thrust coefficient C_F and $d \ln C_F/d\epsilon$ vs. area ratio ϵ for $\gamma = 1.23$ and expansion into vacuum

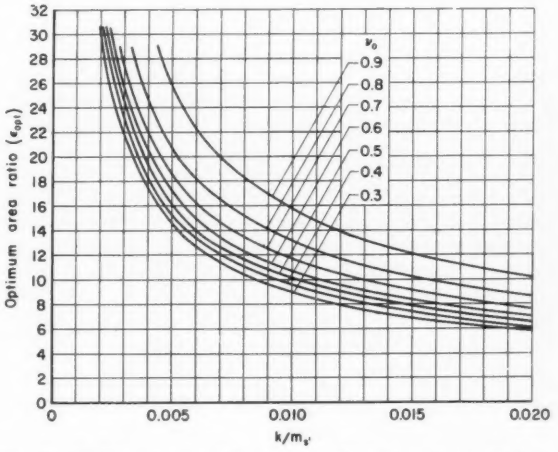

Fig. 2 Optimum area ratio ϵ_{opt} as a function of ν_0 and k/m'_s

In Fig. 2, the values of optimum area ratio ϵ_{opt}, as determined by graphical solution of Equation [7a], are given in terms of ν_0 and k/m_s'. Thus, the designer can enter this figure directly with his own design numbers to obtain the proper value of ϵ_{opt}. Substituting this value of ϵ_{opt} into Equation [1a] yields the velocity increment obtainable for optimum nozzle design.

Examples

Two numerical examples will be given to demonstrate the utility of this method, and the results obtained from the approximate treatment will be compared with the results of exact calculations.

CASE 1

$m_p = 8000$ lb
$m_s = 2500$ lb
$A_t = 30$ in.^{2}
$\rho = 0.275$ lb/in.^{3}
$t = 0.30$ in.
$\alpha = 15$ deg
$\epsilon_0 = 2$

Therefore

$$k = \frac{30 \times 0.275 \times 0.30}{0.259} = 9.56 \text{ lb}$$

$$m_s' = 2500 - 2 \times 9.56 = 2481 \text{ lb}$$

$$\nu_0 = \frac{8000}{8000 + 2481} = 0.763$$

$$\frac{k}{m_s'} = 0.00382$$

ϵ_{opt} = 24.6 from Fig. 2

Next, to afford a check with an exact calculation, values of $\Delta V/c^*$, the performance parameter, have been computed for a range of ϵ, using Equation [1a]. The results are shown in Fig. 3(a).

CASE 2

m_p = 26 lb
m_s = 9.0 lb
A_t = 1.5 in.^{2}
ρ = 0.275 lb/in.^{3}
t = 0.1 in.
α = 15 deg
ϵ_0 = 2

$$k = \frac{1.5 \times 0.1 \times 0.275}{0.259} = 0.159 \text{ lb}$$

$$m_s' = 9.00 - 0.159 \times 2 = 8.68 \text{ lb}$$

$$\frac{k}{m_s'} = 0.0184$$

$$v_0 = \frac{26.0}{26.0 + 8.7} = 0.71$$

ϵ_{opt} = 8.2 from Fig. 2

Examination of Figs. 3(a) and 3(b) reveals, as is to be expected, that the choice of area ratio has little effect on missile performance when the nozzle weight is a very small portion of the burnout weight. The importance of correct choice of area ratio increases as the nozzle weight becomes more significant. Nozzle weights, in conventional practice, seldom become large enough in relation to the rest of the inert weight to invalidate the approximation made in Equation [7]. The gains in velocity increment realized by correct choice of area ratio are usually only a few per cent, which may be important in some applications. In other cases, nozzle design may still be dictated by structural, cooling, etc., requirements.

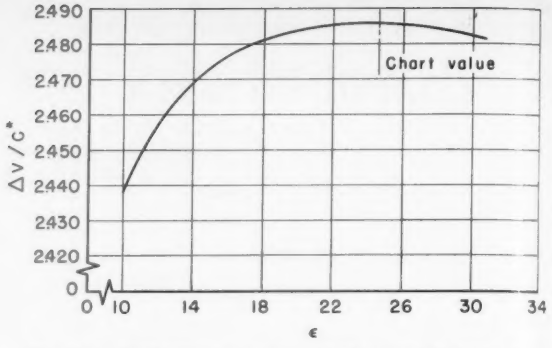

Fig. 3(a) Performance vs. area ratio for numerical case 1

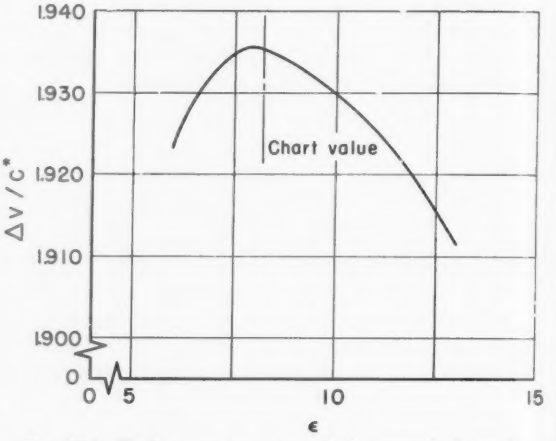

Fig. 3(b) Performance vs. area ratio for numerical case 2

An Analysis of Fuel-Oxidant Mixing in Screaming Combustors

WILLIAM R. MICKELSEN[1]

Lewis Flight Propulsion Laboratory, NACA, Cleveland, Ohio

Vapor fuel-oxidant mixing is analyzed for standing transverse acoustic fields simulating those found in screeching or screaming combustors. The additional mixing due to the acoustic field is shown to be a function of sound intensity, oscillation frequency and stream velocity. The effects of these parameters are shown graphically for a realistic range of combustor conditions. The fuel-oxidant ratio at various combustor stations is shown to have a cyclic fluctuation which is in phase with the pressure fluctuations. Possible mechanisms contributing to screech and scream are discussed.

Received May 20, 1957.

[1] Head, Special Problems Section. Mem. ARS.

Nomenclature

a	=	speed of sound, fps
C_A	=	concentration of oxidant
E	=	activation energy
$\mathfrak{F}$	=	frequency, cps
f/A	=	fuel-air, or fuel-oxidant, ratio by weight
g_c	=	gravitational conversion factor
$J_n(\ )$	=	Bessel function, first kind, order n
$\mathfrak{L}$	=	Lagrangian scale of turbulence, ft
p	=	sound pressure fluctuation, psi
p_0	=	ambient mean static pressure, psia
$\sqrt{\overline{p^2}}$	=	root mean square of sound pressure fluctuation, psi
$\sqrt{\overline{p_R^2}}$	=	root mean square of sound pressure fluctuation at pressure antinode, psi

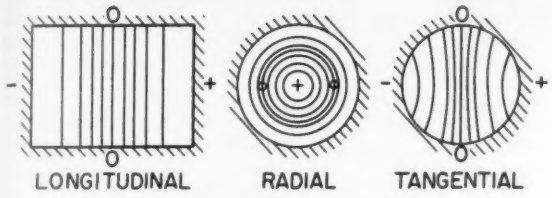

Fig. 1 Modes of oscillation in closed-end cylinders

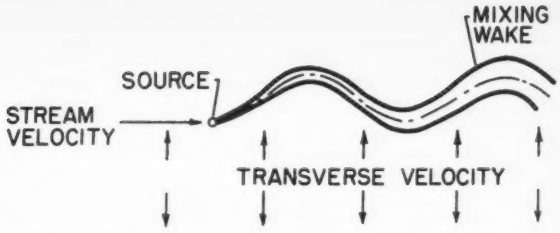

Fig. 2 Deformation of mixing wake by standing transverse acoustic wave

R = radius of cylindrical duct, ft
R_c = gas constant
$\mathcal{R}$ = Lagrangian turbulence correlation coefficient
r = radial coordinate in cylindrical coordinate system, ft
T = flame temperature
t = residence time in fluid stream, sec
U = stream velocity, fps
v = resultant particle velocity, fps
v_c = resultant particle velocity at duct axis, fps
v_r = radial particle velocity, fps
v_θ = tangential particle velocity, fps
$\sqrt{\overline{v^2}}$ = root mean square of particle velocity, fps
$\sqrt{\overline{v_T^2}}$ = intensity of turbulence, fps
w_f = fuel flow rate from point source, lb/sec
X, Y, Z = position of particular point in rectangular coordinates, ft
x = axial coordinate in cylindrical coordinate system, ft
y = lateral displacement of mixing wake center, ft
y_{max} = maximum lateral displacement of mixing wake center, ft
γ = specific heat ratio
θ = angle in cylindrical coordinates
ρ_f = density fluctuation at point source, lb/cu ft
ρ_0 = mean ambient density, lb/cu ft
τ = time scale of acoustic oscillations, sec
ω = turbulent spreading coefficient, sq ft

Introduction

THE effect of acoustic fields on vapor mixing may be of importance to the combustion process in screeching or screaming combustors. If the acoustic oscillations change the fuel-air or fuel-oxidant ratio, the combustion process will be directly affected. To illustrate the effect of acoustic oscillations, an analysis (1)[2] has been made of vapor mixing in cylindrical ducts under conditions found in screeching ramjets and afterburners and in screaming rockets.

Acoustic oscillations in cylindrical chambers have three general modes: longitudinal, radial and tangential. These modes are illustrated in Fig. 1, where pressure contours are shown at an instant in time. The pressure maximums alternate with sign in time, and higher modes can exist for each type. Oscillations in ramjet combustors, afterburners, and rockets may be any combination of these types, depending on a number of acoustic, aerodynamic and combustion factors (2–5).

The pressure fluctuations in each of the modes of oscillation give rise to acoustic particle velocities which can affect the fuel-air or fuel-oxidant mixing process in a manner somewhat similar to that of turbulent velocity fluctuations. It has been shown (6) that the action of a transverse acoustic particle velocity is to produce a sinusoidal-shaped deformation of the concentration pattern downstream from a source of heat or mass, as illustrated in Fig. 2. The analysis showed that if the deformation is sufficiently large, the concentration of heat or mass in the mixing wake will be changed. The pressure fluctuations encountered in screeching (3) and screaming (5) combustors are sufficiently large to imply particle velocities of the same order of magnitude as the stream velocity. Mixing wake deformations caused by acoustic fields of these strengths are great enough to cause a considerable change in the fuel-oxidant ratio throughout the mixing region.

[2] Numbers in parentheses indicate References at end of paper.

Properties of the Acoustic Field

Experiment has indicated that screeching and screaming combustors have acoustic fields approximated by the closed end cylinder case. If the ends are acoustically hard, and the gas is acoustically homogeneous, the transverse modes of oscillation are preserved throughout the length of the cylinder. In realistic combustors, the acoustic field may depart from the ideal, uniform mode. Data from a simulated afterburner (3) show an attenuation and phase shift of the tangential mode upstream of the flame zone. A theoretical analysis (7) of a similar combustion system has predicted an attenuation upstream, but no phase shift. The attenuation in such a case is due to the change in speed of sound between the burned and unburned gases, and to a weak closed-end condition at the combustor inlet. The present analysis will be confined to the ideal, uniform, standing, tangential mode and to pressure amplitudes in the acoustic range.

The general solution of the wave equation (8, p. 398) provides an expression for the rms pressure fluctuation at any point in the first pure standing tangential mode

$$\frac{\sqrt{\overline{p^2}}}{\sqrt{\overline{p_R^2}}\cos\theta} = 1.718\, J_1\left(1.841\,\frac{r}{R}\right) \quad [1]$$

where $\sqrt{\overline{p^2}}$ is the rms pressure fluctuation at the cylindrical coordinates (x, r, θ), $\sqrt{\overline{p_R^2}}$ is the rms pressure fluctuation at the pressure antinodes, $J_1(\ )$ is the Bessel function of the first kind and first order, and R is the chamber radius. The pressure parameter given by Equation [1] is shown in Fig. 3 as a function of the fraction of duct radius.

The particle velocity is related to the pressure fluctuation by (8, p. 295)

$$v = \frac{g}{i\rho 2\pi\mathfrak{F}}\,\mathrm{grad}(p) \quad [2]$$

where v is the particle velocity, g_c the gravitational conversion factor, ρ the fluid density, and the oscillation frequency $\mathfrak{F}$ is given by (8, p. 398)

$$\mathfrak{F} = 0.293\, a/R \quad [3]$$

where a is the speed of sound. Noting that $g/(a\rho) = a/(\gamma p_0)$, where p_0 is the mean pressure of the fluid, the particle velocity components can be derived (1) from the general solution of the wave equation

$$\frac{\gamma p_0\sqrt{\overline{v_\theta^2}}}{a\sqrt{\overline{p_R^2}}\sin\theta} = 0.934\,\frac{R}{r}\,J_1\left(1.841\,\frac{r}{R}\right) \quad [4]$$

$$\frac{\gamma p_0\sqrt{\overline{v_r^2}}}{a\sqrt{\overline{p_R^2}}\cos\theta} = 0.859\left[J_0\left(1.841\,\frac{r}{R}\right) - J_2\left(1.841\,\frac{r}{R}\right)\right] \quad [5]$$

where v_θ and v_r are the tangential and radial components, respectively, and $J_0(\ )$ and $J_2(\ )$ are Bessel functions of the first kind and zero and second orders, respectively. The particle velocity components given by Equations [4, 5] are shown in Fig. 3 as a function of the fraction of duct radius. As illustrated in Fig. 3, the resultant transverse particle velocity reduces to a simple expression at the chamber axis

$$\sqrt{\overline{v_C^2}} = 0.859 \frac{a}{\gamma} \frac{\sqrt{\overline{p_R^2}}}{p_0} \quad \ldots\ldots [6]$$

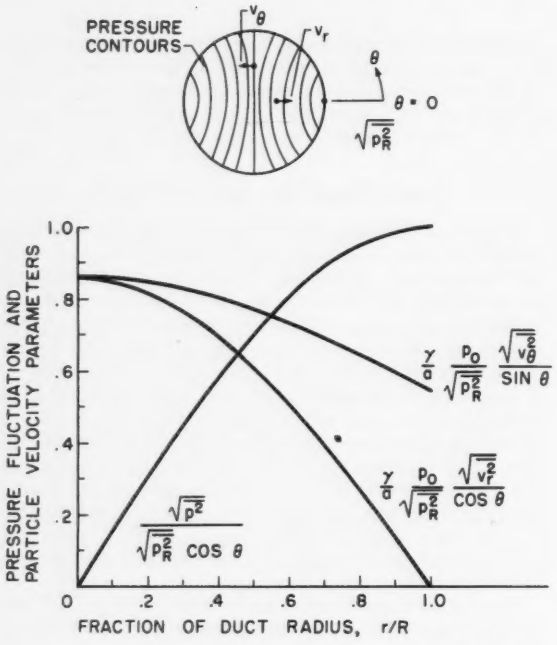

Fig. 3 Pressure fluctuation and particle velocity profiles in first pure standing tangential mode

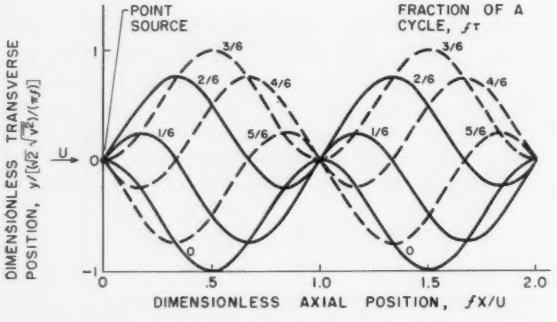

Fig. 4 Position of mixing wake center at various times through one cycle

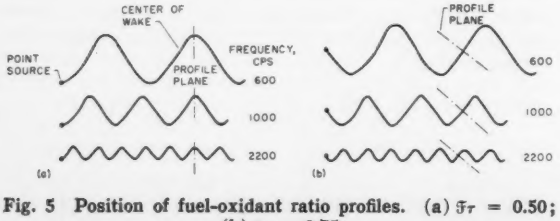

Fig. 5 Position of fuel-oxidant ratio profiles. (a) $f\tau = 0.50$; (b) $f\tau = 0.75$

Mixing Wake Displacement

A previous analysis (6) provides equations describing the motion of the mixing wake caused by a plane transverse sound wave. The analysis assumes that the rms particle velocity $\sqrt{\overline{v^2}}$ is constant in the region encompassing the deformed wake. The particle velocity profiles in Fig. 3 suggest that this condition is approximately met if the source is located on the chamber axis, and if the wake is not displaced too far from the chamber axis. For vapor injection on the chamber axis, then, the displacement of the mixing wake center is (6)

$$y = \frac{\sqrt{2}\sqrt{\overline{v^2}}}{\pi f} \sin\left(\frac{\pi f x}{U}\right) \sin\left(2\pi f \tau - \frac{\pi f x}{U}\right) \quad \ldots\ldots [7]$$

where y is the displacement of the wake center from the chamber axis at the axial station x, τ is the time scale of the particle velocity fluctuation, and U is the stream velocity. The oscillatory motion of the mixing wake is illustrated in Fig. 4, where the dimensionless displacement $y/[(\sqrt{2}\sqrt{v^2})/(\pi f)]$ is plotted against distance downstream from the injector for various times through one cycle of the oscillation. As shown in Fig. 4, the transverse motion of the mixing wake is cyclic, and produces definite nodes at whole number multiples of the dimensionless axial distance $fx/U\mathrm{T}$. he maximum displacement of the wake center occurs at the wake antinodes, and is defined by $y_{\max} = (\sqrt{2}\sqrt{\overline{v^2}})/(\pi f)$.

An estimate of fidelity to the condition of uniform particle velocity in the mixing region may be made by expressing the wake displacement in terms of pressure amplitude. This expression is obtained by substituting Equations [3, 6] into the definition of $y_{\max}$

$$\frac{y_{\max}}{R} = \frac{1.32}{\gamma} \frac{\sqrt{\overline{p_R^2}}}{p_0} \quad \ldots\ldots [8]$$

Comparison of Equation [8] with Fig. 3 shows that up to moderately high acoustic amplitudes

$$0 < \sqrt{\overline{p_R^2}}/p_0 < 0.2$$

the assumption of uniform particle velocity is fairly good for the case of vapor injection on the chamber axis.

Mixing From Source on Chamber Axis

The equation for concentration downstream from a point source emitting fuel vapor at the weight flow rate w_f into a gas stream of homogeneous turbulence (9) may be written in terms of fuel-oxidant ratio

$$\frac{\rho_0 f/A}{w_f} = \frac{1}{(4\pi)^{3/2}} \int_0^\infty \frac{1}{\omega^{3/2}} e^{-((X-Ut)^2+Y^2+Z^2)/4\omega} dt \quad \ldots\ldots [9]$$

where ρ_0 is the mean density of the gas, f/A is the fuel-oxidant (or fuel-air) ratio at the rectangular coordinates (X, Y, Z), t is the residence time, and ω is the turbulent spreading coefficient. The spreading coefficient ω is a function of the time t, the turbulence intensity $\sqrt{\overline{v_T^2}}$ and the Lagrangian correlation coefficient $\mathfrak{R}$. Assuming that

$$\mathfrak{R} = \exp\left[-(\sqrt{\overline{v_T^2}}\, t)/\mathfrak{L}\right]$$

where $\mathfrak{L}$ is the Lagrangian scale of turbulence, the equation for the turbulent spreading coefficient [9] becomes

$$\omega = \mathfrak{L}^2\left(\frac{\sqrt{\overline{v_T^2}}\, t}{\mathfrak{L}} - 1 + e^{-(\sqrt{\overline{v_T^2}}\, t)/\mathfrak{L}}\right) \quad \ldots\ldots [10]$$

The effect of the transverse particle velocity may be included in the mixing equation by accounting for the transverse displacement of the wake center (6)

$$\frac{\rho_0 f/A}{w_f} = \frac{1}{(4\pi)^{3/2}} \int_0^\infty \frac{1}{\omega^{3/2}} e^{-((X-Ut)^2+(Y-y)^2+Z^2)/4\omega}\, dt \ldots . [11]$$

where y is given by Equation [7].

To investigate the effect of oscillation amplitude and frequency, fuel-oxidant profiles were calculated from Equation [11] by numerical integration with a high speed digital computer using Simpson's rule. The profiles were calculated for a fixed axial station $X = 1.25$ ft and for two instants in time $\mathfrak{F}\tau = 0.50$ and 0.75. The turbulent stream properties were fixed at $U = 500$ fps, $\sqrt{\overline{v_T^2}}/U = 0.05$ and $\mathfrak{L} = 0.1$ ft. The profiles were calculated for a range of particle velocities and oscillation frequencies. The profile planes were positioned normal to the wake center as shown in Fig. 5. The fuel-oxidant profiles are shown in Fig. 6. As the particle velocity is increased, the peak fuel-oxidant ratio decreases in all cases shown in Fig. 6. In addition to this general decrease in fuel-oxidant ratio, a cyclic change in fuel-oxidant ratio occurs since the profiles in Fig. 6(a) will be repeated at $\mathfrak{F}\tau = 0, 1.0, 1.5, \ldots$ and those in Fig. 6(b) at $\mathfrak{F}\tau = 0.25, 1.25, 1.75, \ldots$. As shown previously (6) the fuel-oxidant ratio will be highest in portions of the wake having zero slope (dy/dx) and lowest in portions having maximum slope. This indicates that the fuel-oxidant ratios in Fig. 6(a) for $\mathfrak{F}\tau = 0.5$ will form the upper limit, and those of Fig. 6(b) will form the lower limit of the cyclic variation.

It has been shown (1) that a time and position relation exists between the fluctuations in fuel-oxidant ratio and the pressure. When the wake is at its maximum lateral displacement, the fuel-oxidant ratio at the antinodal stations is at a maximum, and the pressure is also at a maximum. This relation is expressed by an equation which defines the pressure change experienced by the wake center during its transverse motion

$$\frac{\gamma p_0 p}{\overline{p_R^2}} = -2.95 \sin\left(\frac{\pi \mathfrak{F} X}{U}\right) \sin\left(2\pi \mathfrak{F}\tau - \frac{\pi \mathfrak{F} X}{U}\right) \cos(2\pi \mathfrak{F}\tau) \ldots . [12]$$

The pressure fluctuation given by Equation [12] is compared in Fig. 7 with values of fuel-oxidant ratio obtained from Fig. 6. The comparison is made for two sets of axial stations $\mathfrak{F}X/U = 0.50, 1.50, \ldots$ and $0.75, 1.75, \ldots$. At the antinodal stations $\mathfrak{F}X/U = 0.50, 1.50, \ldots$, the pressure fluctuations are exactly in phase with the fuel-oxidant ratio fluctuations. At stations away from the antinodal, such as $\mathfrak{F}X/U = 0.75, 1.75, \ldots$, the pressure and fuel-oxidant ratio fluctuations are no longer in phase, but the magnitude of the pressure fluctuation is considerably reduced.

Fuel-oxidant ratio profiles were also calculated from Equation [11] for a range of stream velocities and particle velocities. The profiles were calculated for a fixed axial station of $X = 1.25$ ft and for two instants in time $\mathfrak{F}\tau = 0.50$ and 0.75. The turbulence properties were fixed at $\sqrt{\overline{v_T^2}}/U = 0.05$ and $\mathfrak{L} = 0.1$ ft, and the oscillation frequency was fixed at $\mathfrak{F} = 1000$ cps. The profile planes were positioned in the wake as shown in Fig. 8, and the fuel-oxidant profiles are shown in Fig. 9. The percentage reduction in peak fuel-oxidant ratio with increasing particle velocity is greatest for the lowest stream velocity shown in Fig. 9. Comparison of Figs. 6 and 9 shows that the effect of stream velocity is similar to that of oscillation frequency, but more pronounced. A cyclic variation in fuel-oxidant ratio with time is also evident in Fig. 9.

Injection Away From the Chamber Axis

In the case of vapor injection at points away from the duct axis, pressure fluctuations at the injector may cause cyclic changes in the fuel-oxidant ratio. The mixing equation may be corrected for this effect by noting that the fuel-oxidant ratio of a fluid particle leaving the vicinity of the injector is proportional to $\rho_0/(\rho_0 + \rho_i)$ where ρ_0 is the ambient time-

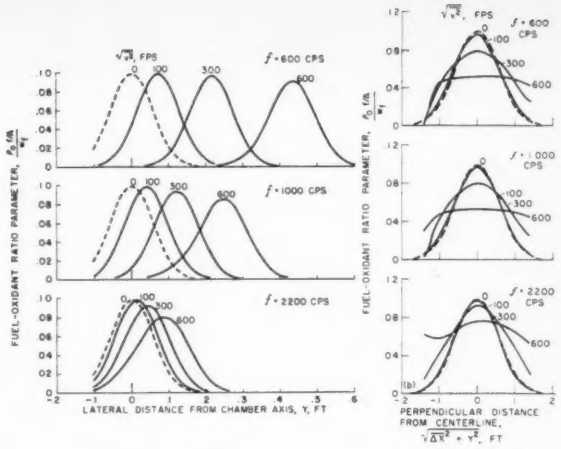

(a) $\mathfrak{F}\tau = 0.50$ (b) $\mathfrak{F}\tau = 0.75$

Fig. 6 Effect of oscillation frequency on mixing in first pure standing tangential mode. Stream velocity, 500 fps; turbulence intensity, 5 per cent; turbulence scale, 0.1 ft; axial station, 1.25 ft

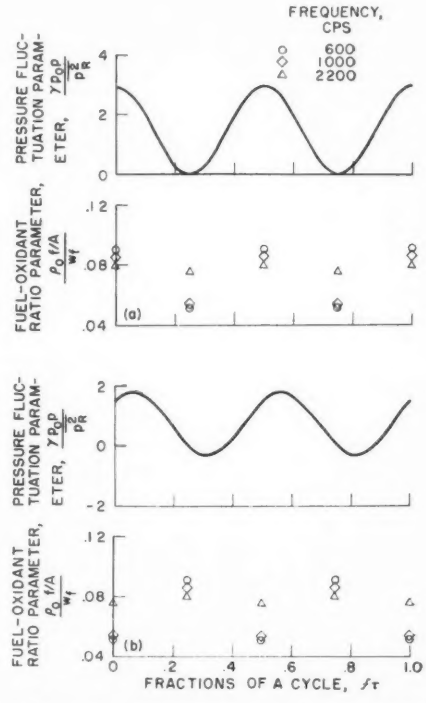

Fig. 7 Time phase relation between pressure and fuel-oxidant fluctuations on wake center during transverse motion. (a) At antinodal stations $\mathfrak{F}X/U = 0.5, 1.5, \ldots$; (b) at stations $\mathfrak{F}X/U = 0.75, 1.75, \ldots$

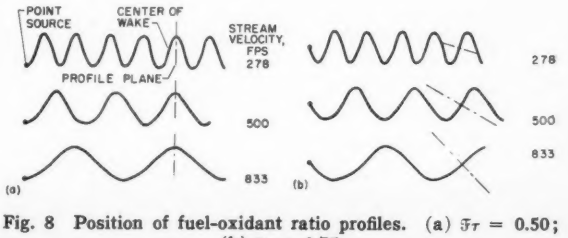

Fig. 8 Position of fuel-oxidant ratio profiles. (a) $\mathfrak{F}\tau = 0.50$; (b) $\mathfrak{F}\tau = 0.75$

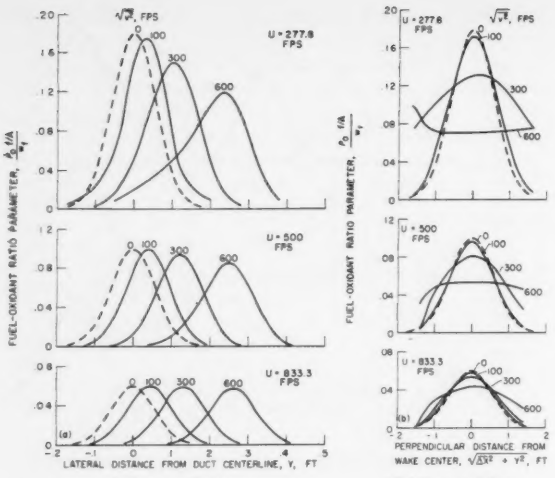

(a) $\mathfrak{F}\tau = 0.50$ (b) $\mathfrak{F}\tau = 0.75$

Fig. 9 Effect of stream velocity on mixing in first pure standing tangential mode. Oscillation frequency, 1000 cps; turbulence intensity, 5 per cent; turbulence scale, 0.1 ft; axial station, 1.25 ft

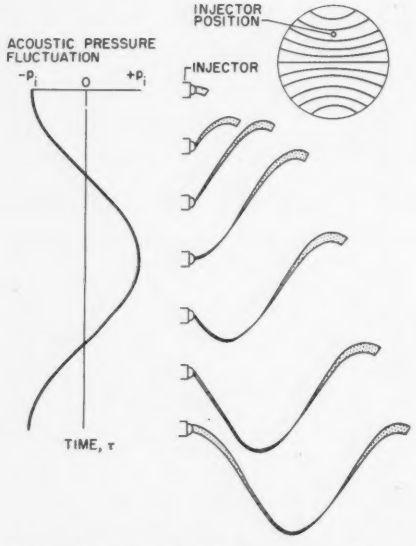

Fig. 10 Mixing in first pure standing tangential mode with injection at points not on pressure node

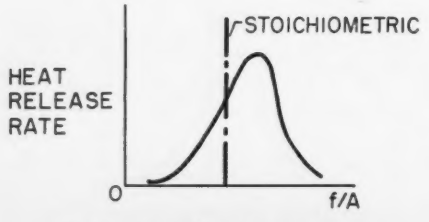

Fig. 11 Typical heat release curve

mean density, and ρ_i is the density fluctuation at the injector. This density ratio may be inserted into the mixing equation

$$\frac{\rho_0 f/A}{w_f} = \frac{1}{(4\pi)^{3/2}} \int_0^\infty \frac{1}{1 + (p_i/\gamma p_0)} \frac{1}{\omega^{3/2}} e^{-((X-Ut)^2+(Y-y)^2+Z^2)/4\omega}\, dt \quad [13]$$

where p_i is the pressure fluctuation at the injector

$$p_i = -2.43 \sqrt{\overline{p_R^2}}\, J_1\left(\frac{2\pi\mathfrak{F}r}{a}\right) \cos\theta \cos(2\pi\mathfrak{F}\tau) \quad [14]$$

With injection away from the chamber axis, the solid body motion expressed by Equation [7] no longer obtains. The pressure gradient encountered by the wake exerts an alternately compressive and expansive motion in the transverse direction. Along the line $\theta = 0$, the exact expression for particle motion is

$$\int_{y_1/R}^{y_2/R} \frac{d(y/R)}{J_0\left(1.841\,\frac{y}{R}\right) - J_2\left(1.841\,\frac{y}{R}\right)} = \frac{0.66}{\gamma} \frac{\sqrt{\overline{p_R^2}}}{p_0} \int_{\tau_1}^{\tau_2} \sin(2\pi\mathfrak{F}\tau) d\tau \quad [15]$$

where y_1 and y_2 are the particle locations at the times τ_1 and τ_2, respectively. Due to the complexity of Equations [14, 15], fuel-oxidant profiles were not calculated for the case of injection away from the chamber axis. By inspection of Equation [14], a qualitative picture of the effect of pressure fluctuation at the injector can be formed as shown in Fig. 10 where the fuel-oxidant wake is shown for successive intervals of time, along with the pressure fluctuation curve. The width of the wake represents the relative magnitude of the fuel-oxidant ratio. The fuel-oxidant ratio at the injector is high when the pressure fluctuation is negative and is low when the pressure fluctuation is positive. The figure shows that when the richest portion of the wake has reached its maximum excursion toward the chamber wall, the pressure fluctuation has reached its maximum positive value. In this way, the pressure fluctuations at the injector tend to accentuate the fuel-oxidant ratio fluctuations caused by wake deformation.

Possible Mechanisms Contributing to Combustor Oscillations

The role of pressure fluctuations in driving screech has been discussed elsewhere (3), where it is suggested that a periodic change in pressure is expected to cause an even larger periodic change in heat release rate. Consideration of the chemical reaction rate equation indicates that fuel-oxidant fluctuations could also cause fluctuations in heat release rate. For example, the second order reaction expression may be written

$$\text{reaction rate} \sim C_A^2 f/A\, e^{-E/R_c T} \quad [16]$$

where C_A is the oxidant concentration, E is the activation energy, R_c is the gas constant, and T is the flame temperature. The flame temperature is a strong function of the fuel-oxidant ratio so that the heat release has the form shown in Fig. 11.

Unpublished data taken in a typical combustor indicated that screeching occurred at over-all fuel-air equivalence ratios between 0.25 and 0.45 based on unburned inlet air. In the absence of screeching, the peaks in the fuel-air ratio profile at the flame front may be expected to be lower than stoichiometric for such lean over-all fuel-air ratios, as shown in Fig. 12(a). As pointed out previously, transverse acoustic oscillations cause a general decrease in peak fuel-air ratio, and also cause a periodic fluctuation in fuel-air ratio as illustrated in Fig. 12(b). In the sketch, the solid line represents the upper

limit of the fuel-air ratio fluctuation, and the dotted line the lower limit. Since the mean value of the peak fuel-air ratio is lower than stoichiometric, then a fluctuation toward higher fuel-air ratio will result in an increased heat release rate as shown by Fig. 11. At antinodal distances $\mathfrak{F}X/U$ downstream from the spray bar, the increase in heat release due to the fuel-air ratio rise is directly in phase with the increase in heat release due to pressure rise, so that screech might be driven to even higher amplitudes. If the mean peak fuel-air ratio were higher than stoichiometric, then a rise in fuel-air ratio would tend to decrease the heat release rate, and thus exert a suppressing effect on the screech driving mechanism. To obtain a mean peak fuel-air ratio higher than stoichiometric, the number of injection points might be reduced, with a higher fuel flow rate through each, resulting in a profile such as shown in Fig. 12(c). An alternate method could be to move the spray bar closer to the flame front as shown in Fig. 12(d).

The effect of off-center injection on the screaming mechanism is not immediately apparent. It was shown earlier that the pressure fluctuation at the off-center injector tends to accentuate the fuel-oxidant fluctuations caused by the deformation of the wake by particle velocity. Since the particle velocity encountered by the wake decreases as the point of injection is moved away from the chamber axis, the fuel-oxidant ratio fluctuations caused by wake deformation will also decrease. Conversely, as the injector is moved away from the chamber axis, the contribution to fuel-oxidant fluctuation by the pressure fluctuation at the injector should increase. In addition to these two effects on fuel-oxidant ratio, the mixing wake will encounter more severe pressure fluctuations during its transverse motion downstream from an off-center injector. Resolution of these three effects awaits further analysis or experiment.

One more possible contribution to the screech mechanism in the first pure standing tangential mode deserves mention. In the case of ramjet combustors and afterburners where injectors are positioned upstream of flameholders, the axial distance between the injector and flameholder stations may be of importance to the screech mechanism. As shown by Fig. 4 and Equation [7], the mixing wake may be periodically displaced a considerable lateral distance at antinodal axial distances from the point of injection. If the injector to flame front distance is at or near a wake antinodal distance, then the fuel-air mixture might pass alternately back and forth across a flameholder and cause significant periodic changes in heat release in the two opposing flame fronts. The cure or control of this type of screech mechanism may lie in the injector to flame front distance. By changing this distance by a fraction of the internodal distance, the time and position phase relation between the fuel-oxidant ratio fluctuations and pressure fluctuations might be altered to attain a suppressing effect on the screech driving mechanism.

Conclusions

In summary, equations have been derived for the calculation of fuel-oxidant ratio profiles downstream from injectors simulating point sources of vapor in cylindrical combustors with the first pure standing tangential mode of acoustic oscillation. From the results of this analysis, the following conclusions are drawn.

1 Acoustic oscillations of the magnitude present in screeching or screaming combustors can cause considerable transverse motion and distortion of the fuel-oxidant mixing wake.

2 In general, the peak fuel-oxidant ratio at all axial stations is lowered by the transverse acoustic oscillations.

3 At all axial stations, the peak fuel-oxidant ratio has a cyclic variation with time. The phase relation between the peak fuel-oxidant ratio and pressure fluctuations is a function of the position of the station, the stream velocity and the oscillation frequency. At the antinodal axial stations, the pressure and fuel-oxidant fluctuations are exactly in phase.

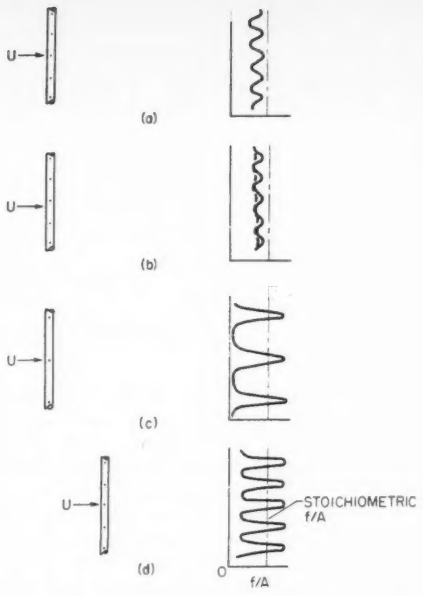

Fig. 12 Fuel-air ratio profiles in combustor

Acknowledgment

The assistance of Lois T. Dellner of the Lewis laboratory, who performed the programming and calculations with the high speed digital computer, is gratefully acknowledged.

References

1 Mickelsen, William R., "Effect of Standing Transverse Acoustic Oscillations on Fuel-Oxidant Mixing in Cylindrical Combustion Chambers," NACA TN 3983, 1957.

2 Truman, John C., and Newton, Robert T., "Why Do High-Thrust Engines Screech?" *Aviation Age*, vol. 23, no. 5, May 1955, pp. 136–143.

3 Blackshear, Perry L., Rayle, Warren D., and Tower, Leonard K., "Study of Screeching Combustion in a 6-Inch Simulated Afterburner," NACA TN 3567, 1955.

4 Berman, Kurt, and Logan, Stanley E., "Combustion Studies with a Rocket Motor Having a Full-Length Observation Window," JET PROPULSION, vol. 22, no. 2, March-April, 1952, pp. 78–85.

5 Smith, R. P., and Sprenger, D. F., "Combustion Instability in Solid-Propellant Rockets," Fourth Symposium (International) on Combustion, Williams and Wilkins, 1953, pp. 893–906.

6 Mickelsen, William R., and Baldwin, Lionel V., "Aerodynamic Mixing Downstream from Line Source of Heat in High-Intensity Sound Field," NACA TN 3760, Aug. 1956. Also, "Aerodynamic Mixing in a High-Intensity Standing-Wave Sound Field," *Journal of the Acoustical Society of America*, vol. 29, 1957, p. 46.

7 Moore, Franklin K., and Maslen, Stephen H., "Transverse Oscillations in a Cylindrical Combustion Chamber," NACA TN 3152, 1954.

8 Morse, Philip M., "Vibration and Sound," 2nd edit., McGraw-Hill, New York, 1948.

9 Mickelsen, William R., "An Experimental Comparison of the Lagrangian and Eulerian Correlation Coefficients in Homogeneous Isotropic Turbulence," NACA TN 3570, 1955.

Heat Transfer in Laminar Pipe Flow With Uniform Coolant Injection[1]

S. W. YUAN[2] and A. B. FINKELSTEIN[3]

Polytechnic Institute of Brooklyn, Brooklyn, New York

The effect of coolant injection at the wall on the temperature distribution of the laminar flow of a fluid in a porous wall pipe has been investigated. The temperature distributions in the pipe for various fluid injection rates are obtained by solving the energy equation in which the velocity distribution terms used are taken from Reference (1). The heat transfer results, expressed as a local Nusselt number, are presented in terms of the Péclet number, the dimensions of the pipe and the coolant flow rate. The relation between the wall temperature and the rate of coolant injection is also calculated. The results also show that the heat transfer coefficient at the wall decreases with an increase in the rate of coolant injection, whereas it was previously found that the friction coefficient at the wall increases with an increase of fluid injection. Thus the usual analogy between heat transfer and momentum transfer does not hold in porous wall cooling of pipe flow.

Nomenclature

x = axial distance in the main flow direction
r = radial distance normal to the main flow direction
φ = azimuthal angle in cylindrical coordinate system
D = diameter of the circular pipe
R = radius of the circular pipe
l = length of the pipe
η = r/R
ξ = x/R
u = fluid velocity in the x direction
v = fluid velocity in the r direction
U = maximum velocity in the Poiseuille flow ($v_0 = 0$)
u_m = average velocity in the Poiseuille flow ($U = 2u_m$)
v_0 = coolant injection velocity at the wall
T = fluid temperature (absolute)
q = heat flow per unit area
p = pressure
μ = dynamic viscosity
ν = kinematic viscosity
ρ = mass density of the fluid
c_p = specific heat at constant pressure
k = thermal conductivity
h = heat transfer coefficient
ϕ = dissipation function
Re = axial Reynolds number ($u_m D/\nu$)
λ = injection Reynolds number ($v_0 R/\nu$)
Pr = Prandtl number ($\mu c_p/k$)
Pe = Péclet number ($PrRe$)
Nu = local Nusselt number (hD/k)

Subscripts

0 = coolant fluid
1 = refers to plane $x = 0$
w = wall of pipe
M = mean value

Received Dec. 24, 1956.

[1] This research was conducted under the auspices of Project SQUID, sponsored by the Office of Naval Research, Department of the Navy.

[2] Professor of Fluid Mechanics, University of Laval, Quebec, P. Q., Canada.

[3] School of Engineering, Science Department, Pratt Institute, Brooklyn, N. Y.

Introduction

THE transpiration cooling problem, i.e., to cool the combustion chamber liners by means of injecting coolant through a porous wall, has been solved to a great extent in the case of a laminar flow over a porous plate (2).[4] It has been assumed that the results obtained from the porous plate solution would yield some indication of the actual case in the combustion chambers. On the other hand, however, the problem of the nonisothermal flow through a porous-wall pipe with injection has not yet been investigated. The purpose of this work was to obtain basic characteristics of this type of flow which in turn would provide guidance for the investigation of transpiration cooling in a turbulent pipe flow, and to verify whether the above assumption made for the plate investigation is valid.

The problem of heat transfer in a steady laminar flow in a circular pipe without injection has been studied by Graetz (3) and Nusselt (4) since the latter part of the last century. In these studies it was assumed that the wall temperature is constant and changes discontinuously at $x = 0$ (Fig. 1), that the physical properties of the fluid are independent of temperature, and that the Poiseuille velocity distribution is maintained throughout the motion. But up to the present, because of the complexity of the problem, there has not been much further improvement in the solution beyond that of an empirical nature.

In the present investigation an exact solution of the energy equation in cylindrical coordinates was obtained in which the velocity component terms used were taken from (1). The solution gives the temperature distribution as functions of coordinate axes, Péclet number, the diameter of the pipe and the rate of coolant injection.

The assumptions made in the present study were:

1 The fluid is incompressible and the free convection, radiation and dissipation are neglected.

2 The molecular heat conduction in the axial direction can be neglected in comparison with that in the radial direction.

3 The coolant flowing through the porous wall is uniform throughout.

4 The wall temperature is constant and changes discontinuously at $x = 0$.

Fundamental Equations

If a curvilinear coordinate system is introduced with the origin at the center of the cross section of a circular pipe where x is taken in the direction of the flow, r in the radial direction and φ the azimuthal angle, then with axial symmetry of flow the Navier-Stokes equations become

$$u\frac{\partial u}{\partial x} + v\frac{\partial u}{\partial r} = -\frac{1}{\rho}\frac{\partial p}{\partial x} + \nu\left[\frac{\partial^2 u}{\partial r^2} + \frac{1}{r}\frac{\partial u}{\partial r} + \frac{\partial^2 u}{\partial x^2}\right] \quad \ldots [1]$$

$$u\frac{\partial v}{\partial x} + v\frac{\partial v}{\partial r} = -\frac{1}{\rho}\frac{\partial p}{\partial r} + \nu\left[\frac{\partial^2 v}{\partial x^2} + \frac{\partial^2 v}{\partial r^2} + \frac{1}{r}\frac{\partial v}{\partial r} - \frac{v}{r^2}\right] \quad \ldots [2]$$

[4] Numbers in parentheses indicate References at end of paper.

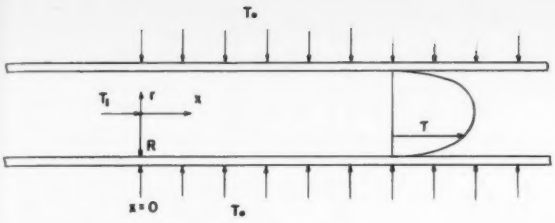

Fig. 1 Temperature distribution along a porous circular pipe

The continuity equation

$$\frac{\partial(ru)}{\partial x} + \frac{\partial(rv)}{\partial r} = 0 \quad \ldots\ldots [3]$$

The energy equation

$$\rho c_p \left(v\frac{\partial T}{\partial r} + u\frac{\partial T}{\partial x}\right) = -u\frac{\partial p}{\partial x} + k\left[\frac{1}{r}\frac{\partial}{\partial r}\left(r\frac{\partial T}{\partial r}\right) + \frac{\partial^2 T}{\partial x^2}\right] + \phi \quad \ldots [4]$$

The velocity distributions of the fluid flow in a porous-wall circular pipe through which uniform injection is applied were obtained by the solution of Equations [1, 2, 3] with appropriate boundary conditions. These solutions were given in (1) and will be used in the present investigation.

For an incompressible fluid it can be shown that the terms in Equation [4] due to the pressure gradient and the dissipation can be neglected, and, furthermore, it is assumed that $\partial^2 T/\partial x^2$ may be neglected in comparison with

$$\frac{1}{r}\frac{\partial}{\partial r}\left(r\frac{\partial T}{\partial r}\right)$$

Hence Equation [4] can be simplified in the nondimensional form

$$\frac{v}{U}\frac{\partial\theta}{\partial\eta} + \frac{u}{U}\frac{\partial\theta}{\partial\xi} = \frac{1}{PrRe}\left[\frac{1}{\eta}\frac{\partial}{\partial\eta}\left(\eta\frac{\partial\theta}{\partial\eta}\right)\right] \quad \ldots\ldots [5]$$

The boundary conditions are

$$\theta = 0 \qquad \text{for } \xi > 0,\ \eta = 1 \quad \ldots\ldots [6]$$

$$\theta = 1 \qquad \text{for } \xi = 0,\ \eta < 1 \quad \ldots\ldots [7]$$

From (1), the nondimensional axial and radial velocity components are given respectively for $0 \leq \lambda \leq 1$ (neglecting terms of order λ^2 with respect to λ) as follows

$$\frac{u}{U} = \left[\frac{1}{1-(\lambda/18)} + 4\frac{\lambda}{Re}\xi\right]F(\eta) + \ldots\ldots [8]$$

and

$$\frac{v}{U} = -2\frac{\lambda}{Re}\left[\eta - \frac{1}{2}\eta^3\right] + \ldots\ldots [9]$$

where

$$F(\eta) = (1-\eta^2) + \frac{\lambda}{36}(-2 + 9\eta^2 - 9\eta^4 + 2\eta^6) + \ldots$$

With these values for the velocity components, Equation [5] becomes

$$\left[\frac{1}{1-(\lambda/18)} + 4\frac{\lambda}{Re}\xi\right]\frac{\partial\theta}{\partial\xi} = 2\frac{\lambda}{Re}\frac{1}{F(\eta)}\left[\eta - \frac{\eta^3}{2}\right]\frac{\partial\theta}{\partial\eta} + \frac{1}{PrRe}\frac{1}{F(\eta)}\left[\frac{1}{\eta}\frac{\partial}{\partial\eta}\left(\eta\frac{\partial\theta}{\partial\eta}\right)\right] \quad \ldots [10]$$

Method of Solution

The energy equation written in the form of Equation [10], again neglecting terms of order λ^2 after multiplying both sides by $1-(\lambda/18)$, yields immediately a solution in the form of an infinite series

$$\theta = \sum_{j=1}^{\infty} A_j\left(1 + 4\frac{\lambda}{Re}\xi\right)^{-C_j^2/4Pr\lambda} M_j(\eta, C_j) \quad \ldots\ldots [11]$$

where the $M_j(\eta, C_j)$ are the solutions of

$$\frac{d^2M}{d\eta^2} + \left[\frac{1}{\eta} + 2Pr\lambda\left(\eta - \frac{\eta^3}{2}\right)\right]\frac{dM}{d\eta} + C^2\left[(1-\eta^2) + \frac{\lambda}{36}(7\eta^2 - 9\eta^4 + 2\eta^6)\right]M = 0 \quad \ldots [12]$$

and the C_j are the eigenvalues of Equation [12] which correspond to the boundary condition $(\theta)_{\eta=1} = 0$. The series solution of Equation [12] corresponding to the eigenvalue C_j, which is free from singularities at $\eta = 0$ is

$$M_j = 1 - \frac{C_j^2}{4}\eta^2 + \frac{1}{16}\left[\frac{C_j^4}{4} + C_j^2\left(Pr\lambda - \frac{7}{36}\lambda + 1\right)\right]\eta^4 + \ldots [13]$$

Multiplying both sides of Equation [12] by the appropriate factor, we can write it as the Sturm-Liouville equation

$$\frac{d}{d\eta}[m(\eta)M_j'] + C_j^2 p(\eta)M_j = 0 \quad \ldots\ldots [14]$$

where

$$m(\eta) = \eta e^{Pr\lambda(\eta^2 - (\eta^4/4))}$$

$$p(\eta) = m(\eta)\left[(1-\eta^2) + \frac{\lambda}{36}(7\eta^2 - 9\eta^4 + 2\eta^6)\right]$$

Hence $M_i(\eta, C_i)$ and $M_j(\eta, C_j)$ for $i \neq j$ are orthogonal functions with respect to the weight function $p(\eta)$; i.e.

$$\int_0^1 p(\eta)M_iM_j d\eta = 0 \qquad \text{for } i \neq j \quad \ldots\ldots [15]$$

The coefficients of the series expansion [11], the A_j, are determined from the boundary condition [7] applied to Equation [11], which is

$$\sum_{j=1}^{\infty} A_jM_j(\eta, C_j) = 1 \quad \ldots\ldots [16]$$

Then multiplying both sides of Equation [16] by $p(\eta)\cdot M_j(\eta, C_j)$ and integrating from 0 to 1

$$A_j = \frac{\int_0^1 p(\eta)M_j(\eta, C_j)d\eta}{\int_0^1 p(\eta)M_j^2(\eta, C_j)d\eta} \quad \ldots\ldots [17]$$

From the differential Equation [14], it can be seen that

$$\int_0^1 p(\eta)M_j(\eta, C_j)d\eta = -\frac{1}{C_j^2}e^{(3/4)Pr\lambda}\left(\frac{dM_j}{d\eta}\right)_{\eta=1} \quad \ldots [18]$$

and

$$\int_0^1 p(\eta)M_j^2(\eta, C_j)d\eta = \frac{1}{2C_j}e^{(3/4)Pr\lambda}\left(\frac{dM_j}{d\eta}\right)_{\eta=1}\left(\frac{\partial M}{\partial C}\right)_{C=C_j,\ \eta=1} \quad \ldots [19]$$

Thus

$$A_j = -\frac{2}{C_j(\partial M/\partial C)_{C=C_j,\ \eta=1}} \quad \ldots\ldots [20]$$

The results of the calculations for the C_j and A_j are given in Table 1 for different values of λ.

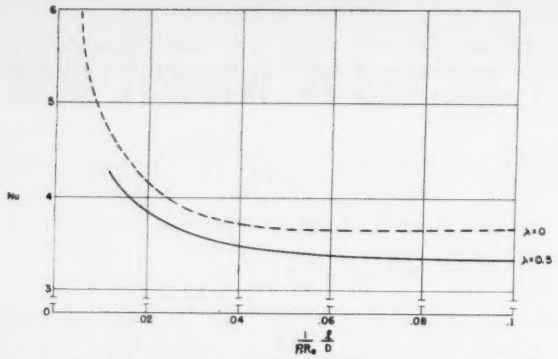

Fig. 2 Local heat transfer coefficient along the length of a pipe

Application of the Solution

The heat transfer coefficient for the flow in a pipe is usually calculated with the difference between the mean temperature of the fluid and the wall temperture. The mean temperature over the cross section considered, weighted with respect to the axial velocity, frequently referred to as the "mixed-mean" fluid temperature, may be defined by

$$\theta_M = \frac{T_M - T_w}{T_1 - T_w} = \frac{\int_0^R \theta u r dr}{\int_0^R u r dr} \quad \ldots\ldots\ldots\ldots [21]$$

The heat transfer coefficient h is then defined by

$$q = h(T_M - T_w) \quad \ldots\ldots\ldots\ldots [22]$$

where the heat flow per unit area at the wall is

$$q = -k\left(\frac{\partial T}{\partial r}\right)_{r=R} = -\frac{k}{R}(T_1 - T_w)\left(\frac{\partial \theta}{\partial \eta}\right)_{\eta=1} \quad \ldots [23]$$

In nondimensional form, the heat transfer coefficient, or local Nusselt number Nu is

$$N_u = \frac{hD}{k} = -\frac{2}{\theta_M}\left(\frac{\partial \theta}{\partial \eta}\right)_{\eta=1}$$
$$= -\frac{2}{\theta_M}\left\{A_1\left[1 + 8Pr\lambda\left(\frac{1}{PrRe}\frac{x}{D}\right)\right]^{-\frac{C_1^2}{4Pr\lambda}} M_1'(1) + \ldots + A_2\left[1 + 8Pr\lambda\left(\frac{1}{PrRe}\frac{x}{D}\right)\right]^{-\frac{C_2^2}{4Pr\lambda}} M_2'(1) + \ldots\right\} \quad \ldots\ldots [24]$$

The temperature distribution given in Equation [11] may be used to determine the amount of coolant required to cool the wall to a predesignated temperature. From the condition of heat balance at the wall, one obtains

$$\int_0^l k\left(\frac{\partial T}{\partial r}\right)_{r=R} dx = -\rho v_0 c_p (T_w - T_0) l \quad \ldots\ldots [25]$$

Using Equations [23, 11] in conjunction with [25], one obtains the temperature difference ratio as follows

$$\frac{T_1 - T_w}{T_w - T_0} = 4Pr\lambda\left(\frac{v_0 l}{u_m D}\right)\left[\frac{A_1 M_1'(1)}{1 - \frac{C_1^2}{4Pr\lambda}}\left\{1 - \left(1 + 4\frac{v_0}{u_m}\frac{l}{D}\right)^{1 - \frac{C_1^2}{4Pr\lambda}}\right\} + \frac{A_2 M_2'(1)}{1 - \frac{C_2^2}{4Pr\lambda}}\left\{1 - \left(1 + 4\frac{v_0}{u_m}\frac{l}{D}\right)^{1 - \frac{C_2^2}{4Pr\lambda}}\right\}\right]^{-1} \quad \ldots [26]$$

where

$$M_j'(1) = \left[\frac{\partial M_j(\eta)}{\partial \eta}\right]_{\eta=1}$$

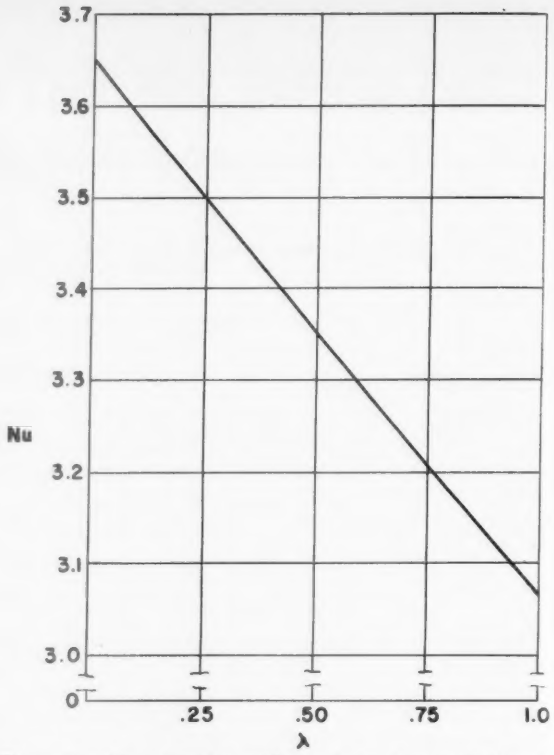

Fig. 3 Local heat transfer coefficient for various rates of coolant injection; $(1/PrRe)\ (l/D) = 0.075$

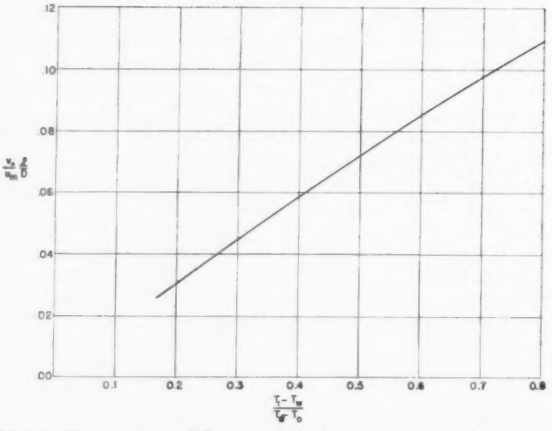

Fig. 4 Temperature difference ratio for various coolant parameters; $(1/PrRe)\ (l/D) = 0.075$

Table 1. Eigenvalues C_j and coefficients A_j for various injection Reynolds numbers λ

λ	C_1	C_2	A_1	A_2
0	2.705	6.66	1.477	−0.810
0.25	2.765	6.67	1.507	−0.861
0.5	2.825	6.67	1.540	−0.920
0.9	2.922	6.67	1.595	−1.020

Discussion

In Fig. 2 the local Nusselt number along the tube length was shown for two cases of coolant Reynolds number λ (see (5) for $\lambda = 0$). The Nusselt number, in both cases, starts with an infinitely large value at the beginning of the heated tube and decreases in flow direction to a constant value asymptotically when $(1/PrRe)(l/D)$ approaches infinity; however, this constant value is approximately reached when $(1/PrRe)\cdot(l/D) = 0.06$.

It can be seen in Fig. 3 that the Nusselt number decreases almost linearly with an increase of the coolant Reynolds number. This is due to the fact that the range of coolant Reynolds numbers considered in the present investigation is rather small ($\lambda \leq 1$). As the coolant Reynolds number increases further ($\lambda > 1$) the Nusselt number then decreases more gradually. This phenomenon was also obtained in the case of nonisothermal flow over a plate with coolant injection.

The ratio of temperature difference, $(T_1 - T_w)/(T_w - T_0)$, was plotted against the coolant flow ratio $v_0\, l/u_m\, D$ in Fig. 4. For a predesignated wall temperature, the amount of coolant required per unit time can be readily determined provided the entrance temperature T_1 and the coolant temperature T_0 are known.

The results obtained from the studies of nonisothermal laminar flow over a plate with coolant injection (2) has shown that the friction coefficient at the wall decreases with the increase of coolant injection. It has also indicated that the heat transfer coefficient decreases with the increase of coolant injection.

Thus, there is a definite direct relationship between the friction coefficient and the heat transfer coefficient. On the other hand the results obtained in (1) indicate that in a pipe flow the effect of fluid injection at the wall is to accelerate the main stream velocity. Hence the velocity gradient at the wall, which determines the wall friction, increases.

This phenomenon thus indicates that the analog between the heat transfer and momentum transfer does not exist in porous wall cooling of pipe flow. In view of the results obtained in the present investigation it is doubtful that the results obtained from the porous plate solution would yield the same trend of the actual case in the combustion chambers.

References

1 Yuan, S. W., and Finkelstein, A. B., "Laminar Pipe Flow with Injection and Suction Through Porous Wall," *Trans. ASME*, vol. 78, May 1956, pp. 719–724.

2 Yuan, S. W., "Cooling by Protective Fluid Films, High Speed Aerodynamics and Jet Propulsion," vol. V, Sect. G, Princeton University Press, 1957.

3 Graetz, L., "Ueber di Wärmeleitungsfahigkeit von Flüssigkeiten," *Ann. der Physik und Chemie*, vol. 18, 1883, pp. 79–94; vol. 25, 1885, pp. 337–357.

4 Nusselt, W., "Die Abhängigkert der Warmeübergangszahl von der Rohrlänge," *Zeitschr. des Vereines deutscher Ingenieure*, vol. 54, 1910, pp. 1154–1158.

5 Goldstein, S., "Modern Developments in Fluid Dynamics," vol. II, Oxford University Press, London, 1938, pp. 661–622.

Influence of Pressure on the Combustion of Liquid Spheres[1]

GEORGE A. AGOSTON[2] BERNARD J. WOOD[3] and HENRY WISE[4]

Stanford Research Institute, Menlo Park, Calif.

An experimental study was made of the influence of pressure on the steady-state mass burning rates of liquid fuels coating the surface of porous Alundum spheres of various diameters. Observations were made on the combustion of a series of liquid organic hydroxy compounds and several heavy hydrocarbons at atmospheric and subatmospheric pressures. These data in addition to flame distance measurements were successfully correlated revealing quantitatively the influence of free convection. At subatmospheric pressures the change in burning rate is so modest that for practical purposes the burning rate of hexadecane drops (for example) less than 1000 μ in diam may be considered independent of pressure under free convection conditions.

Presented at the ARS Semi-Annual Meeting, San Francisco, Calif., June 10–13, 1957.

[1] This paper presents results obtained in research sponsored by the National Advisory Committee for Aeronautics.

[2] Senior Chemical Engineer, Physics Department.

[3] Chemist, Chemical Physics Department.

[4] Manager, Chemical Dynamics Section, Chemical Physics Department.

Nomenclature

B = transfer number $B = \dfrac{q}{L}\dfrac{Y_a}{i} - \dfrac{C_e(T_s - T_a)}{L}$

C_e = specific heat (constant pressure) of air at temperature T_e, cal/(g)(° C)

C_L = specific heat (constant pressure) of liquid at mean temperature between initial liquid temperature and T_s, cal/(g)(° C)

D = drop diameter, cm

D_c = flame diameter based on flame radius at forward stagnation point, cm

D_{co} = flame diameter (spherical flame) with conductive heat transfer in absence of convection, cm

g = gravitation constant, cm/sec^2

Gr = Grashof number $= \dfrac{gD^3\rho^2 d}{\mu_d{}^2}\dfrac{(T_d - T)_b}{T_b} = \Omega D^3$

i = stoichiometric oxygen-fuel ratio g/g

L = heat of vaporization (sensible plus latent heat), cal/g; $L = L_s + C_L(T_s - T_a)$

L_s = heat of vaporization at T_s, cal/g

m = mass burning rate with natural convection, g/sec

m_0 = theoretical mass burning rate with conductive heat transfer in the absence of convection, g/sec

Table 1 Steady-state mass burning rate as a function of pressure and diameter of porous sphere; oxidizer = air at 20 C

Fuel	Sphere Diameter, cm	Pressure P, mm Hg	Burning Rate m x 10^3, g/sec	m/D, (g/sec cm) x 10^3
Hexadecane	0.440	47	2.91	6.61
		64	2.91	6.61
		141	2.75	6.25
		250	2.72	6.18
		450	2.76	6.28
		550	3.06	6.96
		650	3.10	7.05
		760	3.41	7.75
	0.940	18	5.81	6.18
		28	5.43	5.78
		58	5.43	5.78
		101	5.43	5.78
		187	6.28	6.68
		273	6.82	7.25
		538	7.72	8.21
		760	9.0	9.56
	1.208	17	6.86	5.69
		26	6.86	5.69
		30	6.52	5.40
		62	6.67	5.53
		62	6.87	5.69
		103	7.56	6.26
		220	8.80	7.29
		411	10.75	8.9
		604	11.9	9.85
		604	11.9	9.85
		760	12.7	10.5
Xylene	1.208	100	16.1	13.3
		181	15.1	12.5
		400	16.1	13.3
		431	20.4	16.9
		760	23.3	19.5
		760	23.5	19.3
2, 2'-Oxydiethanol	0.312	760	2.46	7.89
	0.440	760	3.58	8.14
	0.638	730	5.38	8.43
	0.940	15	5.82	6.20
		27	6.05	6.44
		27	5.82	6.20
		40	5.55	5.91
		40	6.55	6.96
		40	6.33	6.74
		40	5.55	5.91
		50	5.70	6.06
		53	5.26	5.60
		53	5.55	5.91
		71	5.55	5.91
		71	5.82	6.20
		81	6.05	6.44
		101	6.38	6.78
		101	6.34	6.75
		162	6.77	7.20
		176	6.73	7.17
		302	7.34	7.80
		485	8.40	8.94
		667	9.13	9.71
		667	9.13	9.71
		722	9.40	10.00
		722	9.07	9.65
		724	9.13	9.71
		726	9.40	10.00
	1.208	13	6.85	5.67
		15	6.95	5.83
		15	7.05	5.75
		17	7.61	6.13
2, 2'-Oxydiethanol	1.208	17	7.40	6.30
		27	7.05	6.06
		27	7.34	5.83
		36	7.34	6.08
		64	8.00	6.62
		85	8.40	6.95
		105	8.62	7.14
		105	8.62	7.14
		155	9.15	7.58
		265	10.40	8.6
		423	11.75	9.71
		596	12.50	10.34
		722	12.50	10.34
	1.590	760	20.4	12.83
	1.906	760	26.6	13.96

Pr = Prandtl number = $\frac{C_e \mu_e}{\lambda_e}$

q = heat of combustion (fuel vapor to vapor products), cal/g

T_a = temperature of ambient air, ° K

T_b = mean temperature, ° K; $T_b = \frac{T_s + T_a}{2}$

T_c = adiabatic flame temperature, ° K

T_d = log mean temperature, ° K; $T_d = \frac{T_c - T_b}{2.3 \log (T_c/T_b)}$

T_e = log mean temperature, ° K; $T_e = \frac{T_c - T_a}{2.3 \log (T_c/T_a)}$

T_s = temperature at liquid surface, ° K

Y_a = weight fraction of oxygen in ambient gas, g/g

λ_d = thermal conductivity of air at temperature T_d, cal/(sec)(cm)(° C)

λ_e = thermal conductivity of air at temperature T_e, cal/(sec)(cm)(° C)

μ_d = viscosity of air at temperature T_d, g/(sec)(cm)

μ_e = viscosity of air at temperature T_e, g(/sec)(cm)

ρ_d = density of air at temperature T_d, g/cc

Ω = diameter-free portion of Grashof number, cm^{-3}

Introduction

COMBUSTION in gas turbines at high altitudes is of great concern in aircraft operation. One factor which has been considered to be of possible significance in combustor performance is the influence of pressure on the burning of fuel sprays. Studies of the combustion of individual fuel drops at pressures above atmospheric have indicated that the mass burning rate increases with pressure raised to a power between 0.2 and 0.5 (1, 2).[5] This pressure dependency suggests that natural convection plays a measurable role in the heterogeneous combustion process (3, 4). An object of the present investigation was to provide means for evaluating the mass burning rates of individual drops of various diameters at pressures less than 1 atm.

[5] Numbers in parentheses indicate References at end of paper.

Apparatus

The use of wetted porous spheres in steady-state heterogeneous combustion studies has previously been described (4, 5). In this investigation this method was adapted to studies at subatmospheric pressures. A diagrammatic representation of the equipment is given in Fig. 1. Fuel is fed to the center of the porous Alundum[6] sphere and uniformly wets the surface. A flame is established by ignition of the fuel with an electric spark. The rate of fuel delivery to the porous sphere is then manually adjusted to the steady-state burning rate.

The porous sphere is situated inside a glass cylinder, within which the pressure may be regulated by adjusting the intake and exhaust valves. An air intake of the order of 6000 cm^3/min (S.T.P.) is required to maintain a continually fresh supply of oxidizer to the region of combustion; with this air flow, a high capacity Kinney Vacuum Pump permits the attainment of absolute pressures of the order of 20 mm Hg within the duct. In all the experiments, air velocities were sufficiently low so that forced-convection effects could be neglected (5).

The influence of oxygen concentration on combustion at atmospheric pressure was investigated in the same apparatus by enriching the air with oxygen before admittance to the glass cylinder. Burning rates in air at atmospheric pressure were obtained with the spheres removed from the cylinder and exposed to room air.

[6] The Alundum spheres (catalyst supports) were supplied by the Norton Company, Worcester 6, Mass.

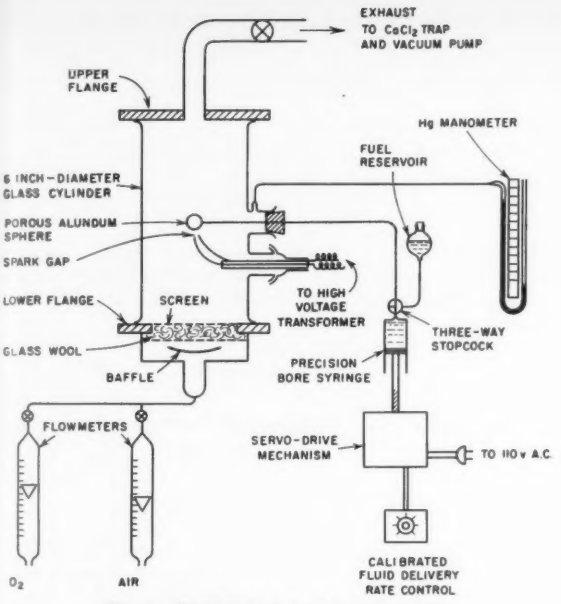

Fig. 1 Steady-state burning apparatus

Results

For several different sphere sizes, measurements were made of the burning rates of 2,2′-oxydiethanol (diethylene glycol), hexadecane (cetane), and xylene in air at subatmospheric pressures. The data obtained are presented in Table 1. Initially the burning rates diminish progressively as the pressure is decreased, but there is some indication of an increase in the burning rates with further reduction in pressure. Such a trend is to be expected because of the variation of latent heat of vaporization with pressure (see next section).

Lowering the pressure causes changes in the flame size and geometry (Figs. 2, 3). The distance of the combustion zone from the drop surface increases with decreasing pressure and the flame envelope approaches a spherical shape at very low pressures. Also, the thickness of the luminous region appears to increase. The distance from the surface of the sphere to the outer surface of the visible flame at the forward stagnation point (i.e., in this case the bottom-most point) was determined from photographs of a number of flames, and the results obtained are presented in Table 2. For comparison purposes flame distance measurements were also obtained from motion pictures of burning fuel drops suspended from silica fibers in air at atmospheric pressure, Table 2.

The mass burning rates of a number of fuels in air at atmospheric pressure were obtained for a series of sphere sizes, Table 3. These data are useful in interpreting the influence of natural convection (see next section). The typical trend of the data is illustrated in Fig. 4, where the burning rate of ethanol (95.5 per cent) is displayed as a function of sphere diameter. Table 3 also includes burning rate data at 1 atm obtained for ethyl alcohol burning in air enriched with oxygen.

Discussion

Similarity considerations in heat transfer problems involving natural and forced convection have led to dimensionless groups which enable the correlation of data obtained under varied conditions. This procedure has been applied to evaporative processes under forced and natural convection conditions by Frössling (6), Ranz and Marshall (7), and others. The combustion of liquid spheres under forced convection conditions has similarly been treated analytically as a heat-transfer controlled process (3). Experimental work has yielded the

Table 2 Flame distance at forward stagnation point

Fuel	Diameter, D_s, cm	Pressure, P, mm Hg	Flame Distance, $(D_c-D)/2$, cm	Flame Diameter Exptl., D_c, cm	Flame Diameter Theor., D_{co}, cm	Gr
Porous Spheres						
2,2′-Oxydiethanol	0.940	15	1.44	3.81	10.5	0.40
		15	1.38	3.70	10.5	0.40
		27	0.992	2.93	10.25	1.24
		90	0.663	2.27	10.0	4.14
		81	0.495	1.93	9.8	10.15
		162	0.386	1.71	9.5	35.0
		302	0.330	1.60	9.21	124.0
		726	0.274	1.49	8.75	688.0
	1.208	15	1.54	4.29	13.3	0.858
		15	1.48	4.16	13.3	0.858
		27	1.045	3.28	13.1	2.64
		64	0.715	2.64	12.65	13.6
		64	0.658	2.51	12.65	13.6
		155	0.495	2.72	12.15	75.7
		423	0.440	2.005	11.60	529.0
		423	0.330	1.87	11.60	529.0
		596	0.384	1.97	11.43	995.0
		722	0.220	1.64	11.30	1438.0
Hexadecane	0.940	18	1.66	4.26	24.7	0.51
		28	1.10	3.14	24.15	1.19
		28	0.99	2.92	24.15	1.19
		58	0.772	2.48	23.3	4.86

Fuel	Diameter, D_s, cm	Pressure, P, mm Hg	Flame Distance, $(D_c-D)/2$, cm	Flame Diameter Exptl., D_c, cm	Flame Diameter Theor., D_{co}, cm	Gr
Hexadecane	0.940	101	0.551	2.05	22.55	14.2
		187	0.440	1.815	21.6	46.3
		273	0.330	1.60	21.05	98.6
		273	0.274	1.485	21.05	98.6
		538	0.330	1.60	20.0	356.0
	1.208	17	1.73	4.65	31.9	0.956
		30	1.29	3.78	30.9	2.90
		33	1.20	3.61	30.8	3.53
		33	1.21	3.63	30.8	3.53
		33	1.27	3.75	30.8	3.53
		33	1.13	3.47	30.8	3.53
		33	1.16	3.53	30.8	3.53
		62	0.868	2.90	29.9	11.6
		62	0.824	2.85	29.9	11.6
		103	0.658	2.53	28.9	31.6
		220	0.467	2.14	27.8	136.0
		411	0.302	1.815	26.4	455.0
		604	0.274	1.755	25.5	958.0
		604	0.274	1.755	25.5	958.0
Xylene	1.208	122	0.490	2.19	32.8	63.4
		181	0.431	2.07	32.2	135.0
		431	0.346	1.71	31.2	707.0
		760	0.287	1.78	30.4	2060.0
Heptane	1.208	760	0.195	1.60	25.8	2380.0

Fuel	Diameter, D_s, cm	Pressure, P, mm Hg	Flame Distance, $(D_c-D)/2$, cm	Flame Diameter Exptl., D_c, cm	Flame Diameter Theor., D_{co}, cm	Gr
Suspended Drops						
Ethanol (95.5%)	0.12	760	0.0707	0.26	2.50	2.55
	0.092		0.0719	0.25	1.92	1.15
	0.092		0.0779	0.25	1.92	1.15
2,2′-Oxydiethanol	0.106	760	0.0707	0.25	0.991	1.055
	0.0636		0.0637	0.19	0.595	0.228
Pentane	0.12	760	0.0920	0.30	4.04	2.80
	0.0708		0.0779	0.23	2.39	0.575
Hexane	0.113	760	0.0920	0.30	3.53	1.92
	0.0708		0.0920	0.26	2.21	0.473
Heptane	0.12	760	0.0779	0.28	3.56	2.32
	0.092		0.0920	0.28	2.73	1.05
Hexadecane	0.106	760	0.0779	0.26	2.18	0.956
	0.092		0.0849	0.26	1.90	0.625

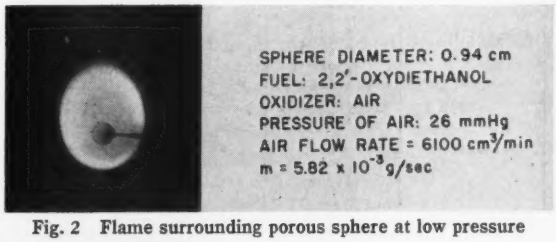
SPHERE DIAMETER: 0.94 cm
FUEL: 2,2′-OXYDIETHANOL
OXIDIZER: AIR
PRESSURE OF AIR: 26 mmHg
AIR FLOW RATE = 6100 cm³/min
m = 5.82 x 10⁻³ g/sec

Fig. 2 Flame surrounding porous sphere at low pressure

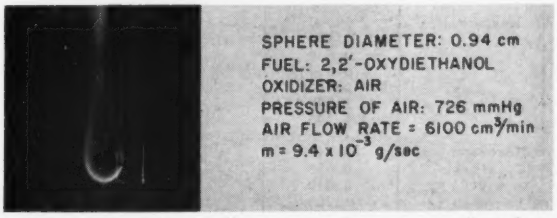
SPHERE DIAMETER: 0.94 cm
FUEL: 2,2′-OXYDIETHANOL
OXIDIZER: AIR
PRESSURE OF AIR: 726 mmHg
AIR FLOW RATE = 6100 cm³/min
m = 9.4 x 10⁻³ g/sec

Fig. 3 Flame surrounding porous sphere at approximately atmospheric pressure

relation between the dimensionless burning rate m/m_0 and the Reynolds number (5, 8).

In the systems under study in this investigation, heat transfer by natural convection is considered to be the mechanism controlling combustion. For such systems Spalding has suggested that the burning rate is some function of the transfer number B, the Grashof number and the Prandtl number (3)

$$\frac{m}{D\mu_e} = f_1(B, Gr, Pr) \quad [1]$$

In the absence of mass transfer Ranz and Marshall (7) have indicated the applicability of an equation of the form

$$\frac{Nu}{Nu_0} - 1 = f_2(Gr, Pr) \quad [2]$$

for heat transfer by natural convection (spheres). On the basis of these equations a relation of the following form is proposed and employed in the correlation of the data of this investigation

$$\frac{m}{m_0} - 1 = \alpha B^M Gr^N Pr^P \quad [3]$$

where α, M, N and P are empirical constants. The burning rate in the absence of convection m_0 is given by

$$\frac{m_0}{D\mu_e} Pr = \frac{m_0 C_e}{D\lambda_e} = 2\pi \ln(1 + B) \quad [4]$$

The ratio m/m_0 is equivalent to Nu/Nu_0 because the Nusselt number is proportional to m/D, (5). Since the Prandtl number for gases is essentially constant (usually close to unity), Pr may be omitted in Equation [3].

It is apparent from Equation [3] that when free convection is reduced to zero ($Gr = 0$), the mass burning rate m becomes identical to the burning rate m_0 for a spherically symmetric flame.

Burning rate determinations over a range of either pressures or sphere diameters are adequate to evaluate the exponent N. In the present analysis this exponent was determined from the

Table 3 Steady-state mass burning rate as a function of diameter of porous sphere and concentration of oxygen in ambient gas; pressure = 1 atm, ambient temperature 20 C

Fuel	Sphere Diameter, D, cm	Oxidizer	Burning Rate, m x 10^3, g/sec
Ethanol (95.5%)	0.440	Air	3.22
	0.638	Air	5.49
	0.940	Air	8.86
	1.208	Air	13.1
	1.59	Air	19.3
	1.906	Air	27.1
	1.208	33 wgt % O_2	14.6
	1.208	46 wgt % O_2	16.4
	0.637	80 wgt % O_2	8.9
	0.940	80 wgt % O_2	13.8
	1.208	80 wgt % O_2	19.5
Butanol-1	0.440	Air	4.1
	0.638		5.83
	0.638		5.66
	0.940		9.8
	1.208		13.9
	1.59		21.6
	1.906		28.2
Pentanol-1	0.440		4.64
	0.440		4.28
	0.638		6.01
	0.638		5.85

Fuel	Sphere Diameter, D, cm	Oxidizer	Burning Rate, m x 10^3, g/sec
Pentanol-1	0.940	Air	9.73
	1.208		14.1
	1.906		28.9
	1.590		22.1
Octanol-1	0.440		3.83
	0.638		5.39
	0.940		9.20
	1.208		13.6
	1.590		20.4
	1.906		27.7
Pentane	0.638		9.7
	0.940		14.2
	1.208		18.2
Hexane	0.638		8.0
	0.940		12.8
	1.208		16.7
Heptane	0.440		5.60
	0.440		5.75
	0.638		7.10
	0.638		7.25
	0.940		12.2
	1.208		16.5
	1.590		24.9
Kerosene ($C_{12.3}H_{24}$) ρ = 0.81	0.44		4.16
	0.638		7.28
	0.940		9.6
	1.208		13.8
	1.590		20.7
	1.906		27.4

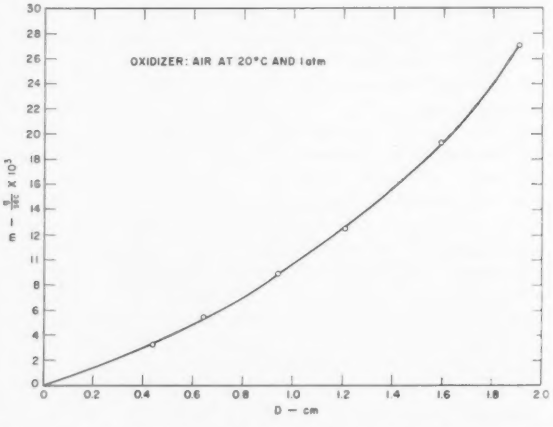

Fig. 4 Mass burning rate of ethanol (95.5 per cent) vs. diameters of porous spheres

Fuel	Sphere Diameter, D, cm	Oxidizer	Burning Rate, m x 10^3, g/sec
Hexadecane	0.440	Air	3.41
	0.940		9.0
	1.208		12.7
	1.590		18.4
	1.906		23.6
2, 2'-Oxydiethanol	0.312		2.46
	0.440		3.58
	1.590		20.4
	1.906		26.6
Xylene	1.208		23.3

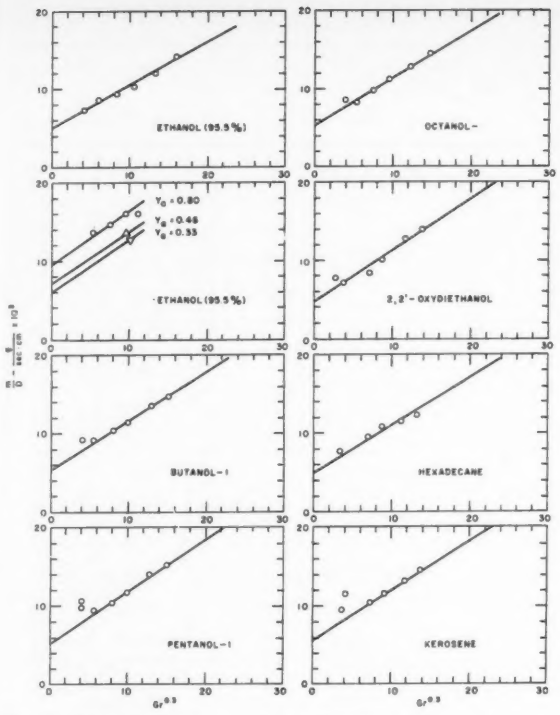

Fig. 5 Mass burning rate data. Porous spheres at atmospheric pressure. Oxidizer: air (unless otherwise noted)

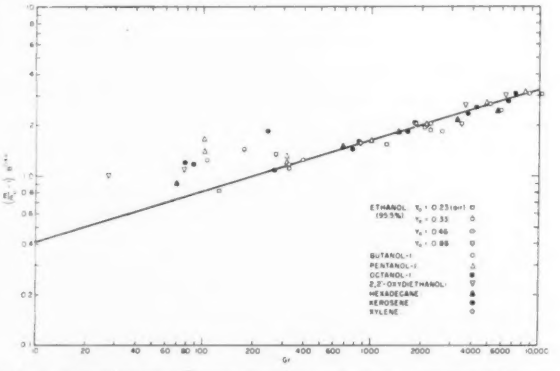

Fig. 6 Correlation of mass burning rate data. Porous spheres at atmospheric pressure. Oxidizer: air (unless otherwise noted)

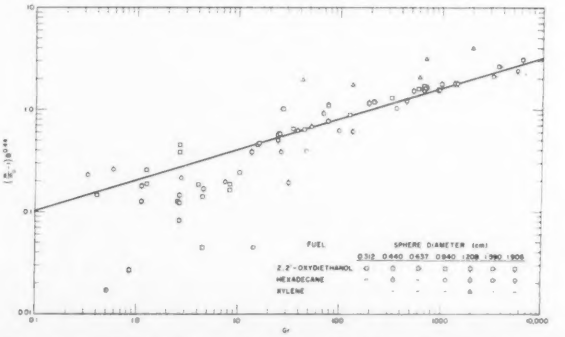

Fig. 7 Correlation of mass burning rate data. Porous spheres at subatmospheric pressures. Oxidizer: air

burning rate data of a number of different fuels at atmospheric pressures, for a series of porous sphere diameters. For the individual fuels, graphical presentation of the parameter $(m/m_0 - 1)$ against Gr on log paper (m_0 is calculated by means of Equation [4], Table 4) gave parallel straight lines with a slope corresponding to $N = 0.30$. In Fig. 5 the linear relationship between m/D and $Gr^{0.30}$ for various fuels is presented. The straight lines drawn through the data intersect the ordinate at the calculated value of m_0/D based on Equation [4]. From the slopes of the lines of Fig. 5, numerical values for the function of B can be evaluated. It is thus found, empirically, that the value of M is equal to -0.44. Replotting the data obtained at atmospheric pressure (Fig. 6) yields a uniform correlation for all the fuels which can be represented by

$$[(m/m_0) - 1]B^{0.44} = 0.20Gr^{0.30} \quad [5]$$

Since $\ln(1 + B)$ is approximately equal to $0.87B^{0.44}$ for the range of values of B in consideration, Equation [5] can be given alternately as

$$\left[\frac{m}{m_0} - 1\right] \ln (1 + B) = 0.17Gr^{0.30} \quad [6]$$

The burning rate data (precision of experiments ±4 per cent) obtained with hexadecane, 2,2′-oxydiethanol, and xylene at reduced pressures (Table 1) are presented in Fig. 7 with the straight line based on Equation [5]. The experimental data summarized in Table 1 are plotted in Figs. 8, 9 also. These curves approach the theoretical curve for burning without convection (Equation [4], Table 5) as pressure is reduced. In the case of hexadecane (Fig. 9) some of the measured values of m fall below the theoretical curves. This overlap suggests that the method for evaluating m_0 is not completely satis-

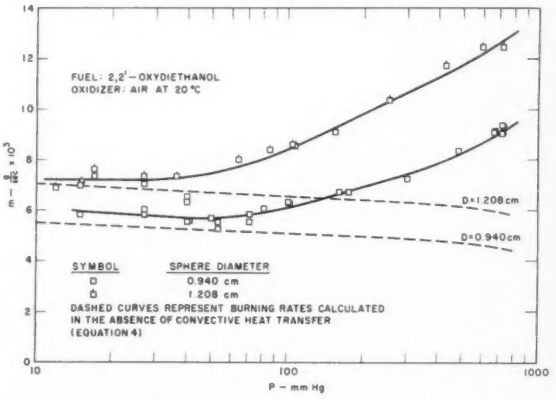

Fig. 8 Mass burning rate as a function of pressure

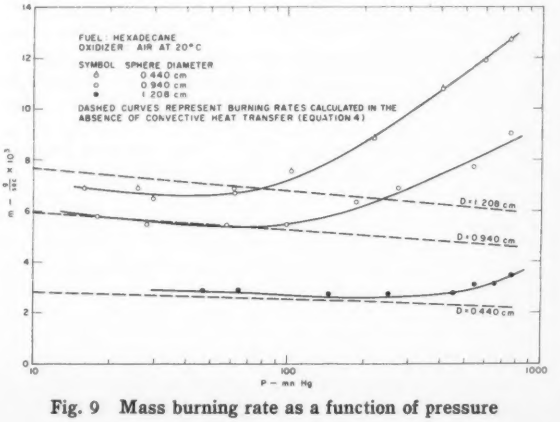

Fig. 9 Mass burning rate as a function of pressure

Table 4 Numerical values of parameters and physical properties employed in the calculation of m_0/D and Grashof number at 1 atm

FUEL AND OXIDIZER	T_s, °K	T_c,* °K	$\mu_d \times 10^4$, g/sec cm	Ω, cm^{-3}	$C_{L(20°C)}$, cal/g°C	$C_{L(T_s)}$, cal/g°C	$L_{S(T_s)}$, cal/g	L, cal/g	q, cal/g	i, g/g	B	$\frac{\lambda_e}{C_e} \times 10^4$, sec^{-1}	$\frac{m_0}{D} \times 10^3$ g/sec cm
Ethanol (95.5%)[a]	351	2250	4.15	1485	0.625	0.85	240	267.5	6,630	1.99	2.88	5.73	4.82
Ethanol (95.5%)[b]	351	2530	4.3	1265	0.625	0.85	240	267.5	6,630	1.99	4.06	5.94	6.00
Ethanol (95.5%)[c]	351	2700	4.48	1178	0.625	0.85	240	267.5	6,630	1.99	5.75	6.04	7.15
Ethanol (95.5%)[d]	351	3020	4.68	1037	0.625	0.85	240	267.5	6,630	1.99	9.90	6.30	9.30
Butanol-1[a]	390	2280	4.22	1270	0.555	0.82	141	207.0	8,051	2.59	3.35	5.75	5.29
Pentanol-1[a]	411	2280	4.29	1178	(0.682 avg.)		120	201.0	8,420	2.72	3.40	5.75	5.36
Octanol-1[a]	468	2300	4.33	1022	0.521	0.890	97.5	221.0	9,060	2.95	3.00	5.78	5.03
Ethylene glycol[a]	471				0.575	0.785	191	312.0	4,290	1.547	1.90	5.75	3.85
2,2′-Oxydiethanol[a]	518	2290	4.40	889	0.550	0.750	146	264.0	5,220	1.507	2.81	5.75	4.80
Pentane[a]	309	2300	4.13	1640	0.560	0.580	85.4	94.4	10,720	3.540	7.48	5.78	7.75
Hexane[a]	342	2300	4.15	1450	0.542	0.597	80.5	108.4	10,720	3.520	6.42	5.78	7.25
Heptane[a]	372	2305	4.20	1345	0.535	0.620	76.5	121.6	10,720	3.510	5.65	5.78	6.88
2,2-4 Trimethyl pentane[a]	372				0.506	0.592	64.9	106.8	10,672	3.510	6.40	5.78	7.26
Hexadecane[a]	561	2310	4.41	804	0.513	0.768	52.9	225.0	10,600	3.460	2.82	5.78	4.88
Xylene (m,p)[a]	413	2330	4.30	1158	0.405	0.504	82.0	137.0	9,850	3.170	5.00	5.79	6.45
Kerosene ($C_{12.5}H_{24}$)[a]	496	2320	4.38	930	0.483	0.665	60.4	176.5	10,400	3.400	3.72	5.79	5.62

* Adiabatic Flame Temperature (Reference 9)

OXIDIZERS: a = air, $Y_s = 0.232$; b = 33 weight % O_2, $Y_s = 0.329$; c = 46 weight % O_2, $Y_s = 0.461$; d = 80 weight % O_2, $Y_s = 0.736$.

factory. Nevertheless, it is believed that the trend displaying a minimum at low pressures is valid. This point is reached when the conductive effects expressed by m_0 begin to control the process of heat transfer. From Equation [4] it is evident that m_0 increases with falling pressure because L, and hence B, decreases. Therefore the burning rate attains a minimum value and then increases with further decrease in pressure.

The deviations of data measured with the porous spheres at low Grashof numbers, corresponding to small sphere diameters (Figs. 5, 6), point to a limitation in the experimental technique. These deviations are accentuated progressively with increasing volatility or increasing B as observed in a similar series of tests on octane, heptane, hexane, pentane, and diethyl ether, all burning in air at atmospheric pressure. When the diameter is diminished, the heat flux (or burning rate per unit area) at the surface increases (see Equations [4, 5]). It is believed that high volatility and high heat flux, combined with a factor such as incomplete wetting of the porous surface, account for this unexpected behavior. Because of this apparent limitation to the technique, the applicability of Equation [5] to the lighter hydrocarbon fuels could not be tested.

In the calculation of m_0, B, and Gr it was necessary to assign values to temperature levels and physical properties. For reasons of expediency, the flame temperature T_c was taken as the equilibrium adiabatic value (9) even though this practice is basically inconsistent with Equation [4] derived for conditions of nondissociation. It has also been shown that as a result of finite thickness of the reaction zone, the actual flame temperature is somewhat lower than the adiabatic value (3, 11). The terms λ and C were evaluated for air at a log mean temperature between T_c and T_a. The use of the log mean instead of the arithmetic mean yielded lower (by 15 per cent) values of m_0 which were more in accord with the observed burning rates at low pressures (Figs. 8, 9). In the calculation of Gr, the properties μ and ρ were similarly taken for air at the log mean temperature between T_c and the temperature of the surroundings. However, since the heated, rising gases are bounded by the liquid surface assumed at the boiling point T_s and the ambient gas at T_a, the temperature of the surrounding T_b was taken simply as the arithmetic mean of T_s and T_a.

Drop combustion studies above atmospheric pressure (1, 2) indicate a proportionality between burning rate and pressure raised to a fractional power j, where j has values between 0.2 and 0.5. Such dependencies, when considered to apply to narrow pressure ranges, are suggested by Equation [6] rearranged in the following form

$$m = m_0 + 0.17\, m_0 K P^{0.60}/\ln(1 + B) \quad \ldots\ldots [7]$$

where P is the pressure and K replaces the pressure-independent terms of the Grashof number. Since $m_0/\ln(1 + B)$ is practically pressure independent, Equation [4], m becomes proportional to $P^{0.60}$ at high Grashof numbers, yielding an upper limiting value of $j = 0.60$.

At constant pressure the distance of the flame at the forward stagnation point from the surface of a sphere or suspended drop $(D_c - D)/2$ (Table 2) decreases with decreasing diameter, but the ratio of flame diameter to sphere or drop diameter increases. Similarly, for a given sphere or drop diameter the flame distance increases with decreasing pressure (Figs. 2, 3). The data presented in Table 2 are useful in relating the natural convection parameter Gr to flame distance. If one assumes that to a first approximation the mass burning rate of a drop is proportional to $D_c D/(D_c - D)$ (Reference 12), Equation [6] may be rewritten

$$\frac{D}{D_{co}} \frac{D_{co} - D_c}{D_c - D} \ln(1 + B) = 0.17 Gr^{0.30} \quad \ldots\ldots [8]$$

Table 5 Numerical values of parameters and physical properties employed in calculation of m_0/D and Grashof number at sub-atmospheric pressures

FUEL	P, mm Hg	T_s, °K	C_L ave, cal/g°C	L_s cal/g	L, cal/g	B	m_0/D, g/sec cm	$\mu_d \times 10^4$, g/cm sec	Ω, cm^{-3}
Hexadecane	15	432	0.58	67.0	148.0	4.55	6.22	4.34	0.429
	20	438	0.58	66.4	150.4	4.47	6.16	4.35	0.756
$(\lambda_g/c_g = 5.78 \times 10^{-4}$	30	448	0.59	65.4	157.0	4.26	6.02	4.35	1.67
g/sec cm)	50	462	0.59	64.4	164.4	4.05	5.87	4.36	4.46
	70	472	0.60	63.5	170.5	3.90	5.76	4.37	8.51
	100	483	0.60	62.6	176.6	3.72	5.64	4.38	16.9
	150	497	0.61	61.2	185.2	3.54	5.50	4.38	36.8
	200	506	0.62	60.2	192.2	3.39	5.36	4.39	64.0
	300	521	0.62	58.4	199.4	3.26	5.25	4.40	138.5
	500	542	0.63	55.6	212.6	3.02	5.05	4.41	367.0
	760	561	0.641	52.8	224.6	2.83	4.88	4.42	803.0
2,2'-oxydiethanol**	15	390	0.60	134.0	197.0	3.94	5.75	4.31	0.486
	20	398	0.60	133.6	202.0	3.83	5.66	4.32	0.843
$(\lambda_g/c_g = 5.75 \times 10^{-4}$	30	408.5	0.60	132.4	207.0	3.72	5.59	4.32	1.86
g/sec cm)	50	422.6	0.61	130.4	215.0	3.57	5.46	4.33	4.97
	70	432.4	0.61	129.1	219.0	3.48	5.40	4.33	9.55
	100	443.3	0.62	127.6	225.0	3.38	5.31	4.34	18.9
	150	456.3	0.62	125.7	232.0	3.27	5.23	4.35	41.0
	200	466.1	0.63	124.4	237.0	3.19	5.15	4.36	70.9
	300	480.5	0.63	122.4	245.0	3.07	5.05	4.37	154.0
	500	500.1	0.64	120.0	255.0	2.92	4.92	4.38	406.0
	760	517.3	0.65	118.0	264.0	2.81	4.80	4.39	886.0
Xylene (m,p)**	100	352.0	0.43	92.8	119.6	5.88	6.99	4.20	25.0
	122	357.0	0.43	92.2	121.3	5.78	6.95	4.20	36.6
$(\lambda_g/c_g = 5.79 \times 10^{-4}$	181	368.0	0.43	90.8	124.9	5.60	6.84	4.22	78.0
g/sec cm)	400	392.0	0.44	87.0	132.0	5.24	6.64	4.25	354.0
	431	394.0	0.44	86.0	132.6	5.21	6.63	4.25	409.0
	760	413.0	0.46	83.6	139.1	4.92	6.45	4.28	192.0

** L_s, heat of vaporization, was calculated using method of Reference 10

OXIDIZER: Air $T_s = 293°K$ $Y_s = 0.232$ (air)

Since (Reference 4)

$$\frac{D_{co}}{D} = \frac{\ln (1 + B)}{\ln \left(1 + \frac{Y_a}{i}\right)} \quad \ldots\ldots\ldots\ldots\ldots\ldots [9]$$

Equation [8] becomes

$$\ln \left(1 + \frac{Y_a}{i}\right) \frac{D_{co} - D_c}{D_c - D} = 0.17 Gr^{0.30} \quad \ldots\ldots\ldots [10]$$

Fig. 10 was prepared utilizing the parameters of Equation [8]. The resulting correlation obtained for different fuels and with suspended drops and porous spheres is rather encouraging although the numerical constants applying to the plotted straight line differ from those predicted by Equation [10].

It is evident from the data presented in Figs. 8, 9 and Table 2 that although the burning rates observed at low pressures (15–100 mm Hg) approach rather closely the values calculated for combustion without convection, the measured and calculated flame diameters, Equation [9], differ appreciably. It may be shown (13) that a possible cause for these large differences is the assumption, in the derivation of Equation [9], of the absence of chemical dissociation of combustion products and the consequent abnormally high flame temperatures. Since this assumption (also used in the derivation of Equation [4]) has little influence on the heat flux at the surface, the mass burning rate calculated does not differ appreciably from that applicable to nonconvective systems with dissociation. However, the introduction of the adiabatic flame temperature markedly reduces the calculated flame distance (12), and for some of the fuels examined the values obtained compare favorably with the flame distances measured.

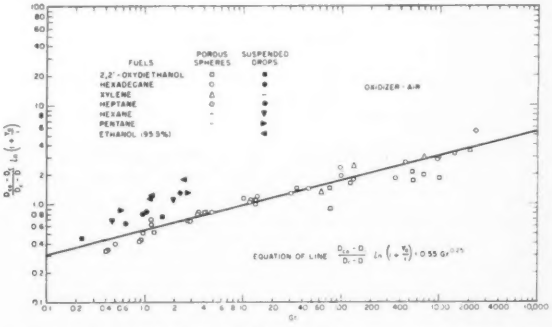

Fig. 10 Correlation of flame distance measurements

Concluding Remarks

A correlation represented by Equation [5] was obtained for a series of liquid organic hydroxy compounds and for several heavier hydrocarbons burning (in air and oxygen-nitrogen mixtures) on the surface of porous Alundum spheres of various sizes at atmospheric and subatmospheric pressures. This correlation demonstrates the contribution of natural convection to the mass burning rate. In the limiting case at high pressures, the burning rate varies linearly with pressure raised to the 0.6 power (cf. Equation [7]), substantiating trends observed by other investigators in drop burning studies at higher pressure levels. As the pressure is reduced heat transfer by conduction becomes the controlling mechanism.

Diameter measurements were made of the flames surrounding both suspended drops at atmospheric pressure and wetted porous spheres at various pressure levels (atmospheric

and below). These data (Fig. 10) also demonstrate the influence of free convection. The flame distances obtained with porous spheres and with suspended drops show conformity in behavior.

It was observed that the steady-state mass burning rate of a liquid sphere goes through a minimum as pressure is reduced. At subatmospheric pressures the predicted pressure dependence for small drops (cf. Equation [5]) is so modest that for practical purposes the burning rate of hexadecane drops (for example) less than 1000μ in diameter, may be considered independent of pressure under free convection conditions.

References

1 Hall, A. R., and Diederichsen, J., "An Experimental Study of the Burning of Single Drops of Fuel in Air at Pressures up to Twenty Atmospheres," Paper 105 of Fourth Symposium (International) on Combustion, Williams and Wilkins Co., Baltimore, Md., 1953.

2 Goldsmith, M., "Experiments on the Burning of Single Drops of Fuel," JET PROPULSION, vol. 26, 1956, pp. 172–178.

3 Spalding, D. B., "The Combustion of Liquid Fuels," Paper 106 of Fourth Symposium (International) on Combustion, Williams and Wilkins, Baltimore, Md., 1953.

4 Wise, H., Lorell, J., and Wood, B. J., "The Effects of Chemical and Physical Parameters on the Burning Rate of a Liquid Droplet," Paper 3 of Fifth Symposium (International) on Combustion, Reinhold Publishing Co., New York, 1955.

5 Agoston, G. A., Wise, H., and Rosser, W. A., "Dynamic Factors Affecting the Combustion of Liquid Spheres," Sixth Symposium (International) on Combustion, Reinhold Publishing Co., New York, 1957, Paper 93.

6 Frossling, N., "The Evaporation of Falling Drops," *Gerlands Beitr. Geophsik*, vol. 52, 1938, pp. 170–216.

7 Ranz, W. E., and Marshall, W. R., Jr., "Evaporation from Drops, Part II," *Chem. Eng. Progress*, vol. 48, 1952, pp. 173–180.

8 Spalding, D. B., "Some Fundamentals of Combustion," Academic Press, New York, 1955.

9 Hottel, H. C., Williams, G. C., and Satterfield, C. N., "Thermodynamic Charts for Combustion Processes, Part I," John Wiley & Sons, New York, 1949.

10 Maxwell, J. B., "Data Book on Hydrocarbons," D. Van Nostrand, New York 1950.

11 Lorell, J., Wise, H., and Carr, R. E., "Steady State Burning of a Liquid Droplet. II. Bipropellant Flame," *Journal of Chemical Physics*, vol. 25, 1956, pp. 325–331.

12 Godsave, G. A. E., "Studies of the Combustion of Drops in a Fuel Spray. The Burning of Single Drops of Fuel," Paper 103 of Fourth Symposium (International) on Combustion, Williams & Wilkins Co., Baltimore, 1953.

13 Goldsmith, M., and Penner, S. S., "On the Burning of Single Drops of Fuel in an Oxidizing Atmosphere," JET PROPULSION, vol. 24, 1954, pp. 245–251.

Technical Notes

Solar Sailing—A Practical Method of Propulsion Within the Solar System

RICHARD L. GARWIN[1]

IBM Watson Scientific Laboratory, Columbia University, New York, N. Y.

It is shown that commercially available metallized plastic film can be used as a solar radiation pressure sail for propulsion of space vehicles within the solar system. The method of propulsion is of negligible cost and is perhaps more powerful than many competing schemes.

IT IS difficult to exaggerate the importance of solar radiation pressure for the propulsion of satellites or space ships within the solar system; but since I have never seen any allusion to this powerful method, while less practical and more difficult schemes are frequently cited, I feel it desirable to publish this paper.

The principle involved is simply to make use of the pressure of the sun's light on a sail to propel a space ship as desired through the solar system. What is important is the area of sail per unit mass, and if, just as a practical example, we use a commercially available 0.1-mil-thick plastic sail equal in mass to the rest of the "space ship," the mass per unit area will be 5×10^{-4} g/cm^2. The sail may be aluminized without significant additional mass, in which case the sun's radiation may be reflected, thereby doubling the maximum pressure which may be exerted on the sail. The magnitude of this pressure on a normally oriented sail is $P = 2W/c$, where W is the energy incident per cm^2 per sec, and c is the velocity of light. At the earth's orbit $W = 2$ cal/cm^2/min or 1.3×10^6 erg/sec/cm^2, so that $P = 0.8 \times 10^{-4}$ dyne/cm^2. The acceleration of the space ship is, therefore, $a = p/\sigma$, where σ is the mass/cm^2 and in the example is 5×10^{-4} g/cm^2. Therefore $a = 0.16$ cm/sec^2. Thus on a space ship so constituted one may obtain an acceleration of as much as 1.6×10^{-4} times that of gravity even with a gross 0.1-mil sail.

The thrust may be varied from the maximum calculated, smoothly almost to zero by manipulation of the "shroud lines"; and the thrust may be directed almost without loss in magnitude to any angle within 45 deg of the radius vector from the sun, while smaller thrust (as cos θ) is available up to 90 deg from the radius vector.

Although the acceleration is numerically small, the velocity changes in reasonable times by significant amounts. Thus $\Delta v = 1.4 \times 10^4$ cm/sec/day, so that the escape velocity from the earth (8×10^5 cm/sec) may be acquired in two months, and a velocity large enough to escape from the solar system entirely may be reached in a time of the order of a year.

Before comparing the merits of solar sailing with those of ion propulsion, hydrogen expulsion by solar batteries, or nuclear or thermonuclear reactors, let us discuss two situations in which solar sailing might well be used. To have a definite example, consider an earth satellite with reflective sails, each weighing 20 lb (10 kg). The sail will have an area

$$\frac{2 \times 10^4 \text{ g}}{5 \times 10^{-4} \text{ g/cm}^2} = 4 \times 10^7 \text{ cm}^2$$

Received Nov. 28, 1957.

[1] Staff Member and Adjunct Associate Professor of Physics.

EDITOR'S NOTE: The Technical Notes and Technical Comments sections of JET PROPULSION are open to short manuscripts describing new developments or offering comments on papers previously published. Such manuscripts are published without editorial review, usually within two months of the date of receipt. Requirements as to style are the same as for regular contributions (see masthead page).

and will be more or less a circle of plastic film 70 meters in diameter. There are, of course, no requirements as to absence of holes, tears, flaws, etc. The reflective coat plays a perhaps important role in eliminating electrostatic forces which might easily prevent opening of the sail. The sail may be attached to the ship by "shroud ribbons" ~200 meters long. Since the forces on the shroud ribbon will not exceed 2 grams weight, the ribbons may be narrow strips of the same material as the sail. Let us for the moment grant that the sail may be expelled from its packing container after the "space ship" is in a satellite orbit at reasonable altitude. It is of interest to compute the time required for the sail to "fill with sunlight." This is the time for the sail to go from a flat circle to a dished configuration of the order of 10 meters deep and is

$$t_f = \left(\frac{2 \times 10^3}{0.32}\right)^{1/2} = 80 \text{ sec}$$

Thus the sail may be furled and unfurled quickly compared with the 90-min period of its orbit around the earth.

The simplest program for increasing the altitude of the satellite, at the same time increasing its energy and *reducing* its velocity about the earth, is to furl the sail by slacking half the shroud lines while the satellite approaches the sun and to unfurl the sail while receding from the sun. Clearly then, the mean projected acceleration along the velocity vector is $\pi^{-1} \times 0.16$ cm/sec^2 or 5×10^{-2} cm/sec^2, and the rate of decrease of orbital velocity is then $\dot{v} = 5 \times 10^{-2}$ cm/sec^2. Thus, an initial velocity of 8×10^5 cm/sec will decrease to zero in a time on the order of $(8 \times 10^5)/(5 \times 10^{-2}) = 1.6 \times 10^7$ sec, or 6 months. The orbit eccentricity grows during this time, and, depending on details, the altitude at perigee may remain constant or increase.

It should be noted parenthetically that the torque exerted on a satellite by radiation pressure is ordinarily larger than that due to differential gravity effects. Indeed, if half of a 20-in.-diam Vanguard sphere is painted black, while the other half is reflecting, and if the moment of inertia is 2×10^6 gm cm^2, the torque is of magnitude ~1 dyne-cm, and angular acceleration will be $\sim 10^{-6}$ radians per sec. The sphere will, therefore, revolve one radian in ~30 min due to this cause. For this same sphere with maximum gravitational quadrupole (two 5-kg masses at opposite ends of a diameter), the differential gravity torque is 10 dyne-cm at 45 deg inclination. On this small-area device, the torque due to radiation pressure is not negligible. For less symmetrical devices (cones, etc.) a stable equilibrium may be reached pointing into the sun, while damping of long-period oscillations about this equilibrium may be achieved by slightly viscous fluids in some portion of the satellite.

The energy required for operating the shroud lines is at most (2×10^3 dynes) $\times$ (10^4 cm) or ~2 joules each 90 min, even if a nonconservative actuator is used. This is 20 milliwatts, while the kinetic energy delivered to the satellite by the sail averages 60 watts. The maximum power falling on the sail is $\sim 4 \times 10^6$ watts (4 megawatts) so that it is evident that the propulsion efficiency is not very high ($\sim 10^{-5}$ or, in fact, v/c). A solar battery ~1cm^2 area supplies enough power to manipulate the shroud lines.

As a second example let us consider a space ship of the same fairly high mass per unit area (0.1-mil sail of mass equal to that of the rest of the ship) $\sim 5 \times 10^{-4}$ g/cm^2. Now we want to go from the earth's orbit to that of Venus and back again.

The optimum sail tilt to go slowly with a small sail from one circular orbit to another is $\theta = \sin^{-1} \sqrt{3}/3$, since this angle gives the maximum component along the velocity vector and thus allows the ship to lose or gain energy as rapidly as possible. In order to move in to Venus we must *brake* the ship to *increase* the orbital velocity (because the potential energy is twice the kinetic energy and negative). In the field of our sun with the space ship given above we have

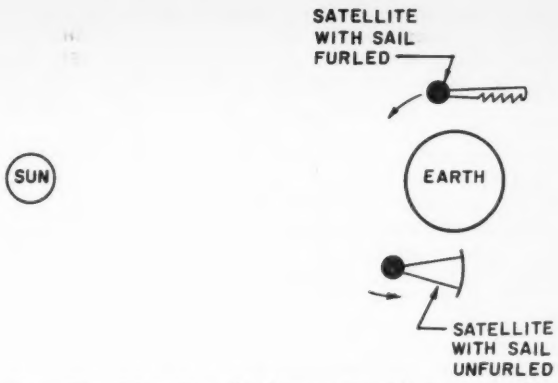

Fig. 1 Use of the solar sail to increase the altitude of a satellite and to escape the earth

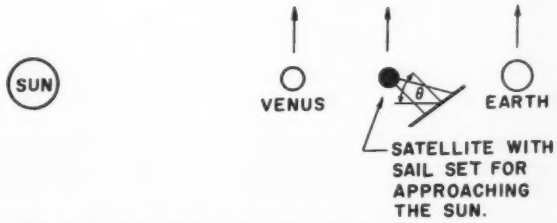

Fig. 2 Cruising within the solar system by use of the sail

$$\dot{v} = \frac{(0.8) \times (0.8 \times 10^{-4})}{(5 \times 10^{-4})} \left(\frac{r_0}{r}\right)^2 = 0.1 \left(\frac{r_0}{r}\right)^2 \text{ cm sec}^{-2}$$

where r/r_0 is the distance of the ship from the sun measured in earth's orbit radii ($\sim 1.5 \times 10^{13}$ cm). But

$$v = 2.4 \times 10^6 \left(\frac{r_0}{r}\right)^{1/2}$$

Thus we find for the rate of change of r with time

$$\frac{\dot{r}}{r} = 10^{-7} \left(\frac{r_0}{r}\right)^{3/2}$$

showing that the orbit is an equiangular spiral, opening or closing by a large factor each turn (indeed, by a factor ~20 per year if the initial conditions were right for the motion to be an equiangular spiral in this noncentral-force field).

The orbit equations are not difficult to solve in detail, but we may here be content with observing that the radiation pressure in our example is one-half the gravitational force between sun and space ship, so that the space ship is entirely free to go "tacking" about in the solar system, arriving at any specified radius in times considerably less than a "year" for the planet at that radius. For instance, one can go to Venus and back in less than an ordinary year with this first gross sail.

Compared with escape from the earth, the efficiency of the sail rises for operation near the earth's orbit, from $\sim 10^{-5}$ for earth satellite propulsion to $\sim 10^{-4}$ for solar navigating, since the pertinent velocity is higher and the duty cycle more favorable. We may compare alternative schemes for propulsion, the one currently most popular being, perhaps, acceleration of the interplanetary ions ($\sim 10^3$/cm^3) by an accelerator in the vehicle, powered by solar energy or nuclear or thermonuclear reactor. To achieve the 4×10^3 dynes thrust contemplated here with gentle use of a sail, one would have to accelerate to, say, 100 kev energy one ampere of interplanetary protons.

This would require only 100 kilowatts of power rather than the 4 megawatts of sunshine reflected (lower, of course, by the ratio of proton exhaust velocity to light velocity); but the space ship swallows up only $(2.4 \times 10^6) \times (10^3) \times (A)$ protons per sec, where A is the frontal area of the accelerator. Thus $A \geq 10^9$ cm^2, and the space ship must have a maw larger than the sail contemplated here. The use of a thermonuclear reactor to eject $\sim$1 gram of hydrogen per day at 100 kev (in our 20-kg ship) would be an eminently satisfactory solution if such reactors existed and were of zero mass. Even so, one must eject one's own mass every 30 years to compete with the solar sail for cruising.

It is obvious that there are considerable difficulties connected with space travel, but those connected with the sail appear relatively small. We note that a reasonable chemical fuel with exhaust velocity $\sim$2 km/sec, requiring a ratio of take-off mass to final mass of $e^{v/V}$, were V is the jet velocity and v the desired final rocket velocity, or a mass ratio of $e^4 = 250$ to reach 11 km/sec (escape velocity from the earth) would require to reach 24 km/sec a mass ratio of 1.6×10^5, if rocket engines and tanks had zero mass. In actuality the mass ratios are very much larger.

Possible Improvements

It should be no great trick to make large areas of sail of thickness 2×10^{-5} cm (as is used for beta-ray source backing), thus reaching a space ship area per gram twelve times smaller than that considered above. With this improved sail a satellite could escape the earth within a week, and could fall to Venus in less than a month and come back in a week (at high velocity, albeit).

Combustion Instability in Solid Propellant Rocket Motors

E. W. PRICE[1] and J. W. SOFFERIS[2]

U. S. Naval Ordnance Test Station, China Lake, Calif.

RECENT results of an experimental program have revealed some new and crucial information regarding the mechanism of excitation of combustion instability in solid propellant rocket motors, and the effect of oscillatory behavior on the quasi-steady burning rate of the solid propellant. The nature of this information and the tests which revealed them are described in the following.

In conventional rocket motors the structure and orientation of the flow oscillations that correspond to acoustical modes of vibration of the combustion chamber cavity are very complex and not necessarily stationary with time (1,2).[3] Thus it is difficult to know where to place a pressure gage for meaningful measurements of the oscillation; difficult to know what aspect of the burning and what region of the charge surface are responsible for, or associated with, the excitation process; and difficult to assess the effects of the different aspects of oscillatory behavior (e.g., velocity oscillation and pressure oscillation) on a partially burned charge.

To circumvent these difficulties, an experimental burner was designed to favor oscillations in a stationary mode, and studies were made of the conditions favorable for combustion instability. A burner having a combustion chamber with circular cylindrical geometry was chosen in order to obtain longitudinal oscillations of very simple geometry, with frequencies comparable to those of the transverse oscillations in much larger motors. The burner is sketched in Fig. 1. In order to minimize the attenuation of oscillations in the longitudinal mode, the nozzle vent was placed midway between the ends of the burner, at a point of zero pressure oscillation of the fundamental mode of longitudinal vibration of the cavity (Fig. 2). The ends of the motor were made as flat as practicable and the propellant charge was made a very close fit in the burner to avoid dissipation of oscillation energy in the annular space between burner and inhibited outer surface of

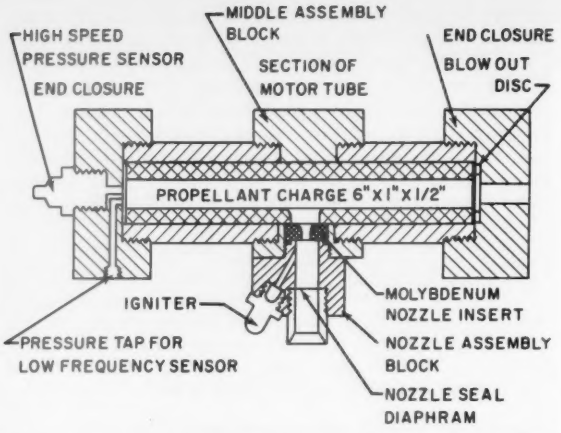

Fig. 1 No. 1 research burner for studies of combustion instability

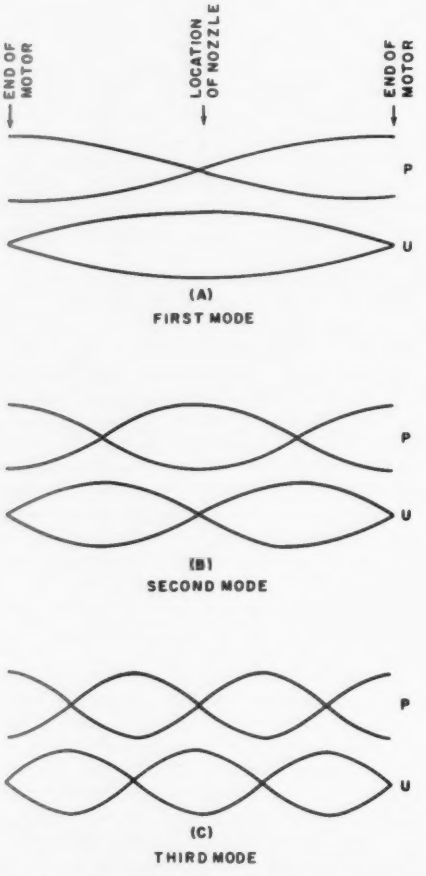

Fig. 2 Envelopes of standing pressure and velocity waves in the longitudinal mode of the burner cavity

Received Dec. 16, 1957.

[1] Physicist. Head, Fluid Dynamics Branch, Research Department. Mem. ARS.

[2] Physicist, Research Department.

[3] Numbers in parentheses indicate References at end of paper.

the charge. In this design (Fig. 1) the pressure gage is always located at a point of maximum pressure oscillation (antinode) on the standing longitudinal pressure wave. The blowout disk at the opposite end of the burner provides protection for the equipment and leads to partial burns of the charges when the (normally progressive) pressure reaches blowout pressure.

The experimental burner described has been used in a number of tests designed to verify or disprove (for one propellant so far) the following contentions of various writers regarding combustion instability:

1 Combustion oscillations are excited by periodic fluctuations in mass burning rate induced by pressure oscillations (as opposed to velocity oscillations or periodic fluctuations in turbulence in the region of velocity oscillations) (1,2,3,4).

2 The most readily excited mode of oscillation of a circular cylindrical cavity is a traveling tangential mode (2).

3 The flow at the downstream end of the charge (where channel discontinuities occur) generates noise which in turn excites combustion oscillations (5).

4 Quasi-steady burning rate may or may not be increased by the action of the oscillatory flow and combustion (6).

5 Changes in burning rate during unstable performance are favored by conditions of high quasi-steady stream velocity in the conduit of the burner (7).

The conclusions regarding these issues and the supporting evidence were as follows:

1 Flow oscillations were excited by action of pressure oscillations on combustion but not by velocity oscillations. To determine this, tests were run on charges made up partly of dummy (cellulose acetate) propellant as shown in Fig. 3. The charges with dummy propellant in the middle would presumably oscillate much like full charges in the first mode if pressure (or density or temperature) oscillations were of primary importance to the excitation process, since the burning continues to be present in the principal region of oscillation of pressure.

On the other hand, the charges with propellant in the middle section would be expected to oscillate like full charges if velocity oscillation were primarily responsible for the excitation of oscillations. The pressure records of two tests on these charges are shown in Fig. 4, with a pressure record from a full charge for comparison. The records show that only relatively minor oscillations occurred in the test with propellant in the vicinity of the velocity oscillations, while the oscillations with the charge having propellant at the ends of the burner where pressure oscillation predominates were almost as severe as those obtained with the full propellant charge.

Probably equally significant is the fact that the charge with propellant in the central section "chose" to oscillate in a mode that placed pressure antinodes in the region of the propellant material. From the observed frequency, the mode was found to be the third mode of the longitudinal mode (about 8700 cps), the structure of which is sketched relative to the charge configuration in Fig. 2c. It is presumed that the second mode was not "chosen" because that mode has a pressure antinode adjoining the nozzle, and acoustic pressure tends to "leak out" through the nozzle in that mode.

2 Contrary to predictions of Grad (1) and Cheng (3), the mode of oscillation most readily excited in the tests reported here was the longitudinal one. However, the time lag concept used by both these authors could permit this result in any particular design because the geometry change during burning might not lead to any tangential frequencies compatible with the time lag involved. It was found that use of a longitudinal resonance rod (which would tend to suppress any transverse oscillations) did not affect the oscillations materially. The changes in amplitude of the oscillations during burning, although to some extent reproducible, were not found to be associated with any multiple relationship between calculated frequency of the longitudinal modes and frequency of transverse modes (thus there apparently wasn't much coupling between modes). The instrumentation used was

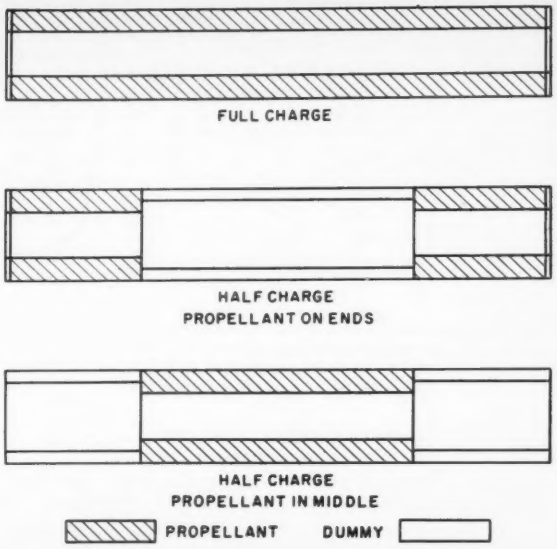

Fig. 3 Partial charges to localize the region of excitation

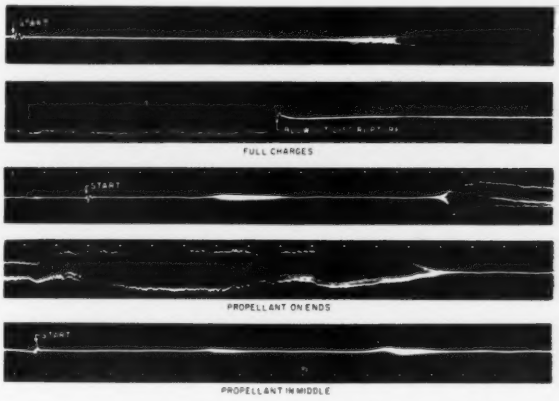

Fig. 4 Longitudinal pressure oscillations in the motor shown in Fig. 1 using the charge configuration shown in Fig. 3; double base propellant, 80 F

linear only to 15 kc, so that no transverse oscillations would have been recorded if they had been present. However, the above comments support the belief that no transverse oscillations were present.

3 Test results indicated that the intensity of fluid dynamically excited noise was not a conspicuous factor in exciting combustion instability. Flow velocities in the combustion chamber were very low in the tests reported as compared to conventional motors, being in the vicinity of Mach 0.06 at the midpoint of the burning period when the majority of instabilities developed. The configuration did not have channel discontinuities comparable to conventional motors where vortex shedding processes would readily excite fluid dynamic noise.

4 For the double-base propellant used in these tests, the burning rate during periods of oscillatory behavior was observed to decrease by as much as 50 per cent at lower pressures (500 to 1700 lb/in.^{2}), and to increase more than 50 per cent at higher pressures. The first effects are illustrated in Fig. 5, where an observed pressure-time curve is compared with a theoretical one. The pressure level is severely depressed during the period of oscillation, rises some about two-thirds of the way through burning when the oscillations temporarily de-

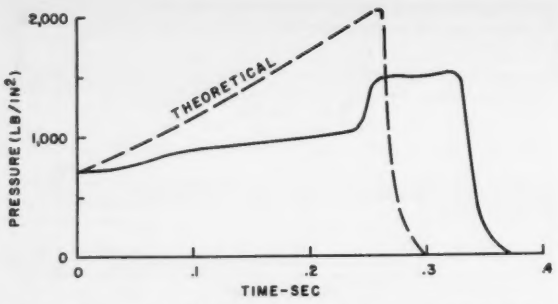

Fig. 5 Comparison of theoretical pressure-time curve with one obtained on test with combustion instability; double base propellant, 80 F

crease in amplitude, and then becomes further depressed below normal as the oscillations grow again.

5 Results of tests with full charges indicate that high mean stream velocity is not essential to the modification of quasi-steady burning rate accompanying flow-combustion oscillations. The motor used in these experiments had an effective ratio of throat area to port area of 0.21 at the start of burning, 0.05 at the end of burning. This ratio should result in Mach numbers of 0.12 and 0.03 at the start and end of the burn, respectively. These values are very low compared to most rockets (which have initial ratios of throat area to port area of 0.4 to 0.8). The modification of burning rate does not seem to follow the change in mean gas velocity, but rather primarily the amplitude of the pressure oscillations.

References

1 Grad, Harold, "Resonance Burning in Rocket Motors," *Communications on Pure and Applied Mathematics*, vol. 2, 1949, pp. 81, 82, 96–99.

2 Smith, R. P., and Sprenger, D. F., "Combustion Instability in Solid-Propellant Rockets," Fourth Symposium (International) on Combustion, Williams and Wilkins, Baltimore, 1953, pp. 903–905.

3 Cheng, Sin-I, "High-Frequency Combustion Instability in Solid Propellant Rockets, Part I," JET PROPULSION, vol. 24, Jan.-Feb. 1954, p. 28.

4 Geckler, Richard D., "Unsolved Problems in Solid-Propellant Combustion," Fifth Symposium (International) on Combustion, Reinhold, New York, 1955, p. 35.

5 Green, Leon, Jr., "Unstable Burning of Solid Propellants," JET PROPULSION, vol. 24, July-Aug. 1954, p. 252.

6 Green, Leon, Jr., "Observations on the Irregular Reaction of Solid Propellant Charges," JET PROPULSION, vol. 26, Aug. 1956, p. 657.

7 Green, Leon, Jr., "Studies on the Reaction Stability of Solid Propellant Charges," Aerojet-General Corp. Report 1077, AFOSR-TR-56-10, 1956, p. 7.

A Preliminary Study of Vortex-Boiling Burnout Heat Fluxes

W. R. GAMBILL[1] and N. D. GREENE[2]

Oak Ridge National Laboratory,[3] Oak Ridge, Tenn.

Nomenclature

A_i = internal surface area of test section, ft²
D_i = internal diameter of test-section tube, in.
L = test section heated length, in.
P_f = power required for fluid flow across test section, hp
P_q = power corresponding to heat absorption rate q, hp
ΔP = test section pressure drop, psi
q = rate of heat transfer, Btu/hr
V = axial fluid velocity, fps
W = water weight flow rate, lb/hr
x = steam quality at test section exit, per cent by weight
ρ_L = liquid density evaluated at exit temperature, lb/ft³

Subscripts

b = burnout condition
i = internal

Received Dec. 12, 1957.

[1] Development Engineer.

[2] Development Engineer.

[3] Operated by Union Carbide Nuclear Co. for the Atomic Energy Commission.

RECENT experiences with source-vortex flow of fluids (air and water) in forced-convection heating without boiling (to be published) led the authors to believe that this type of flow field might be especially advantageous in a boiling system. By "source-vortex flow" is meant fluid flow with both axial and tangential velocity components; more specifically, it refers in the present instance to the flow of a swirling or whirling fluid from one end of a tube to the other. With source-vortex flow, steam bubbles formed at the inner surface of the heated tube wall are surrounded by a rapidly rotating body of liquid of much higher density, and the gravitational acceleration arising from the vortex motion would be expected to cause a much stronger inward radial displacement

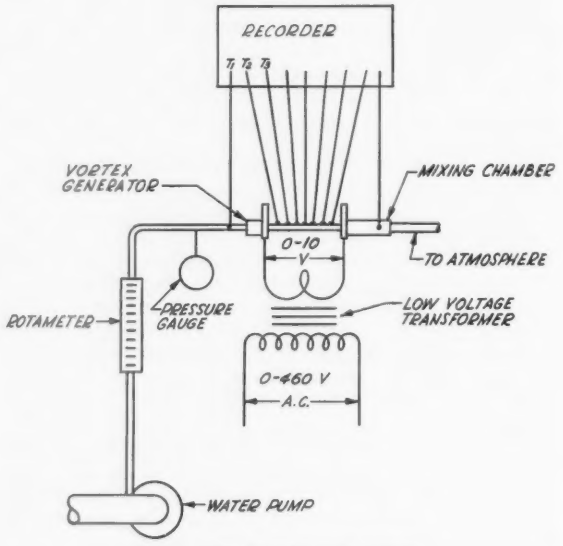

Fig. 1 The experimental system

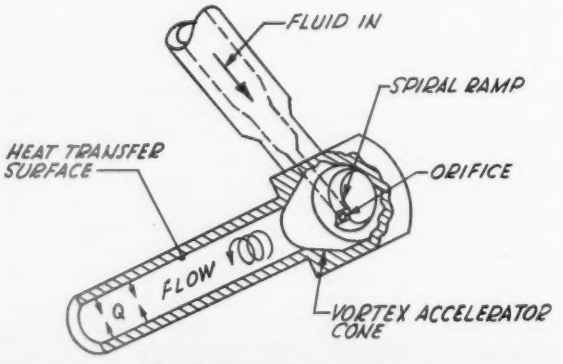

Fig. 2 The vortex generator

Table 1 Results of Investigation

Run	Voltage variation	Axial velocity, fps	Degree of subcooling at exit, °F	Inlet static pressure, psig	Test Section					x, exit quality, %	$\left(\frac{P_f}{P_q}\right)\%$	$(q/A_i)_b$, Btu/hr-ft²
					ID, in.	OD, in.	Heated length, in.	L/D_i	Material			
1	Step taps	12.1	36	93	0.275	0.300	3.063	11.14	Copper	0.0	0.26	5,940,000
2	Variacs	11.8	0	94	0.275	0.300	3.187	11.60	Copper	1.24	0.19	8,240,000
3	Variacs	12.35	0	99	0.275	inlet—0.2875 exit—0.300	2.875	10.44	Copper	1.49	0.20	9,690,000
4	Variacs	13.61	72	100	0.250	0.300	1.20	4.80	Inconel	0.0	0.43	10,980,000
5	Variacs	13.18	135	248	0.300	0.375	3.05	10.16	Copper	0.0	0.37	8,630,000
6	Variacs	16.3	150	248	0.250	inlet—0.270 exit—0.281	2.25	9.00	Inconel	0.0	0.39	10,810,000
7	Variacs	24.0	49	285	0.250	inlet—0.270 exit—0.278	1.625	6.50	Inconel	0.0	1.01	17,250,000

of bubbles away from the inner wall toward the tube center than in the case of linear liquid motion. Were this effect sufficiently strong, the inner surface would be freer of bubbles at a given heat flux than in standard straight-through flow, thereby permitting the attainment of a greater peak flux before burnout. These considerations led the authors to carry out the study described herein. The large measured heat fluxes empirically demonstrate the qualitative validity of these early concepts.

A schematic representation of the experimental system is given as Fig. 1. The test-section inlet, shown as Fig. 2, consisted of a spiral-ramp fluid introduction zone followed by a convergent cone section which accelerates the rotation rate of the water through reduction of radius. This same vortex generator, with orifice diameter of 0.104 in., was used with all of the test section tubes. The available flow rates, in conjunction with the design of the vortex generator, permitted the attainment of several thousand gravities (calculated) at the test section inlet. The resistance-heated, thin-walled tubes (of copper or Inconel) were cooled by the vortex water flow within them.

The tubes for runs 3, 6 and 7 were tapered, possessing thinner walls at the inlet than at the exit. The use of this geometry was motivated by an attempt to more efficiently utilize the greater circulation in the freshly formed vortex at the test section inlet by generating more power in this zone, and reducing the power generation with length to at least qualitatively match the decreasing vorticity of the water flow. This sort of variation of heat-generation rate with length is similar to that obtainable by selective placement of fuel in a nuclear reactor. It might be noted here that in all tests about four tube diameters separated the inlet orifice and the initial heated portion of the test section, so that some vortex decay had taken place before heating began.

The degree of subcooling listed is the minimum for the system (at exit conditions) and is equal to the saturation temperature of water at the exit static pressure (always just above atmospheric, except in run 6) minus the actual exit water temperature. The inlet static pressure was measured at the small orifice of the vortex generator at the tube inlet.

The results of this investigation are summarized in Table 1[4] for the seven experiments believed to be of highest accuracy (estimated maximum over-all error in burnout heat flux of ±10 per cent, probable error of 3 to 4 per cent).

The quantity designated (P_f/P_q) per cent represents the ratio of calculated power required to force the water through the test section to the rate of heat absorption by the water at the burnout point, expressed in the same power units. This was calculated from

$$P_f = \frac{W\Delta P}{13{,}750\ \rho_L}\ \text{hp} \qquad [1]$$

and

$$P_q = \frac{(q_{\text{total}})_b}{2545}\ \text{hp} \qquad [2]$$

The flow in all tests exhibited high stability right to the burnout point, and the system could apparently be operated indefinitely a few per cent below the burnout condition.

The heat fluxes reported in this paper are extremely large for the conditions of operation; in fact, at least five times greater than any values previously reported for comparable system conditions. The largest experimental values of burnout heat flux that have been reported in the literature, to the knowledge of the authors, for flow through straight, round tubes, are those of Rohsenow and Clark (1)[5] (3.1×10^6 Btu/hr-ft² for water at 2000 psia, 30 fps, 240 F average subcooling, and $L/D = 52$), and of Buchberg et al. (2) (3.8×10^6 Btu/hr-ft² for water at 507 F exit temperature, 44 fps, 236 F exit subcooling, and $L/D = 110$). This latter value corresponds to about 5.3×10^6 Btu/hr-ft² for $L/D = 7$, according to the approximate rule that halving L/D increases $(q/A_i)_b$ by ~10 per cent (3). The highest value for any geometry or experimental conditions is apparently that of Gunther (4), who obtained 11.4×10^6 Btu/hr-ft² for water at 114 psia exit pressure, 40 fps, and 256 F subcooling at exit. Gunther obtained his values with a thin (0.004 in.) electrically heated metal strip in a rectangular channel of $L/D_e = 6$; the strip was cooled from both sides. Since Gunther's values are consistently among the highest reported in the literature, a comparison of our run 4 and his test 5, for which conditions are almost identical, is revealing (see Table 2).

Were all of Gunther's experimental conditions identical with those of our run 4, it is estimated that his $(q/A)_b$ would be 2.3×10^6 Btu/hr-ft², which gives a 377 per cent higher peak heat flux for the vortex case. When comparisons are made with other literature data, the advantage becomes more nearly 500 per cent for the vortex case.

It might be noted that the burnout heat flux for run 7 corresponds to an average volumetric heat release rate within

---

[4] Added in proof: Burnout heat fluxes for runs 2 to 7 of Table 1 (Variac control) have been empirically correlated, with a 4.8% average error, by

$$(q/A_i)_b = (15{,}750\ V^2 + 8{,}070{,}000)(1.18 - 0.03\ L/D_i)$$

For the bulk exit subcooling range of 0 to 150 F, there was only a very small dependence of $(q/A_i)_b$ on degree of subcooling.

Recent preliminary comparisons on an over-all power expenditure basis indicate that linear and vortex flow patterns will give approximately equal burnout fluxes at equal flow power in the low flow power range, but that vortex boiling exhibits an increasing superiority with increase of flow input power.

[5] Numbers in parentheses indicate References at end of paper.

Table 2

	Gambill-Greene Run 4	Gunther (4) Test 5
Axial water velocity, fps	13.6	12.3
P_{exit}, psia	15.0	14.4
Subcooling at exit, °F	72	71
L/D_e	4.8	6[a]
$(q/A)_b$, Btu/hr-ft²	10.98×10^6	2.0×10^6

[a] Based on hydraulic diameter of ½ in. given by Gunther (4).

the tube wall of about 173 kw/cc, based on water heat absorption alone.

The ascending magnitude of burnout heat flux with run number (Table 1) is primarily attributable to improvements in experimental technique as more was learned of the nature of the process of burnout in this new flow system. Run 2, e.g., gives a $(q/A)_b$ greater than that in run 1 because a transition was made from the use of step transformer taps for voltage control to Variacs, by which power level could be increased gradually and smoothly rather than by finite increments only. The result is still higher in run 3 because of slower Variac adjustment as a result of having learned the approximate burnout point from run 2. Another factor tending to further increase burnout heat flux in run 3 was the use of the tapered-wall test section, which provided an area for electrical current flow at inlet about half that at the exit. The calculated heat flux at the inlet for the burnout condition is 14.8×10^6 Btu/hr-ft² for this run. The further increase in $(q/A)_b$ of run 4 is primarily associated with the reduction of L/D from ~10 to ~5.

In run 5, the tube (thick-walled copper) probably failed because of a combination of undesirable mechanical stress conditions that existed. Runs 6 and 7 serve as the basis of one important conclusion that has been reached concerning the relative importance of the pertinent variables. In run 6, the exit pressure was held at a constant 100 psig but the burnout flux showed little change, except as expected from differences in velocity and L/D, from that of run 4. In run 7, exit pressure was reduced to atmospheric, a maximum inlet pressure was attained, and the effect of the greater velocity showed up in a much greater burnout flux. This comparison indicates that the velocity effect is more important than any pressure level effects. This is to be expected, since, in the case of a vortex, increased circulation or vorticity also brings about greater static pressure of the fluid at the wall, greater local degree of subcooling, and possibly greater radial bubble migration.

Heat flux at the inlet (zero length) of the tapered tube of run 7 is computed to be 20.9×10^6 Btu/hr-ft² at the burnout condition.

Burnout in run 7 was prematurely triggered by a small temporary decrease in water flow. The water circuit used in all tests was open and subject to small fluctuations in supply pressure.

The large heat fluxes obtained for the case of net steam generation, runs 2 and 3 of Table 1, suggest another possible advantage of vortex boiling—that any gas released or vapor generated will be transported to the center of the tube where it will do the least harm. This action occurs to some extent in linear flow because of Bernoulli forces, but many investigators have nevertheless concluded that greater amounts of dissolved gas will decrease peak flux in subcooled boiling with linear flow.

Some idea of the excessive velocities required in standard axial flow systems for attainment of these high heat fluxes can be obtained from the following comparison. Both Buchberg (2) and Gunther (4) indicate that for constant subcooling and pressure in a given tube

$$(q/A)_b \propto V^{0.5} \quad [3]$$

By a correlation proposed by Gunther (4) the $(q/A)_b$ to be expected for axial flow under the conditions of our run 7 is 1.68×10^6 Btu/hr-ft². The vortex value of 17.25×10^6 is 10.27 times greater and, by Equation [3], a linear velocity of $(24)\ (10.27)^2 = 2540$ fps would be required to attain 17.25×10^6 for an exit subcooling of 49 F.

In practice, of course, this velocity would be neither available nor necessary, since the high pressure required would at the same time increase the subcooling and thus decrease the required velocity. Nevertheless, the comparison does illustrate the variation required in the velocity variable alone.

A new heat-transfer mechanism apparently is acting in vortex boiling, and the high fluxes obtained are by no means due solely to higher velocities and degrees of subcooling at the wall. The burnout fluxes obtained are much larger than values calculated for linear flow even when the orifice velocity (maximum tangential in the system) is used in available burnout equations. All comparisons and analyses point to the existence of some mechanism such as postulated previously.

The burnout values presented here can quite likely be increased to considerably higher levels by the use of greater velocities, pressures and degrees of subcooling, all of which decrease the maximum attainable bubble size and increase the burnout heat flux. None of the conditions of the present study (except L/D) approach the optimum for maximum $(q/A)_b$, which further emphasizes the immense heat fluxes possibly attainable.

An effort will be made to extend this study of heat-transfer effects within a vortex flow field to other ranges of experimental variables. It is felt that a $(q/A)_b$ value of 40,000,000 Btu/hr-ft² is not unattainable, and that further refinements of experimental technique may be expected to reduce the maximum error for $(q/A)_b$ to below ±5 per cent. Further studies will involve determination of more than $(q/A)_b$ and the additional data will permit an attempt to formulate a generalized correlation.

Further results will be published as they are produced.

References

1 Rohsenow and Clark, "Heat Transfer and Pressure Drop Data for High Heat Flux Densities to Water at High Sub-Critical Pressures," Heat Transfer and Fluid Mechanics Institute Reprints, 1951, pp. 193–207.

2 Buchberg et al., "Heat Transfer, Pressure Drop, and Burnout Studies With and Without Surface Boiling for De-aerated and Gassed Water at Elevated Pressures in a Forced Flow System," Heat Transfer and Fluid Mechanics Institute Reprints, 1951, pp. 177–191.

3 Griffith, P., MIT, personal communication, Sept. 1957.

4 Gunther, "Photographic Study of Surface-Boiling Heat Transfer to Water with Forced Convection," *Trans. ASME*, vol. 73, 1951, pp. 115–123.

Burning Rate Studies. III. Correlation of Experimental Results With the Thermal Model

D. L. HILDENBRAND[1] and W. P. REID[2]

U. S. Naval Ordnance Test Station, China Lake, Calif.

Received Nov. 22, 1957.

[1] Physical Chemist, Research Department. Present address: Thermal Laboratory, The Dow Chemical Co., Midland, Mich.

[2] Mathematician, Research Department. Present Address: Michigan State University, East Lansing, Mich.

Condensed phase temperature distributions, experimentally determined for several burning liquid systems, have been compared with distributions predicted for various modifications of the thermal combustion model. Reasonably good agreement exists between the theory and experiment, and the results have been analyzed with respect to the relative importance of various types of heat production. In general, the temperature distribution can be largely accounted for by thermal conduction alone. The effects of radiation absorption and chemical reaction are discussed.

Introduction

PREVIOUS papers (1,2)[3] in this series have dealt with the measurements of the combustion wave temperature distribution in burning liquid systems and the application of the method to a fundamental study of the mechanism of combustion. This paper describes a portion of these studies in which the experimental condensed phase temperature profiles are compared with those expected for a thermal model of the combustion process, i.e., one in which the flow of heat is the process of primary importance.

According to the thermal theory, the temperature at any point in the condensed phase of a burning system is determined by three possible processes: The conduction of heat, the absorption of radiation from hot gases above the surface, the generation (or absorption) of heat by chemical reaction.

The desired procedure would be to describe the situation in mathematical terms and then to inspect the resulting expressions for the distribution of temperature. Unfortunately, the presence of the chemical reaction term gives rise to a nonlinear differential equation, which must be solved to obtain the temperature distribution. Because of this nonlinearity, one cannot obtain an analytical solution giving the temperature as an explicit function of distance. Numerical solutions of this equation have been obtained by Olds and Shook (3), and an analysis of their results indicates that the chemical reaction term influences the over-all temperature distribution only in the region extremely close to the burning surface. For example, a numerical solution containing a chemical term of $13.6 \times 10^{16} \exp(-35400/RT)$ cal cm^{-3} sec^{-1}, a surface temperature of 450 C, an initial temperature of 20 C, a thermal diffusivity of 6.9×10^{-4} cm^2 sec^{-1} and a burning rate of 1.0 cm sec^{-1} showed that the effect of the chemical term was felt only at temperature above 420 C.

The major portion of the temperature-distance curve (covering the region from 20 to 420 C) could, however, be fit quite accurately by solutions to the above heat flow problem obtained by considering only heat conduction and radiation absorption. The nature of this "conduction-radiation" solution has been described by Reid (4). It thus appears that useful information about the radiation and conduction parameters may be obtained by comparing the experimental temperature-distance curves with the "conduction-radiation" solutions. The method used in making this comparison follows.

The Curve-Fitting Method

The experimental profile data were obtained by having a liquid burn past a thermocouple, as described in (1). From the observed liquid consumption rate and the thermocouple readings, one has values for the temperature at different distances from the burning surface. Attempts were made to fit the data so obtained by means of functions of the sort

$$T = Ae^{-\beta x} + Be^{-\gamma x} + C \quad \ldots\ldots [1]$$

$$T = Ae^{-\beta x} + C \quad \ldots\ldots [2]$$

From (4) it is seen that

$$A = \left(T_0 - T_\infty + \frac{I}{\rho c(h^2\alpha - v)}\right) \qquad B = -\frac{I}{\rho c(h^2\alpha - v)}$$

$$\beta = \frac{v}{h^2} \qquad C = T_\infty \qquad \gamma = \alpha$$

[3] Numbers in parentheses indicate References at end of paper.

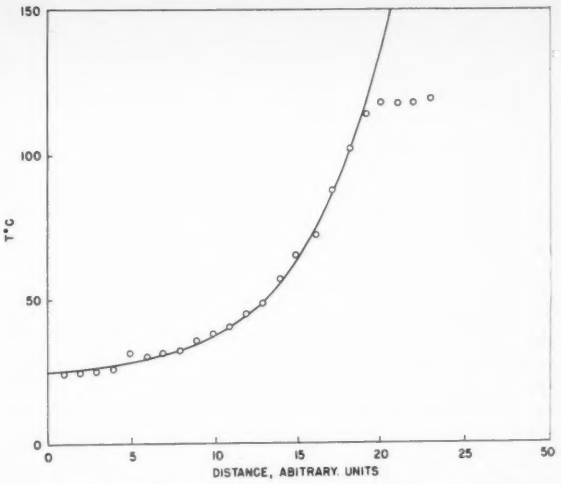

Fig. 1 "Best fit" to the ethyl nitrate data at 7.7 atm

where T_0 is the maximum temperature, T_∞ is the initial temperature, I is the radiation intensity at the burning surface, α is the radiation absorption coefficient, h^2 is the thermal diffusivity, v is the liquid consumption rate, and ρ and c are density and specific heat, respectively.

The temperature distribution is given by Equation [1] when heat conduction and radiation absorption are the contributing factors, and by Equation [2] when there is heat conduction alone.

The procedure used in attempting to fit the data by the above functions was to consider first a series of points well below the surface and obtain a best fit (in the least square sense) by means of Equation [2]. The curve fitting was then extended to progressively higher temperatures so as to include points closer and closer to the surface. For each set of points a curve was obtained, and the sum of the squares of the deviations of the points from the curve was calculated. Upon dividing this value by $N - 1$ (where N is the number of points) and taking the square root, one obtains the rms (root mean square) error. This value was used to measure how well the equation fit the data. An excellent fit could usually be obtained when just points well away from the burning surface were used. In addition, good fits could sometimes be obtained almost up to the burning surface. The results obtained with ethyl nitrate at lower pressures, for instance, were of this type. In some cases the fit to the data by means of Equation [2] became unsatisfactory when too many points were included. In these cases it was found that the use of Equation [1] made it possible to obtain a better fit over a wider range of points.

From the mathematical standpoint, it is not easy to obtain a best fit of a set of points by means of a sum of two exponentials. Several procedures were tried before a satisfactory one was found. The method used was as follows: First trial values for β and γ were taken, and with them "best" values for A, B and C were determined by the method of least squares. Values for T were then computed at each point by means of Equation [1] and compared with the experimental data. Again, the rms error was used as a measure of how well the curve fit the data. The trial values of β and γ were then systematically varied until a minimum value of the rms error was obtained. That is, the β and γ were such that if either was increased or decreased, the rms error would increase. The curve obtained with these values for β and γ was considered to be the "best" fit in the least square sense. Fortunately a high speed electronic computer (IBM 701) was available for the calculations. A sample fit is shown in Fig. 1. The circles are experimental points and the heavy line represents the calculated curve.

Table 1 Curve-fitting the ethyl nitrate data

Pressure, atmosphere	Cons. rate, cm sec^{-1}	Equation fitted	β, cm^{-1}	$h^2 \times 10^4$, cm^{2}sec^{-1}	rms error, °C
4.3	0.028	[2]	34.4	8.1	2.3
7.7	0.052	[2]	73.1	7.1	2.2
11.1	0.083	[2]	140	5.9	2.2
14.5	0.122	[1]	164	7.4	1.0

Results and Discussion

Ethyl nitrate data. The extent to which the ethyl nitrate condensed phase profiles obtained at various combustion pressures can be fitted by Equation [1 or 2] is shown in Table 1. Shown from left to right are the combustion pressure, the liquid consumption rate, the equation to which the data were fitted, the value of the parameter β obtained from the curve-fitting, the thermal diffusivity calculated from β and the rms error. In deciding whether to fit the data with Equation [1 or 2], the curve-fitting was considered adequate whenever the rms error was less than 3 deg. This estimate was based on a consideration of the reproducibility of a given set of experimental results.

It can be seen that up to a combustion pressure of 11.1 atm, the measured temperature distributions can be satisfactorily fitted by the single exponential or "conduction only" solution. At all four pressures, essentially the entire liquid phase profile can be fitted. Although it appears to be necessary to bring in the radiation term at the highest pressure, an analysis of the data shows the rms error to be extremely sensitive to small changes in the conduction parameter, but relatively insensitive to changes in the radiation parameter. Thus the temperature distributions, even at 14.5 atm, can be accounted for primarily by thermal conduction, with radiation absorption being a second order effect, at best. For this reason, no significance is attached to the calculated values of the radiation parameters, although they appear to be of the correct order of magnitude.

A further check on the validity of the curve-fitting method can be made by comparing the predicted thermal diffusivity values, as in Table 1, with values obtained by independent measurement. An analysis of twelve sets of profile data obtained at various combustion pressures gave values for h^2 that agreed to within 15 per cent and for which an average value of 7.1×10^{-4} cm^2 sec^{-1} was obtained. Combining this value with an average specific heat (5) of 0.45 cal g^{-1} deg^{-1} and an average density (5) of 1.05 g cm^{-3}, one obtains a predicted value of 3.4×10^{-4} cal cm^{-1} sec^{-1} deg^{-1} for the thermal conductivity of liquid ethyl nitrate. The average value of the thermal conductivity over the temperature range involved, as obtained by direct measurement (6) is 4.7×10^{-4} cal cm^{-1} sec^{-1} deg^{-1}. Considering the error involved in the temperature profile work, the agreement between the predicted and observed thermal conductivities is felt to be satisfactory and would indicate that the experimental results are compatible with the thermal theory.

Table 2 Curve-fitting the metriol trinitrate data

T_0, °C	rms error, Equation [1], °C
187	1.8
208	2.0
226	2.2
242	2.8
256	3.7
264	4.6
271	5.8

Metriol trinitrate data. In treating the temperature data obtained on the metriol trinitrate[4] (82 per cent)-triacetin[5] (18 per cent) system at a combustion pressure of 34.9 atm, only the portion of the profile below about 240 deg can be fitted satisfactorily. The surface temperature is about 290 deg. Table 2 shows the way in which the rms error begins to diverge when the data are fitted to Equation [1] and the curve-fitting is extended toward the surface. Given in the table are the maximum temperature attained in the curve-fitting and the rms error. When the data were fitted to the "conduction only" solution, rms errors of 3.0 and 4.6 deg resulted at T_0 values of 187 and 208 deg. Even so, an analysis of the variation in the rms error with small changes in β and γ indicates, as before, that the shape of the profile is determined largely by thermal conduction and that radiation absorption is, at most, a second order effect.

The data of Table 2 are in qualitative agreement with the results of a series of thermal stability measurements made on the metriol trinitrate mixture. For these observations, the liquid sample was pressurized to 35 atm in the combustion chamber and temperature-time curves were recorded as the liquid was heated at varying rates with stirring. In all cases, rapid self-heating due to exothermic chemical reaction occurred at temperatures of 190–210 deg. Thus the failure of Equation [1] to fit the profile data above 240 deg can be accounted for on the basis of interference from chemical reaction.

Here also a comparison can be made between the liquid thermal conductivity value predicted from the curve-fitting and that obtained by direct measurement. An analysis of four separate sets of profile data obtained at 34.9 atm gave values for the thermal diffusivity agreeing to within 8 per cent, the average being 6.7×10^{-4} cm^2 sec^{-1}. Combining this value with an average specific heat (5) of 0.43 cal g^{-1} deg^{-1} and an average density (5) of 1.20 g cm^{-3}, one obtains a predicted thermal conductivity of 3.5×10^{-4} cal cm^{-1} sec^{-1} deg^{-1}. The average value of the liquid thermal conductivity over the temperature range of interest, as obtained by direct measurement (5), is 3.2×10^{-4} cal cm^{-1} sec^{-1} deg^{-1}. Again, the comparison indicates that the experimental data are in reasonable agreement with the thermal theory.

Acknowledgment

The authors are indebted to C. H. Shomate for supplying the specific heat data on the nitrate esters.

References

1 Hildenbrand, D. L., Whittaker, A. G., and Euston, C. B., *Journal of Physical Chemistry*, vol. 58, 1954, p. 1130.

2 Hildenbrand, D. L., and Whittaker, A. G., *Journal of Physical Chemistry*, vol. 59, 1955, p. 1024.

3 Olds, R. H., and Shook, G. B., U. S. Naval Ordnance Test Station, Tech. Memo. 917, 1952.

4 Reid, W. P., *Journal of Physical Chemistry*, vol. 57, 1953, p. 242.

5 Unpublished measurements, U. S. Naval Ordnance Test Station.

6 Hildenbrand, D. L., and Happe, J. A., *Journal of Physical Chemistry*, vol. 61, 1957, p. 1415.

[4] Methyl trimethylolmethane trinitrate.

[5] Glycerol triacetate.

Technical Comments

Terminology in Rocket Combustion Instability

E. W. PRICE[1]

U. S. Naval Ordnance Test Station, China Lake, Calif.

THE problem of oscillatory performance of rocket motors has been studied and discussed to some extent during the past 15 years by every agency in the rocket business. The isolated nature of the various studies has lead to a diversity of terminology which often results in misinterpretation of the reported information, e.g. (1,2).[2] This is further complicated by the fact that much of the terminology was established in the early days when knowledge of the phenomenon was little more than speculation. Confusion continues to be injected into the issue by the fact that the majority of measurements are made by instruments which are unresponsive to the rapid oscillations which occur during combustion instability. In view of this situation, some clarification of terminology seems in order. The remarks below on this subject pertain primarily to solid propellant rockets, although the situation is much the same with liquid propellant rockets.

The phenomenon of combustion instability with solid propellants is advantageously viewed as consisting of two major aspects. The first is the self-excited oscillation of the gas flow-combustion system. The second aspect is the "cumulative effect" of this oscillatory phenomenon on the mean burning rate of the solid propellant (averaged over several cycles of oscillation). The first aspect is referred to as "sonance" by Green (3), and is referred to as "dynamic instability" by Cheng (4).

The terminology "resonance" was originally applied to the combustion instability phenomenon at a time when actual oscillations had not been successfully measured. Thus the term "resonance" was introduced because of a speculation that oscillatory behavior was present, but was in practice associated primarily with very different, low-frequency measurements properly involving the second aspect of combustion instability noted above. It may end up that this trend toward application of the term "resonance" to the mean burning rate aspect of the problem was fortunate, since it is not accurate when applied to the self-excited oscillations,[3] and since recent work by Green (3) suggests that the mean burning rate effect may actually be a true resonance phenomenon between the oscillating gas phase system (forcing function) and the "natural frequency" of the solid phase combustion process determined by the reciprocal of the time lag of the solid phase process. At present the terms "resonance" and "resonant burning" are widely and indiscriminately applied to all aspects of combustion instability.

The terminology "combustion instability" or "unstable burning" has become increasingly evident. Its meaning is sufficiently vague and general to avoid actual *incorrect* interpretation. However, it implies that it is the combustion that is unstable, whereas, it is the interaction between the combustion and the flow oscillations that is actually unstable. By selective reference to the combustion, this terminology is misleading, and blocks the way to subsequent terminology distinguishing the high speed and the low speed aspects of the phenomenon mentioned above.

In the case of solid propellant rocket motors, the oscillatory phenomena occur at very high frequencies (pressure oscillations higher than 50 kc have been observed), and the pressure sensing and recording equipment used in routine testing is usually unresponsive to these high frequencies. As a result, only the effect (if there is any) due to the change in mean burning rate is detected. This often leads to failure to detect combustion instability, or erroneous identification of other performance anomalies with combustion instability. The resulting looseness in meaning and interpretation further confuses the meaning of combustion instability. In view of this situation it is undoubtedly wise to use increased discretion in interpretations of test results and wording in the description of results and interpretations. This writer does not consider any of the terminologies currently in use to be accurately descriptive of the phenomenon and at the same time unambiguous with respect to the aspect of the phenomenon. It is suggested that terminology be sought which covers the three concepts indicated in the diagram below.

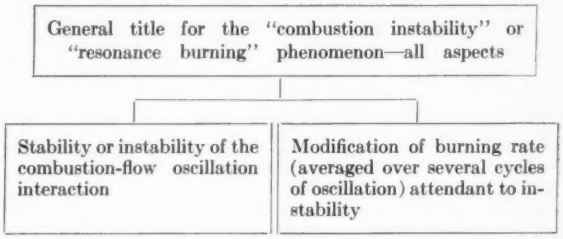
General title for the "combustion instability" or "resonance burning" phenomenon—all aspects
Stability or instability of the combustion-flow oscillation interaction
Modification of burning rate (averaged over several cycles of oscillation) attendant to instability

Received Dec. 16, 1957.

[1] Physicist. Head, Fluid Dynamics Branch, Research Department. Mem. ARS.

[2] Numbers in parentheses indicate References at end of paper.

[3] Resonance is a concept which applies to systems with forced oscillations rather than self-excited ones (5).

References

1 Green, Leon, Jr., "Unstable Burning of Solid Propellants," JET PROPULSION, vol. 24, July-Aug. 1954, p. 252.

2. Cheng, Sin-I, "On Unstable Burning of Solid Propellants," JET PROPULSION, vol. 25, Feb. 1955, p. 79.

3 Green, Leon, Jr., "Non-Steady Behavior of a Simplified Model of Solid-Propellant Burning," Aerojet-General TN-15, OSR-TM-55-475, Nov. 1955.

4 Cheng, Sin-I, personal communication.

5 Hartog, Den, Pieter, Jacob, "Mechanical Vibrations," McGraw-Hill, New York, 1947, 3rd edit., Chap. 7.

A Remark on the Free Vibration of a Variable Mass

GEORGE LEITMANN[1]

University of California, Berkeley, Calif.

Nomenclature

M = mass of body (tank)
M_0 = initial mass of body
$\mathbf{r}_c$ = position vector of center of mass of body relative to an inertial reference system
$\mathbf{R}_c$ = position vector of center of mass of body relative to a reference system fixed in the invariant part of the body (body system)

Received Nov. 21, 1957.

[1] Assistant Professor of Engineering Science, Department of Engineering.

$\mathbf{R}_L$ = position vector of "effective center" of exit surface relative to body system
$\mathbf{l}$ = $\mathbf{R}_c - \mathbf{R}_L$
$\boldsymbol{\omega}$ = angular velocity of body system
$\mathbf{F}$ = resultant of external forces
$\mathbf{V}_e$ = exit velocity (of out-flowing mass) relative to body system
t = time
d/dt = differentiation with respect to time in inertial system
$\partial/\partial t$ = differentiation with respect to time in body system
x = linear displacement of mass center of body

IN A recent note in this Journal, Miesse (1)[2] discussed the solution of a differential equation which was to describe the free vibration of a variable mass, a tank in which the mass of liquid decreases linearly with time. However, the basic equation, Equation [1] of (1), is incorrect for two reasons:

1 The linear momentum of a body of variable mass, i.e., of a body which loses mass across a portion of its bounding surface is not merely $M(d\mathbf{r}_c/dt)$, (2 and 3), but is given by

$$M\frac{d\mathbf{r}_c}{dt} + \mathbf{l}\frac{dM}{dt}$$

2 Newton's Second Law, which was originally stated for particles, cannot be applied directly to a variable mass such as the one under study. A correct application of Newton's Second Law, as used in (2 and 3), yields the equation of motion

$$M\frac{d^2\mathbf{r}_c}{dt^2} = \mathbf{F} - \mathbf{l}\frac{d^2M}{dt^2} + \left[\mathbf{V}_e - 2\boldsymbol{\omega}\times\mathbf{l} + \frac{\partial\mathbf{R}_L}{\partial t} - 2\frac{\partial\mathbf{R}_c}{\partial t}\right]\frac{dM}{dt} \quad \ldots\ldots[1]$$

The second of these reasons is probably the more important one.

If it is assumed that the "effective center" of the exit surface and the center of mass of the body are stationary in the body system

$$\frac{\partial\mathbf{R}_L}{\partial t} = \frac{\partial\mathbf{R}_c}{\partial t} = 0$$

If, in addition, the body system does not rotate relative to the inertial system

$$\boldsymbol{\omega} = 0$$

Then for linear mass flow

$$M\frac{d^2\mathbf{r}_c}{dt^2} = \mathbf{F} + \mathbf{V}_e\frac{dM}{dt} \quad \ldots\ldots[2]$$

Equation [2] also results under the assumption that the linear momentum of the body is approximated by $M d\mathbf{r}_c/dt$, (4). If now

$$\mathbf{V}_e\frac{dM}{dt} \ll \mathbf{F}$$

then for the one-dimensional case

$$M(t)\frac{d^2x}{dt^2} = F = -\left(Kx + c\frac{dx}{dt}\right) \quad \ldots\ldots[3]$$

which differs from Equation [1] of (1) by the term $(dM/dt)\cdot(dx/dt)$. Equations [3 and 6] of (1) then become, respectively

$$u\ddot{x} - \frac{Gc}{M_0}\dot{x} + \frac{KG^2}{M_0}x = 0 \quad \ldots\ldots[4]$$

$$v^2f'' - vf' + (v^2 - p^2 - 2p)f = 0 \quad \ldots\ldots[5]$$

References

1 Miesse, C. C., "The Free Vibration of a Variable Mass," JET PROPULSION, vol. 27, Oct. 1957, p. 1103.

2 Rankin, R. A., "The Mathematical Theory of the Motion of Rotated and Unrotated Rockets," *Philosophical Transactions of the Royal Society of London*, Series A, vol. 241, 1949, p. 457.

3 Leitmann, G., "On the Equation of Rocket Motion," *Journal of the British Interplanetary Society*, vol. 16, 1957, p. 141.

4 Sibert, H. W., "Relation of Force, Acceleration, and Momentum of a Body Whose Mass Is Varying," *Journal of the Aeronautical Sciences*, vol. 20, 1953, p. 141.

[2] Numbers in parentheses indicate References at end of paper.

On the Free Vibration of a Variable Mass

J. J. MARCINEK[1]

Convair Division of General Dynamics Corp., Pomona, Calif.

IN OCTOBER 1957 JET PROPULSION, C. C. Miesse (1)[2] presented work on the free vibration of a variable mass. In establishing the force balance for the system, Newton's Second Law was used incorrectly. The Second Law, as commonly stated, applies only to mass conservative systems.

In a variable mass system momentum changes are the result of (a) velocity changes caused by the impressed force and (b) mass changes that add or remove momentum of the system. Thus:

time rate of (system momentum change + momentum entering or leaving system) = force

A formal explanation and proof can be obtained in (2).

Using Miesse's nomenclature throughout, the force equation for a vibrating system of decreasing mass is

$$Kx + c\frac{dx}{dt} = -\frac{d}{dt}M_0\left(1 - \frac{t}{G}\right)\frac{dx}{dt} - \dot{m}\frac{dx}{dt} \quad \ldots\ldots[1]$$

where

$$\dot{m} = \frac{M_L}{T} = \frac{M_0}{G}$$

so that

$$Kx + c\frac{dx}{dt} = -M_0\left(1 - \frac{t}{G}\right)\frac{d^2x}{dt^2} \quad \ldots\ldots[2]$$

Substituting

$$v = 2G\sqrt{\frac{K}{M_0}\left(1 - \frac{t}{G}\right)} \quad \ldots\ldots[3]$$

$$x = v^{p+1}f(v) \quad \ldots\ldots[4]$$

into Equation [2] results in

$$v^2f'' + vf' + [v^2 - (p+1)^2]f = 0 \quad \ldots\ldots[5]$$

for which the solution is

$$f = AJ_{p+1}(v) + BY_{p+1}(v) \quad \ldots\ldots[6]$$

which differs from Miesse's solution by one order.

The frequency approximation, Equation [20] of (1), is then written as

$$f \approx \frac{1}{2\pi}\sqrt{\frac{K}{M}}\left[1 - \frac{4(p+1)^2 - 1}{8v^2}\right] \quad \ldots\ldots[7]$$

More important, the amplitude variation for large values of

Received Nov. 27, 1957.

[1] Thermo-Mechanics Group Supervisor. Mem. ARS.

[2] Numbers in parentheses indicate References at end of paper.

v is (Equation [22] of (1))

$$v^{p+1}J_{p+1}(v) \leq \sqrt{\frac{2}{\pi}}\, v^{p+(1/2)} \quad \ldots\ldots\ldots\ldots [8]$$

Therefore the amplitude will decrease with time for all positive values of p. The amplitude can only increase if p is a velocity-dependent forcing function with a value less than $-\frac{1}{2}$.

For the case of the system to which mass is added, Equation [1] becomes

$$Kx + c\frac{dx}{dt} = -M_0\left(1 + \frac{l}{G}\right)\frac{d^2x}{dt^2} \quad \ldots\ldots\ldots [9]$$

If now

$$v = 2G\sqrt{\frac{K}{M_0}\left(1 + \frac{l}{G}\right)} \quad \ldots\ldots\ldots\ldots [10]$$

and

$$x = v^{1-p}f(v) \quad \ldots\ldots\ldots\ldots [11]$$

then Equation [9] becomes

$$v^2f'' + vf' + [v^2 - (p-1)^2]f = 0 \quad \ldots\ldots\ldots [12]$$

The approximate frequency is then given as

$$f \approx \frac{1}{2\pi}\sqrt{\frac{K}{M}}\left[1 - \frac{4(1-p)^2 - 1}{8v^2}\right] \quad \ldots\ldots\ldots [13]$$

The amplitude variation is obtained as

$$v^{1-p}J_{1-p}(v) \leq \sqrt{\frac{2}{\pi}}\, v^{(1/2)-p} \quad \ldots\ldots\ldots\ldots [14]$$

Since v increases with time in this case, the amplitude of the oscillations will decrease for values of $p > \frac{1}{2}$, and increase for $p < \frac{1}{2}$.

References

1 Miesse, C. C., "The Free Vibration of a Variable Mass," JET PROPULSION, vol. 27, Oct. 1957, p. 1103.

2 Rosser, J. R., Newton, R. R., Gross, G. L., "Mathematical Theory of Rocket Flight," McGraw-Hill, New York, 1947, p. 6.

New Patents

George F. McLaughlin, *Contributor*

Tracking system (2,817,081). W. Van B. Roberts, Princeton, N. J., assignor to the U.S.A.

System for measuring the speed and course of a rocket. A continuous wave transmitter is tuned to resonate with the length of the rocket. Recorders located below the expected trajectory are synchronized with the firing of the rocket to be observed.

Variable-area inlet constrictor for ramjet engine (2,817,209). C. W. Besserer, Silver Spring, Md., assignor to the U. S. Navy.

A bellows connected to a pitot-tube presented forwardly adjacent to the intake. Expansion of the bellows, in response to velocity and atmospheric density, shifts a central body forward within the intake.

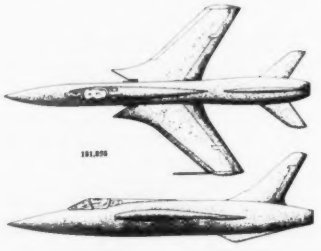

Airplane design (181,858). A. Kartvelli, Huntington, N. Y., assignor to Republic Aviation.

Fighter bomber known as the F-105 Thunderchief, driven by a P&W J-75 turbojet engine of 15,000-lb-thrust class. It features swept forward air intake ducts to shatter shock waves.

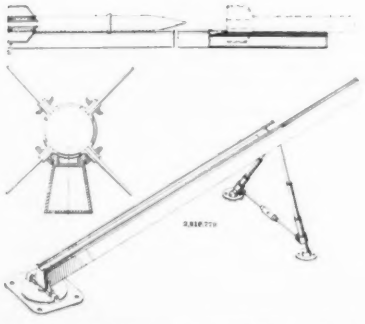

Non-tip off launcher (2,818,779). C. J. Koeper, Hunstville, Ala., assignor to the U. S. Army.

Steel section with parallel upper and lower plates carrying a flange forming a double rail receiving notches in the rocket fin section to guide the missile during initial flight. After the rocket has traveled beyond the end of the double rail to a single rail extension, a collar encircles the forward end of the rocket.

Firing pin for rocket fuze (2,817,245). H. B. Wylie, Barrington, Vt., assignor to the U. S. Navy.

An intermediate thin-walled section crushable upon application of a sudden axial force. A spring-loaded shutter in a compartment containing an explosive element is prevented from movement to an armed position until the inertial force has subsided to a predetermined level.

Aircraft control force modifier (2,817,483). T. C. Hill, Harford County, Md., assignor to The Martin Co.

Ram air led from an intake port at the leading edge of a vertical fin surface to pressure responsive means within the fin. When the rudder is out of its neutral position, the pressure actuates linkage connected to a tab at the rudder trailing edge.

Self-supporting shell for flying body (2,817,484). F. M. B. Stenzel, Alamogordo, N. Mex., assignor to Machine Tool Works Oerlikon.

Hollow metal wire helically coiled to form a body shell. Longitudinal stringers contact the shell; an agent bonds adjacent turns of the wire to one another and to the stringers.

Jet powered adjustable pitch helicopter rotor (2,818,122). J. G. Johnston, Palmdale, Calif.

Fluid lines extending radially outward from a center post to a pair of rotor blades. A valve in the post selectively and simultaneously opens the lines to fluid passage in either or both blades for controlling their thrust and pitch.

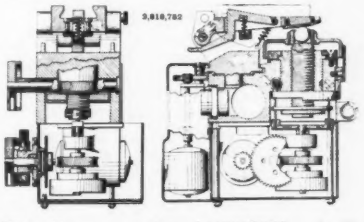

Directing apparatus (2,818,782). J. R. Jasse, Paris, France, assignor to Societe Nouvelle des Etablissements Brandt.

System of launching self-propelled projectiles. An anemometic device driven by electric motors receives corrections in elevation and direction, one of which is dependent on the wind component in the plane of fire and the other on the transverse wind component.

Jet propulsion of helicopters (2,818,223).

EDITORS NOTE: Patents listed above were selected from the Official Gazette of the U.S. Patent Office. Printed copies of Patents may be obtained from the Commissioner of Patents, Washington 25, D. C., at a cost of 25 cents each; design patents, 10 cents.

ENGINEERS

Aerodynamics & Propulsion

Information manual about APL and its programs now available

The Applied Physics Laboratory (APL) of The Johns Hopkins University is unique in that we are neither an industrial nor an academic organization, but rather a composite, having drawn freely from the methodologies of each.

For thirteen years APL has pioneered in guided missiles. Today we are engaged in a broad program of R & D for the Navy; in addition, we are responsible for technical direction of industrial and academic contractors in developing the Terrier, Talos and other major weapons and weapons systems. Our staff members enjoy not only the stimulus of association with their immediate colleagues at APL, but also with those in other organizations of considerable stature.

NEW 30-PAGE PUBLICATION

A few positions for senior engineers and scientists are now open. Information on our accomplishments and goals is available in a new 30-page publication, just off the press.

In it staff leaders representing each of the various disciplines and fields outline the nature of their programs. Information on our new laboratory in Howard County, Md. (equidistant between Baltimore and Washington) is also included, together with facts on the outstanding communities in which our staff members live.

Quantity is somewhat limited. May we suggest you send now to: Professional Staff Appointments,

The Johns Hopkins University
Applied Physics Laboratory
8617 Georgia Avenue, Silver Spring, Md.

F. L. Doblhoff, Zell am See, Austria, assignor to The Fairey Aviation Co., Ltd. (England).

Turbine gases directed through at least one rotor blade propulsion nozzle to cause blade rotation. Gases are also directed against the rudder to achieve orientation about a vertical axis during hovering.

Jet engine fuel, pressure ratio and nozzle area control (2,818,703). I. W. Victor, Cincinnati, Ohio, assignor to General Electric Co.

Means responsive to the ratio of compressor discharge pressure to turbine exhaust pressure to control the variable area discharge section. A ratio is maintained at a first predetermined value when the shutoff valve is open, and at a second predetermined value when the valve is closed.

Turbine engine starting system (2,818,704). H. C. Karcher, Mansfield, Ohio, assignor to General Motors Corp.

Control valve with a radial array of pivotal overlapping shutter flaps at the inlet of the combustion chamber. The valve closes the flaps upon ignition of the combustible charge.

Rotary jet propelled engine (2,818,705). L. L. Ledet, Charleston Heights, S. C.

Rotor including a jet exhaust within a frame, and mounted in a housing. Louver openings in the housing permit air under pressure to enter the combustion chamber. Heated air escaping to the atmosphere creates thrust, imparting motion to the rotor.

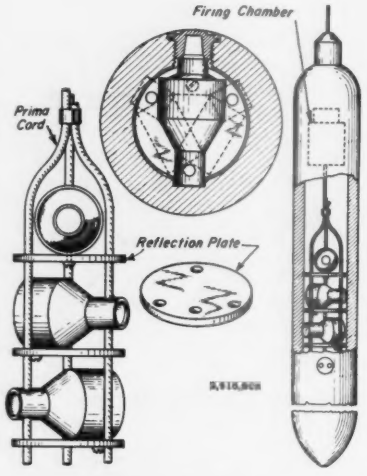

Jet perforating gun (2,818,808). W. S. Dill, Midland, Tex.

Gun for perforating casing in oil wells. Series of shaped charges are stacked in a carriage so each directs a jet outwardly through the casing at an angle of 120 deg from the jets of adjacent shaped charges. A firing Primacord has parallel burning paths of travel, firing charges in regular unidirectional sequence.

Valve arrangement for afterburner igniter control (2,819,587). R. J. Coar, Hartford, Conn., assignor to United Aircraft Corp.

Two pistons displace fuel into the combustion chamber. The smaller piston is moved by the larger one to supply additional fuel through nozzles into the afterburner.

Ventilated suit refrigeration unit (2,819,590). F. H. Green, Palos Verdes Estates, Calif., assignor to The Garrett Corp.

Heat exchanger for cooling hot compressed air supplied to an airtight enclosure. An expansion turbine further cools and reduces the pressure of a portion of the cooled air. Temperature responsive means controls a valve in response to the temperature of air flowing into the enclosure.

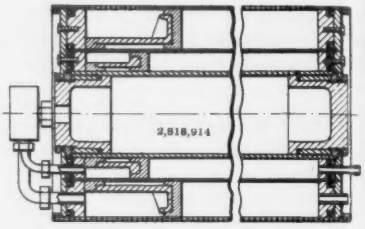

System of containers for at least two liquids and a pressure gas (2,818,914). H. Thomann and A. Steck, Vaduz, Bartlegrosch, Liechtenstein, assignors to Machine Tool Works Oerlikon.

Central tube with two lids slidably inserted from each end to form a pressure gas chamber. Two liquid containers surround the gas chamber and one another. Pistons in the containers put gas into controllable communication with the liquid containers.

Variable area turbine entrance nozzle (2,819,732). R. A. Faetz, University Heights, Ohio, assignor to Thompson Products, Inc.

Movable fluid directing vanes between a pair of radially spaced coaxial rings. A third ring operates to controllably move pivotal vanes, regulating flow between the movable and fixed vanes.

Turbojet engine fuel and nozzle control system (2,820,340). J. Dolza, O. P. Prahar, and J. B. Wheatley, Indianapolis, Ind., assignors to General Motors Corp.

Means for varying the fuel rate coordinately with the effect of the ambient air condition on fuel requirements.

Braking and reverse turbine for gas turbine engines (2,820,341). C. A. Amann, Birmingham, Mich., assignor to General Motors Corp.

Exhaust duct receiving motive fluid from a forward turbine and a radial inflow reverse turbine. A valve controls the flow of fluid from the turbines to the duct.

Air-jacketed annular combustion chamber for a jet-propulsion engine (2,821,066). J. S. Clarke, S. R. Jackson and G. J. Hudson, Burnley, England, assignors to Joseph Lucas Industries Ltd.

Walls with corrugations shaped and arranged to form inner and outer boundaries of combustion zones in the combustion chamber. Walls are positioned so air from the jackets can enter the combustion zones and set up a circular motion around the axis of each burner nozzle.

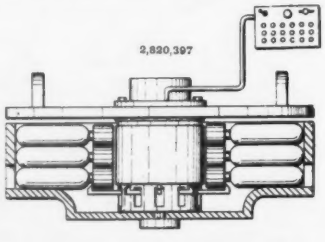

Airborne missile dispenser (2,820,397). T. H. Durkin, Roslyn, Pa.

Rotatable container from which missiles may be released from an aircraft by centrifugal force in a sequential order, or simultaneously over a wide area beneath the line of flight.

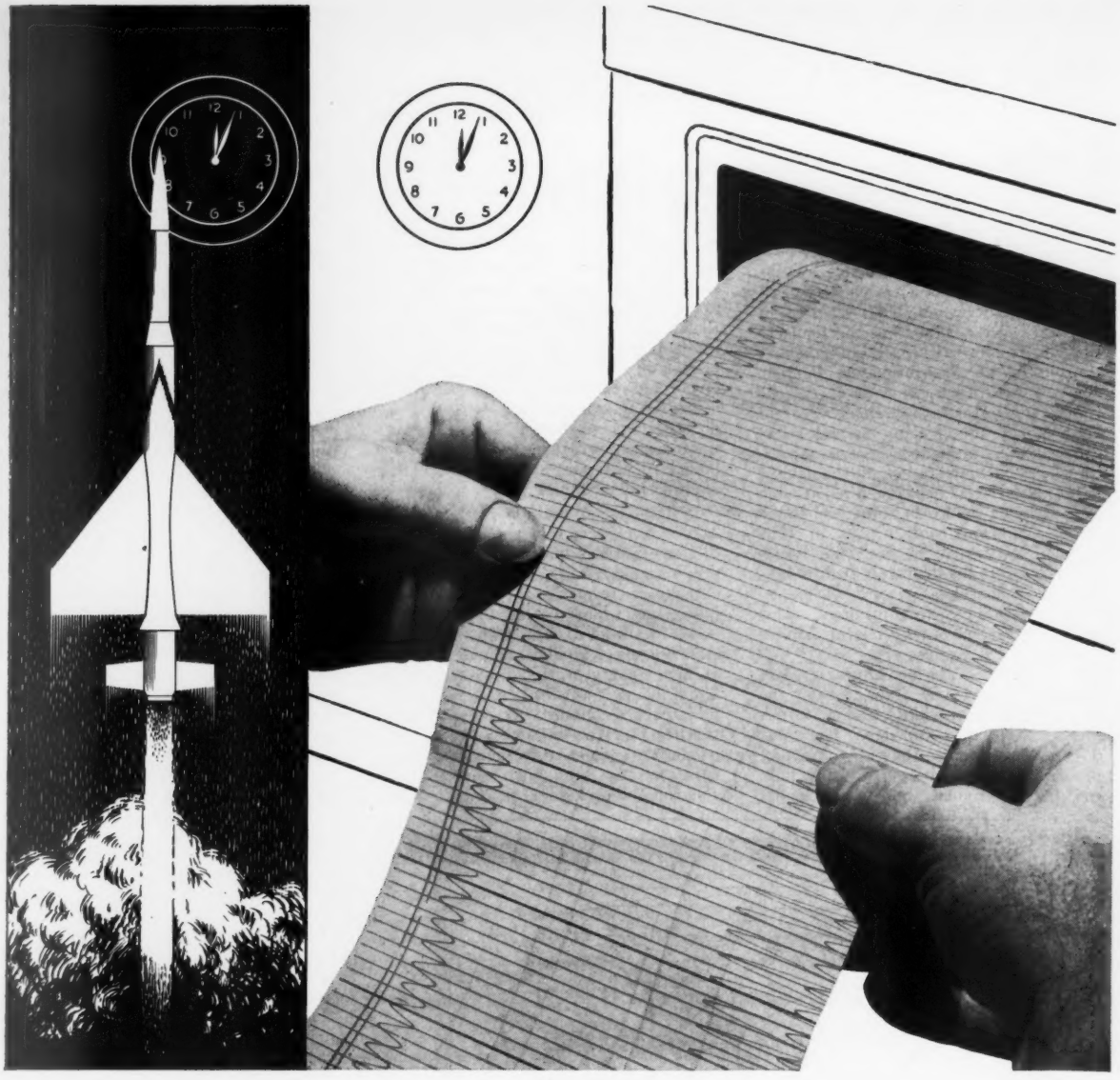

For records you can read <u>at once</u> . . .
new Kodak Linagraph Direct Print Paper

This paper is designed for use when you must know what's happening while it's happening . . . in such applications as rocketry, control, computing, product design, component testing and nuclear research. It requires no processing, comes out of the recording instrument ready to read.

To get such instant monitoring of high-speed variables you eliminate the powerful energy amplification factor of photographic development. Traces must be put down by a high-intensity u-v light source.

Kodak Linagraph Direct Print Paper gives you a wide range of recording speeds—from 0 to 3,000 cps. Records have adequate permanence for extended storage. If used under sunlight or fluorescent lamps they should be stabilized. The surface of the paper takes notations in pencil or ink. Records are suitable for use in recording system readers.

Several major manufacturers now offer recording instruments based on the characteristics of Kodak Linagraph Direct Print Paper. We'll gladly send you their names on request. If you want more detailed information on the paper, we'll send that too.

EASTMAN KODAK COMPANY
Graphic Reproduction Division
Rochester 4, N. Y.

Kodak

Book Reviews

Ali Bulent Cambel, Northwestern University, *Associate Editor*

Heat Transfer—Volume II, by Max Jakob, Wiley, New York, 1957, 652 + xxxii pp. $15.

Reviewed by J. Edward Sunderland
Purdue University

The second volume of Jakob's treatise on heat transfer completes the most comprehensive survey of heat transfer in existence. Dr. Jakob was particularly well qualified for writing a treatise on heat transfer as he was intimately familiar not only with American research in heat transfer, but also with German research. He has made use of many German references and has presented the most significant German contributions to the field of heat transfer. He has done a remarkable job in giving credit to those who have made significant contributions in heat transfer. Although the book was essentially complete before Jakob died in January 1955, considerable work was necessary in order to prepare it for press. This work was carried out by one of Jakob's colleagues, S. P. Kezios.

As in Volume I, the author uses a partly historical approach in order to show the development of the ideas leading to our present state of knowledge. The book does not lend itself to the easy solution of problems by merely substituting into convenient formulas, but its particular asset comes from a clear and concise presentation of theoretical, mathematical and experimental analyses.

The book is divided into three parts: Heat Radiation in Spaces of Simple Configuration, Selected Fields of Application, and Supplements to Volume I. The first part, dealing with radiation, continues the material on radiation which is covered in Volume I. In the first volume some basic laws and properties of radiation are given, but the treatment is limited to cases where surfaces are separated by nonabsorbing mediums. In Volume II the treatment is extended to cover various boundary configurations and the effects of absorbing mediums.

In the second division of Volume II Jakob selected certain specialized topics of heat transfer applications. The topics are: Applications of thermometry, heat exchangers, regenerators, cooling towers, falling liquid films, cooling of surfaces exposed to hot gases, heat transfer through laminar and turbulent boundary layers at high fluid velocities, heat transfer in liquid metals, and steady state heat transfer in packed columns. In the chapter on thermometry the author discusses methods for the accurate determination of temperature and heat flow measurements. Following the chapter on ordinary heat exchangers (recuperators), in which a general theoretical analysis is made of unidirectional and counterflow heat exchangers, there is a most complete treatment of regenerator theory. Due to the extreme complexities encountered in regenerator theory, the author discusses only some of the relatively simple analytical solutions, but treats with more detail the numerical and graphical solutions. An analysis is given for the working conditions of cooling towers. The theoretical and experimental results for both laminar and turbulent film cooling are presented in the chapter on cooling by falling liquid films. As a result of the increasing importance of cooling surfaces which are exposed to hot gases, the author includes a chapter covering the following topics: The effect of radiation from furnace gases to boiler tubes, the cooling of hollow gas turbine blades by a fluid in forced or free convection inside the blade, and transpiration cooling. Boundary layer theory is given for the case of high velocity flow with laminar boundary layers; for instance, a method is given for determining the temperature distribution in a fluid flowing parallel to a plane plate with a uniform or an arbitrary surface temperature. The theoretical methods and experimental results are presented for recovery factors for both laminar and turbulent boundary layers. An excellent survey is given for heat transfer in liquid metals which includes a detailed presentation of Lyon's modification of Martinelli's analogy, Jenkins' and Deissler's modified mixing length theories, a discussion of contact resistance between solid surfaces and liquid metals, and a comparison of theoretical and experimental data. In the chapter on packed columns, heat transfer is studied between a fluid and a bed of packed solids and the container wall. The fluid flow and heat transfer are assumed to be under steady state conditions.

In order to incorporate in Volume I many of the recent papers associated with heat transfer, a short supplement to Volume I is included as the last major division of Volume II. It must be noted, however, that the most recent references quoted in the Supplement as well as the rest of the book have been written in 1953 and 1954. Although there has been much work done since the book was written, it will continue for many years to be a most outstanding reference for those engaged in the field of heat transfer.

Spectroscopy at Radio and Microwave Frequencies, by D. J. E. Ingram, Philosophical Library, New York, 1956, 332 pp. $15.

Reviewed by S. F. Singer
University of Maryland

Since the war the development of microwave techniques for radars has stimulated research in a new region of spectroscopy. It turns out that the microwave region is as useful as the optical region for many

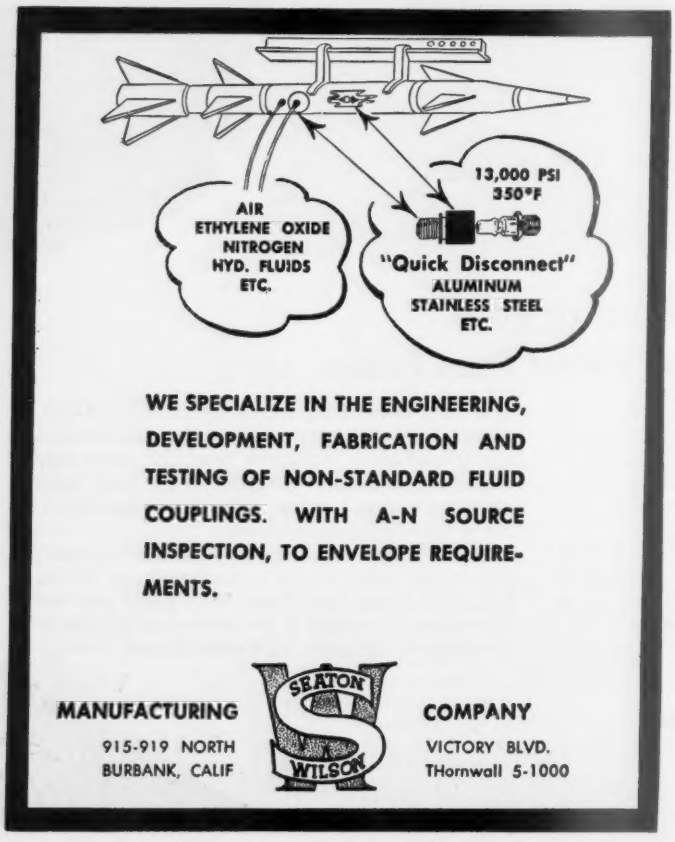

WHY DOUGLAS ENGINEERS AND SCIENTISTS GO FURTHER...
At DOUGLAS
...your missiles assignment can be as big as your talents
Now in its 17th year, the Douglas missiles program is projected far into the future by such exciting new projects as THOR
Out of such veteran projects as Nike and Honest John are coming fantastic new missile systems to challenge the finest engineering talents in the land.
Since early in World War II, Douglas has been engaged in missile projects of prime importance. New engineering teams are constantly being formed for research, design, development and production. Engineers advance rapidly as Douglas expands its leadership in this challenging field.
You are stimulated to accelerate your career by the importance of each assignment ... by the help of your associates who are recognized experts in missile work ... by the vastness of opportunity for engineers in this company that is run by engineers.
There is no more promising future than that which awaits you in the Douglas Missiles Divisions.
THOR—an intermediate range ballistics missile now going into mass production—has top priority in our country's program for national defense.
For complete information, write:
E. C. KALIHER,
MISSILES ENGINEERING
PERSONNEL MANAGER,
DOUGLAS AIRCRAFT COMPANY,
BOX J-620,
SANTA MONICA, CALIFORNIA
GO FURTHER
WITH
DOUGLAS
FIRST IN MISSILES

Spheres of titanium alloy represent the optimum configuration and material of maximum strength/weight for the storage of gases and liquids under extremes of pressure and temperature.

Rheem Aircraft, presently supplying pressure units to current ICBM programs, is directing its years of experience to the development and production of all types of vessels and propellant chambers.

RHEEM MANUFACTURING CO.
AIRCRAFT DIVISION

11711 woodruff avenue, downey, california

Rheem

Engineers: Join Rheem in challenging technical work.

applications. Research workers, although nonspecialists in this field, will want to know about the various applications to their own problems. Microwave spectroscopy can be used for gases as well as for solid state work. One of the most important applications, for example, is the detection and measurement of free radicals. Although not specifically discussed in the book, one of the important applications might be to combustion problems.

The first portion of the book discusses techniques, the production and detection of microwaves and various wave guide techniques. For the person who buys a ready-made microwave spectroscopy setup these chapters are of lesser importance; but in many cases one will wish to build his own setup. In any case the information presented is unusually detailed; many clear circuit diagrams are given and references to the literature are quite up-to-date.

Next, microwave spectroscopy *systems* are discussed, together with information on resolution and sensitivity. Then there follow discussions on the theory and results of gaseous spectroscopy, paramagnetic resonance and ferromagnetic resonance. Next follows a discussion on radiofrequency spectroscopy covering the region up to about 300 mc (10^{-4} electronvolts per quantum). Radiofrequency spectroscopy has been useful for solid state problems.

To give a view of the wide field applications of these techniques, one can list determination of nuclear spins, magnetic moments and electrical quadrupole moments of nuclei, methods for aligning nuclei by different techniques, and finally the wide field of measurement of various chemical parameters.

Applications of a more practical nature include the construction of frequency standards by means of atomic clocks, the measurement of magnetic fields using, for example, nuclear precession methods, stabilization of magnetic fields by resonance methods, chemical analysis by various nondestructive methods, detection of free radicals, the study of irradiation damage and applications in solid state research, gas discharges and radio astronomy.

Analysis of Feedback Control Systems, by Robert A. Bruns and Robert M. Saunders, McGraw-Hill, New York, 1955, 383 pp.

Scott H. Cameron
Armour Research Foundation

This book is concerned more with the practical or applied aspects of control system design than with the theoretical. Also no prior knowledge of servomechanism theory is needed in order to deal easily with the material presented. In fact, the only background required is a knowledge of the steady state theory of a-c networks, the fundamental laws of dynamics and a familiarity with elementary differential equations.

The first ten chapters of this book treat the characteristics of the components of which control systems are comprised, since it is the author's view that a real understanding of feedback control theory can be most readily obtained after one is already familiar with the operational characteristics of the components. This portion of the text is particularly good in that it treats not only the usual electrical and electromechanical components, but the hydraulic and pneumatic components of which so many of our modern systems are composed. The operation and construction of each of the components is explained and, where appropriate, the transfer function derived. The transfer function is treated throughout as a simple generalization of steady state a-c network theory rather than a ratio of Laplace transforms.

The following chapters deal with various aspects of feedback theory; while these chapters are adequate, they certainly find their counterpart in any number of recent texts. The material which is presented is adequate in detail and each chapter is concluded with a set of excellent problems. The two concluding chapters present rather sketchy discussions of the describing function and phase plane methods of nonlinear analysis. This reviewer thought that the chapter on experimental techniques for the determination of transfer functions was particularly good.

This book is apparently intended and, in the opinion of the reviewer, would serve very well as a text for an introductory course in servomechanism theory and practice.

Books Received

Electro-Technology, by M. G. Say, Philosophical Library, New York, 1955, 167 pp. $6.

Principles of Metal Casting, by Richard W. Heine, McGraw-Hill, New York, 1955, 639 pp. $7.50.

Magnetic Materials in the Electrical Industry, by P. R. Bardell, Philosophical Library, New York, 1955, 288 pp. $10.

The Sun, by Giorgio Abetti, MacMillan, New York, 1957, 336 pp. $12.

The Inexplicable Sky, by Arthur Constance, Citadel Press, New York, 1957, 288 pp. $3.50.

Introduction to Electrical Applied Physics, by N. F. Astbury, Philosophical Library, New York, 1957, 241 pp. $10.

Introducing Astronomy, by J. B. Sidgwick, MacMillan, New York, 1957, 259 pp. $3.50.

Automation: Its Purpose & Future, by Magnus Pyke, Philosophical Library, New York, 1957, 191 pp. $10.

Zirconium, by G. L. Miller, Butterworths Scientific Publications, London, 1954, 382 pp.

Electro-Magnetic Machines, by R. Langlois-Berthelot, Philosophical Library, New York, 1955, 535 pp. $15.

Atomic Energy Research at Harwell, by K. E. B. Jay, Philosophical Library, New York, 1955, 144 pp. $4.75.

Electricity and Magnetism, by J. Newton, Philosophical Library, New York, 1956, 613 pp. $10.

Radio Telemetry, by M. H. Nichols and L. L. Rauch, Wiley, New York, 1956, 461 pp. $12.

Basic Physics, by Alexander Efron, John F. Rider Publisher, Inc., New York, 1957, 724 pp. $8.95.

Technical Literature Digest

M. H. Smith, *Associate Editor,* **and M. H. Fisher,** *Contributor*
The James Forrestal Research Center, Princeton University

Materials of Construction

Studies of Structural Failure Due to Acoustic Loading, by Robert W. Hess, Robert W. Fralich and Harvey H. Hubbard, *NACA TN* 4050, July 1957, 11 pp.

Lithium Emerges as Major Aircraft Material, by William Beller, *Amer. Aviation,* vol. 21, July 15, 1957, pp. 47–55.

Effect of Stress on Creep at High Temperatures, by H. Laks, C. W. Wiseman, O. D. Sherby and J. E. Dorn, *J. Appl. Mech.,* vol. 24, June 1957, pp. 207–213.

Cermets and Metallic Refractories, by Robert Steinitz, pp. F-6–7, **Metal Strengths at High Temperatures** (Table), pp. F-8–9, **Ceramic Materials** (Table), pp. F-8–9, **Thermal Limits of Non-metals and Chemicals** (Graphs), pp. F-10–11, **Beryllium Properties** (Table), p. F-12, *Aviation Age, Res. and Dev. Tech. Handbook, 1957–1958,* Section F. Materials: Research and Development Trends, pp. F-3–5 (Metals-non-metals-chemicals).

Corrosion and Ignition of Titanium Alloys in Fuming Nitric Acid, by John B. Rittenhouse, Nicholas D. Stolica, Stephen P. Vango, Julia S. Whittick and David M. Mason, *Wright Air. Dev. Center, TR* 56-404, (*ASTIA AD* 118028), Feb. 1957, 57 pp.

Tensile Properties of Inconel X Sheet Under Rapid-heating and Constant-temtemperature Conditions, by Ivo M. Kurg, *NACA TN* 4065, Aug. 1957, 20 pp.

Compressive Stress-Strain Properties of 17-7 PH and AM 350 Stainless-steel Sheet at Elevated Temperatures, by Bland A. Stein, *NACA TN* 4074, Aug. 1957, 21 pp.

Torquing of Bolts for Nuclear Reactors, by F. J. Mehringer, *Atomic Energy Comm.,* KAPL-1645, Aug. 22, 1956, 124 pp.

Uranium Alloys for High-temperature Application, by Henry A. Saller, Ronald F. Dickerson and William E. Murr, *Atomic Energy Comm.,* BMI-1098, June 25, 1956, 45 pp.

Optimum Stresses of Structural Elements at Elevated Temperatures, by Arthur Schnitt, M. A. Brull and H. S. Wolko, *Trans. ASME,* vol. 79, July 1957, pp. 959–966.

Instrumentation, Telemetering, Data Recording

Electroanalogic Methods, 3, by T. J. Higgens, *Appl. Mech. Revs.,* vol. 10, no. 2, Feb. 1957, pp. 49–54.

An Evaporated Gold Bolometer, by E. Archbold, *J. Sci. Instruments,* vol. 34, no. 6, June 1957, pp. 240–241.

A Thermistor Probe, by W. Belfield and R. W. Johnson, *J. Sci. Instruments,* vol. 34, no. 5, May 1957, pp. 209–210.

EDITOR'S NOTE: Contributions from E. R. G. Eckert, J. P. Hartnett, T. F. Irvine Jr. and P. J. Schneider of the Heat Transfer Laboratory, University of Minnesota, are gratefully acknowledged.

Simple Equipment for a Small Low Temperature Laboratory, by R. F. Broom and A. C. Rose-Innes, *J. Sci. Instruments,* vol. 33, Nov. 1956, pp. 420–421.

Measuring Instruments for Resistance Thermometers, by Jaroslav Edl, *Elektrotechniky, Obzor,* vol. 45, Dec. 1956, pp. 609–616 (in Czech).

Temperature and Pressure Measurements in an Overcompression Cloud Chamber, by D. W. Hadley, J. C. Bower and J. Walker, *J. Sci. Instruments,* vol. 33, Dec. 1956, pp. 507–509.

Design of Total Temperature Probes, by D. H. Henshaw and D. F. Daw, *Canada, NAE LR*-184, Jan. 1957.

Edge Effects in Electromagnetic Flowmeters, by J. A. Shercliff, *J. Nuclear Energy,* vol. 3, no. 4, Nov. 1956, pp. 305–311.

Measurements of Heat Transfer from Fine Wires in Supersonic Flows, by John Laufer and Robert McClellan, *Calif. Inst. Tech., Jet Propulsion Lab., Rep.* 20-101, June 29, 1957, 26 pp., 10 ref.

Recent Developments in Electronic Instrumentation, by P. G. Hubbard, reprinted from *Hydraulics Conference, 6th, 1956 (Iowa State Univ., Studies in Engng., Bull.* 36), pp. 101–100, 16 ref.

Potential-flow Analogs and Computers, by S. C. Ling, reprinted from *Hydraulics Conference, 6th, 1956 (Iowa State Univ., Studies in Engng., Bull.* 36), pp. 167–186, 10 ref.

All Metal Apparatus for the Determination of the Density of Liquefied Gases, by Roger L. Jarry, *Rev. Sci. Instruments,* vol. 28, Aug. 1957, pp. 641–642.

Effects of Thermal Relaxation and Specific-heat Changes on Measurements with a Pneumatic-Probe Pyrometer, by P. W. Kuhns, *NACA TN* 4026, July 1957, 67 pp.

Temperature Transducers for High Speed Gases, by S. G. Darevskii, *Gt. Brit., Royal Aircraft Estab., Translation* 598 (*ASTIA AD* 121650), (Translation of *USSR Akademia Nauk Doklady,* vol. 107, no. 3, 1956, pp. 373–376), Oct. 1956, 5 pp., 4 fig.

The Development of a Mass Flow Probe, by E. R. Wolff, *Univ. Toronto, Inst. Aerophys., TN* 12, Jan. 1957, 18 pp.

Automatic Data Plotter for F-M/F-M Telemetering, by H. B. Riblet, *Electronics,* vol. 30, Aug. 1, 1957, pp. 182–187.

Note on Strain Gauge Recording Equipment for the RAE Intermittent Supersonic Wind Tunnels, by K. G. Winter and E. J. Petherick, *N. Atlantic Treaty Organization, Advisory Group Aeron. Res. Dev., Rep.* 64, Aug. 1956, 11 pp.

Accuracy of CEP Estimates, by M. L. Eaton, *Naval Air Missile Test Center, Tech. Mem. Rep.* 105, Jan. 1957, 49 pp.

A Generalization of the Nyquist Stability Criterion with Particular Reference to Phasing Error, by R. H. Merson, *Gt. Brit., Aeron. Res. Council, Current Paper* 330 (formerly *ARC Tech. Rep.* 18747; *Royal Aircraft Estab., TN GW*316), 1957, 8 pp., 1 fig.

Determination of Equilibrium Gas Emissivities from Spectroscopic Data, by S. S. Penner and A. Thomson, *Calif. Inst. Tech., Daniel and Florence Guggenheim Jet Propulsion Center, Tech. Rep.* 25, July 1957, 63 pp.

Microflowmeters at a Loss of D.F.G. Charge, by F. Bebeauvais, R. Feidt and C. Gebel, *France, Ministere de l'Air, Pub. Sci. Tech. Notes Techniques* 64, 1957, 23 pp. (in French).

Response of Mechanical Systems to Random Excitation, by W. T. Thomson and M. V. Barton, *J. Appl. Mech.,* vol. 24, June 1957, pp. 248–251.

Research and Development Trends, pp. H-3–4 (Research Testing-Development Testing-Flight Testing-Service Testing-the Future), **Airborne FM-FM Telemetering Units** (Table), pp. H-5–9, **Airborne Data Recorders** (Table), pp. H-10–17, **Environmental Testing Facilities** (List), pp. H-18, 22–36, *Aviation Age, Research and Development Technical Handbook, 1957–1958:* Section H: Testing.

Research and Development Trends, p. I-3, **Computers for Aviation Research and Development** (Table), pp. I-4–11, **Data Review,** pp. I-12–16, *Aviation Age, Research and Development Technical Handbook, 1957–1958,* Section I: Computers and Data Processing.

Guidance Systems and Components

Theoretical Investigation Based on Experimental Frequency-Response Measurements of an Automatic Altitude Control in Combination with a Supersonic Missile Configuration, by Ernest C. Seaberg, Edward S. Geller and William W. Willoughby, *NACA RM* L54F04, Aug. 1954, 28 pp. (Declassified from Confidential by authority of *NACA Res. Abs.* 116, p. 22, 7/5/57.)

Principles of Self-contained Navigation, by H. H. Bailey, *Aeron. Engng. Rev.,* vol. 16, Aug. 1957, pp. 68–73.

Cytac—A Multi-purpose Precision Navigation System, by Wilbert P. Frantz, *Sperry Engng. Rev.,* vol. 10, May-June 1957, pp. 2–6.

Supersensitive Giant Antennas Will Track Long Range Missiles, by A. J. Garon, J. K. Van Hock and C. H. New, *Aviation Age,* vol. 28, Aug. 1957, pp. 116–119.

Hughes Latest Falcon Has Infra-red Seeker, *Missiles and Rockets,* vol. 2, Aug. 1957, p. 52.

Project Vanguard Report No. 18, Minitrack Report No. 1—Phase Measurement, by C. A. Schroeder, C. H. Looney, Jr., and H. E. Carpenter, Jr., *Naval Res. Lab., NRL Rep.* 4995, July 26, 1957, 28 pp.

Flight Vehicle Design and Testing

Missile Progress by the Corps of Engineers, by Maj. Gen. David H. Tulley, USA, *Missiles and Rockets,* vol. 2, July 1957, pp. 89–90.

Progress in Army Missile Research and Development, by Maj. Gen. August Schomburg, USA, *Missiles and Rockets,* vol. 2, July 1957, pp. 91–94.

Navy Rockets and the Future of Man,

MISSILE HARDWARE

By

NEWBROOK

• • • we have the "Know-How!"

We have developed new techniques, new methods, new processes that effect production economy so necessary to a successful missile program.

Here at Newbrook you will find men with experience gained from doing . . . a modern plant with up-to-date equipment . . . precision inspection to meet your most exacting quality control requirements.

And most important, Newbrook specialization results in strict reliability ! Let us help you with your Missile Hardware problems.

Specializing in

- **Motor Cases** *Solid and Liquid propellants*
- **Jato Cases**
- **Nozzles**
- **Plenum Chambers**
- **Blast Tubes**
- **Fuel Injectors**

Phone or Write

NEWBROOK MACHINE CORPORATION

20 Mechanic Street ***Phone 45***

SILVER CREEK, NEW YORK

by Rear Adm. Rawson Bennett, USN, *Missiles and Rockets*, vol. 2, July 1957, pp. 97–98.

Navy Missile Progress, by Rear Adm. John E. Clark, USN, *Missiles and Rockets*, vol. 2, July 1957, pp. 101–102.

Progress in Air Force Scientific Research, by Brig. Gen. Hollingsworth F. Gregory, AFOSR, *Missiles and Rockets*, vol. 2, July 1957, pp. 105–109.

Missile Encyclopedia, *Missiles and Rockets*, vol. 2, July 1957, pp. 123–164. US Army: Nike Ajax, Hawk, Nike Hercules, Dart, LaCrosse, Little John, Honest John, Corporal, Sergeant, Redstone, Jupiter, pp. 124–136. US Navy: Bullpup, Corvus, Diamondback, Sidewinder, Zuni, Sparrow, Torpedoes, Terrier-Tartar, Regulus I, Talos, Triton, Regulus II, Polaris, pp. 137–150. US Air Force: Mighty Mouse, Falcon, Bomarc, Rascal, Matador, Snark, Navaho, Thor, Atlas, Titan, Miscellaneous Missiles, pp. 151–164.

Rockets and Satellites and Cranfield, *Flight*, vol. 72, Aug. 2, 1957, pp. 153–156.

Trident Blents Simplicity, Performance, by David A. Anderton, *Aviation Week*, vol. 67, Aug. 19, 1957, pp. 50–59.

RTV-N-12a Viking Rockets 8-10, Design Summary, *Martin Co., Rep.* ER-6534, Aug. 1955, 199 pp., 78 ref.

Development of a High-velocity Free-flight Launcher—the Ames Light-gas Gun, by A. C. Charters, B. Pat Denardo and Vernon J. Rossow, *NACA RM* A55G11, Dec. 1955, 97 pp. (Declassified from Confidential by authority of *NACA Res. Abs.* 118, p. 6, 8/16/57.)

SBAC Display Suggests British Missile Policy Is Premature, by David A. Anderton, *Aviation Week*, vol. 67, Sept. 9, 1957, pp. 26–30.

Some Observations on Guided Missiles, by Th. von Kármán, *Interavia*, vol. 12, Aug. 1957, pp. 777–778.

Missiles at the Paris Show, by M. Decker, *Interavia*, vol. 12, Aug. 1957, pp. 792–794.

The West's Guided Missiles, *Interavia*, vol. 12, Aug. 1957, pp. 795–798.

Air-to-Air Rocket Weapons, by F. I. Ordway, *Interavia*, vol. 12, Aug. 1957, pp. 806–807.

Britain's Guided Weapons, by D. Wood, *Interavia*, vol. 12, Aug. 1957, pp. 808–809.

High-Velocity, Light-Gas Gun, by W. D. Crozier and William Hume, *J. Appl. Phys.*, vol. 28, Aug. 1957, pp. 892–894.

Research and Development Trends, pp. A-3–4 (Aircraft Systems-Ballistic Missile Systems-The Future), **Weapon System Programs Need Better Organization,** by Milton W. Mohr, pp. A-5–7, **Missiles** (Table), pp. A-8–13, *Aviation Age, Res. and Dev. Tech. Handbook, 1957–1958:* Section A: System Engineering.

Guided Missile Progress, by John H. Sides, *Ordnance*, vol. 42, July-Aug. 1957, pp. 44–46.

Combustion, Fuels and Propellants

Bibliography on Aerosols, 1950-1955, Supplement to Report SO-1003, by W. J. Scheffy, *Atomic Energy Comm.*, COO-1016, June 1, 1956, 109 pp.

Burning of a Liquid Droplet, III. Conductive Heat Transfer within the Condensed Phase During Combustion, by Henry Wise and C. M. Ablow, *J.*

Chem. Phys., vol. 27, Aug. 1957, pp. 389–393.

Heats of Combustion of Some Peroxides and the Heats of Formation of Acetate, Propionate, and Butyrate Radicals, by L. Jaffe, E. J. Prosen and M. Szwarc, *J. Chem. Phys.*, vol. 27, Aug. 1957, pp. 416–420.

Hydrogen Bonding in Radical Reactions, Some Remarks on CF_3 Radicals, by M. Szwarc and H. Smid, *J. Chem. Phys.*, vol. 27, Aug. 1957, pp. 421–422.

Free Energy Functions for 54 Gaseous Elements, by Harwood G. Kolsky, Ruth M. Gilmer and Paul W. Gilles, *J. Chem. Phys.*, vol. 27, Aug. 1957, pp. 494–495.

On the Existence of Higher Than Normal Detonation Pressures, by Donald R. White, *J. Fluid Mech.*, vol. 2, July 1957, pp. 513–514.

Effect of Plastic Viscosity and Yield Value on Spray Characteristics of Magnesium-slurry Fuel, by George M. Prok, *NACA RM* E56J19a, Jan. 1957, 23 pp. (Declassified from Confidential by authority of *NACA Res. Abs.* 116, p. 20, 7/5/57.)

Experimental Performance of Chlorine Trifluoride-hydrazine Propellant Combination in 100 pound Thrust Rocket Engine, by Paul K. Ordin and Riley O. Miller, *NACA RM* E9F01, Aug. 1949, 22 pp. (Declassified from Confidential by authority of *NACA Res. Abs.* 116, p. 14, 7/5/57.)

Status of Combustion Research on High-energy Fuels for Ram Jets, by Walter T. Olson and Louis C. Gibbons, *NACA RM* E51D23, Oct. 1951, 75 pp. (Declassified from Confidential by authority of *NACA Res. Abs.* 116, p. 14, 7/5/57.)

Preparation and Physical Properties of Metal Slurry Fuel, by James B. Gibbs and Preston N. Cook, Jr., *NACA RM* E52A23, March 1952, 36 pp. (Declassified from Confidential by authority of *NACA Res. Abs.* 16, p. 14, 7/5/57.)

Study of the Physical Properties of Petrolatum-stabilized Magnesium-hydrocarbon Slurry Fuels, by Murray L. Pinns and Irving A. Goodman, *NACA RM* E53J16, Jan. 1954, 58 pp. (Declassified from Confidential by authority of *NACA Res. Abs.* 116, p. 16, 7/5/57.)

A Preliminary Study of the Preparation of Slurry Fuels from Vaporized Magnesium, by Walter R. Witzke, George M. Prok and Thomas J. Walsh, *NACA RM* E53K23, Feb. 1954, 21 pp. (Declassified from Confidential by authority of *NACA Res. Abs.* 116, p. 16, 7/5/57.)

Study of Some Dielectric Properties of Suspensions of Magnesium Particles in Mineral Oil, by Aubrey P. Altshuller, *NACA RM* E53L09, Feb. 1954, 42 pp. (Declassified from Confidential by authority of *NACA Res. Abs.* 116, p. 17, 7/5/57.)

The Effect of Magnesium Particles of Various Equivalent Diameters on Some Physical Properties of Petrolatum-Stabilized Magnesium-Hydrocarbon Slurries, by Joseph M. Lamberti, *NACA RM* E54A22, April 1954, 48 pp. (Declassified from Confidential by authority of *NACA Res. Abs.* 116, p. 17, 7/5/57.)

Space Flight

Designing a Recoverable Scientific Satellite, by Carl Gazley, Jr. and David J. Masson, *Aviation Age*, vol. 28, Aug. 1957, pp. 44–51.

The Atmosphere of Mars, by R. M. Goody, *J. Brit. Interplanet. Soc.*, vol. 16, April-June 1957, pp. 69–83.

"Electro-gravitics": What It Is—or Might Be, by A. V. Cleaver, *J. Brit.*

NOW IN VOLUME PRODUCTION AT C.A.E.

. . . the TC-106 (USAF TYPE MA-1A) PORTABLE STARTING UNIT for LARGE JET AIRCRAFT

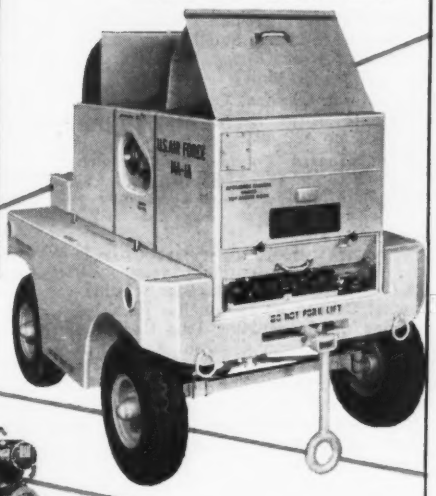

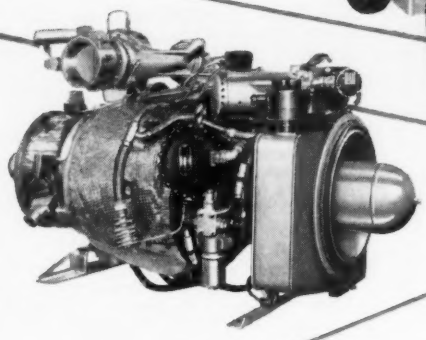

MODEL 141 TURBO-COMPRESSOR ENGINE

Typical of the fine results of Continental development is the TC-106 portable starting unit for large jet aircraft. This advanced new model, with a high performance turbine compressor as its heart, weighs one-third less than its predecessor, yet has 17 per cent higher output, and in addition, other important qualities: greater mobility, less noise, and a completely automatic control system. . . . It is now in volume production at the Continental Aviation and Engineering Toledo plant.

C.A.E. gas turbine models—the J69-T-9, the J69-T-2, and the J69-T-19A are being built for Cessna's T-37A twin jet trainer, Temco's TT-1 Navy jet trainer, the Beech jet Mentor trainer, and the Ryan Q-2A Fire Bee target drone.

CONTINENTAL AVIATION & ENGINEERING CORPORATION
12700 KERCHEVAL AVENUE, DETROIT 15, MICHIGAN
SUBSIDIARY OF CONTINENTAL MOTORS CORPORATION

Interplanet. Soc., vol. 16, April-June 1957, pp. 84–94.

Soviet IGY Rocket Program Revealed, *Missiles and Rockets*, vol. 2, Aug. 1957, pp. 40–41.

Vanguard Engines Pass Qualification Test, *Missiles and Rockets*, vol. 2, Aug. 1957, p. 50.

Space Travel and Our Technological Revolution, by Wernher von Braun, *Missiles and Rockets*, vol. 2, July 1957, p. 75.

Meteoric Dust Erosion Problem and Its Effect on the Earth Satellite, by Stuart A. Hoenig, *Aeron. Engng. Rev.*, vol. 16, July 1957, pp. 34–38.

Spiral and Elliptical Orbits, by Brian Egerton, *J. Royal Aeron. Soc.*, vol. 61, June 1957, pp. 422–423.

Algae Hazard Found Facing Space Travel, *Aviation Week*, vol. 67, Sept. 9, 1957, p. 65.

Astrophysics, Aerophysics

A Consideration of Radio Star Scintillations as Caused by Interstellar Particles Entering the Ionosphere, Part III: The Kind, Number, and Apparent Radiant of the Incoming Particles, by G. A. Harrower, *Canadian J. Phys.*, vol. 35, July 1957, pp. 792–798.

The Study of the Upper Atmosphere by Means of Rockets, at the Academy of Sciences, USSR, by S. M. Poloskov and B. A. Mirtov, *J. British Interplanet. Soc.*, vol. 16, April-June, 1957, pp. 95–100.

Nuclear Propulsion

Promising Nuclear Powerplants, by Leo Seren, *Aviation Age*, vol. 28, July 1957, pp. 42–49.

Dose Rates Produced from Gamma Ray Sources, by J. G. Lewis, *Ind. Engng. Chem.*, vol. 49, July 1957, pp. 1197–1202.

Oscillations of a Cylindrical Plasma, by Thomas H. Stix, *Physical Rev.*, vol. 106, June 15, 1957, pp. 1146–1150.

The Lithium Hydride, Deuteride, and Tritide Systems, by F. K. Heumann and O. N. Salmon, *Atomic Energy Comm.*, KAPL-1667, Dec. 1, 1956, 54 pp., 25 ref.

Decomposition and Recombination in Irradiated Static Water Systems at High Temperatures, by J. R. Humphreys, E. K. Abers and Y. Solomon, *Atomic Energy Comm.*, ANL-5004, March 1953 (declassified Feb. 23, 1957), 55 pp.

High-energy Particle Data, vol. 1, by Beverly Hill Willis and Charles V. Stableford, *Atomic Energy Comm.*, UCRL 2426, rev. Nov. 1956, 87 pp.

Criticality Calculations for Hydrogenous Systems, by J. R. Knight, *Atomic Energy Comm.*, K-1260, Nov. 25, 1955 (declassified April 22, 1957), 20 pp., 14 ref.

Neutron Shielding Materials, by T. M. Snyder, *Atomic Energy Comm.*, KAPL-704, Feb. 12, 1952 (declassified April 30, 1957), 6 pp.

Investigation of Burnout Heat Flux in Rectangular Channels at 2000 Psia, by H. S. Jacket, J. D. Roarty and J. E. Zerbe, *Atomic Energy Comm.*, WAPD-AlW(IM)-3, Dec. 5, 1955, 52 pp.

Reactor Heat Transfer Progress, No. 13, ed. by John E. Viscardi (Nuclear Dev. Corp. of America), *Atomic Energy Comm.*, NDA-33 (2008-18), Feb. 14, 1957, 27 pp.

Conference on the Use of Organic Materials in Nuclear Reactors, Aug. 5–6, 1953, Downey, Calif. (North American Aviation, Atomic Energy Res. Dept.) *Atomic Energy Comm.*, TID-10041, Dec. 1, 1953 (declassified April 23, 1957), 146 pp.

Nuclear Ramjet Study, *Aviation Week*, vol. 67, Aug. 19, 1957, p. 27.

Nuclear Heat Won't Be Used Directly in Near Future, by A. A. Kucher, T. F. Nagey and H. J. Ogorzaly, *SAE J.*, vol. 65, Aug. 1957, pp. 24–25.

Heat Generation by Inelastic Scattering Gamma Rays, by J. P. Davis, *Comb. Engng., Inc., Reactor Dev. Div. (U.S. Atomic Energy Comm.)*, GERDSIC-108, April 1956, 8 pp.

Liquid Metals and Nuclear Power, by C. D. Boadle, *Atomics and Nuclear Energy*, vol. 8, Feb. 1957, pp. 41–45, March 1957, p. 83.

Aerodynamics of Jet Propelled Missiles

Performance Comparison of Three Canard-Type Ram-jet Missile Configurations at Mach Numbers from 1.5 to 2.0, by Evan A. Fradenburgh and Emil J. Kremzier, *NACA RM* E53F11, Aug. 1953, 31 pp. (Declassified from Confidential by authority of *NACA Res. Abs.* 116, p. 16, 7/5/57.)

A Method for Simulating the Atmospheric Entry of Long-Range Ballistic Missiles, by A. J. Eggers, Jr., *NACA RM* A55I15, Dec. 1955, 19 pp. (Declassified from Confidential by authority of *NACA Res. Abs.* 116, p. 14, 7/5/57.)

Flight Measurements of Boundary-Layer Temperature Profiles on a Body of Revolution (NACA RM-10) at Mach Numbers from 1.2 to 3.5, by Andrew G. Swanson, James J. Buglia, and Leo T. Chauvin, *NACA TN* 4061, July 1957, 40 pp.

An Experimental Investigation of the Flow over Simple Two Dimensional and Axial Symmetric Bodies at Hypersonic Speeds, by I. E. Vas, S. M. Bogdonoff and A. G. Hammitt, *Princeton Univ., Dept. Aeron. Engng., Rep.* 382 (*Wright Air Dev. Center, TN* 57–246; *ASTIA AD* 130826), June 1957, 11 pp., 9 fig.

Two-dimensional, Steady, Cavity Flow about Slender Bodies, by Hirsh Cohen and Robert Gilbert, *J. Applied Mech.*, vol. 24, June 1957, pp. 170–176.

Research and Development Trends *Aviation Age, Research and Development Technical Handbook, 1957–1958*, Section B. Aerodynamics and Structures. pp. B-3–5. (Space Dynamics Aerodynamics-Structures.)

Calculating Thermal Stresses in Sandwich Panels, by W. C. Schoeller, *Aviation Age, Research and Development Technical Handbook, 1957–1958*, Section B. Aerodynamics and Structures, pp. B-6–8.

Data Review, *Aviation Age, Research and Development Technical Handbook, 1957–1958*, Section B. Aerodynamics and Structures, pp. B-10, 12.

Analysis of Inequalities of Flow Field, by L. Frager, *Fusées et Recherche Aeron.*, vol. 2, May 1957, pp. 133–134 (in French).

The Prediction of Nonlinear Pitching and Yawing Motion of Symmetric Missiles, by Charles H. Murphy, Jr., *J. Aeron. Sci.*, vol. 24, July 1957, pp. 473–479.

Optimum Nose Shapes for Missiles in the Superaerodynamic Region, by W. J. Carter, *J. Aeron. Sci.*, vol. 24, July 1957, pp. 527–532.

Two-Dimensional Bow Shock Wave Detachment Distances, by R. A. A. Bryant and J. N. G. Grant, *J. Roy. Aeron. Soc.*, vol. 61, June 1957, pp. 424–426.

The Effect of a Spike Protruding in Front of a Bluff Body at Supersonic Speeds, by D. Beastall and J. Turner, *Gt. Brit., Aeron. Res. Council, Rep. and Mem.* 3007 (formerly *ARC Tech. Rep.* 14892; *Royal Aircraft Estab., TN Aero* 2137) 1957, 26 pp.

Measurement of Projectile Motion during Engraving Process, by J. A. Petersam, H. G. McGuire, and T. E. Turner, *Aberdeen Proving Ground, Ballistic Res. Labs., Mem. Rep.* 1070, May 1957, 53 pp.

An Introduction to the Equations of Magnetogasdynamics, by J. A. Steketee, *University of Toronto, Inst. Aerophys., TN* 13, May 1957, 13 pp.

Investigation of Some Wake Vortex Characteristics of an Inclined Ogive-Cylinder Body at Mach Number 1.98, by Leland H. Jorgensen and Edward W. Perkins, *NACA RM* A55E31, Aug. 1955, 47 pp. (Declassified from Confidential by authority of *NACA Res. Abs.* 118, p. 6, 8/16/57.)

A Flight Investigation of Mach Numbers from 0.67 to 1.81 of the Longitudinal Stability and Control Characteristics of a 60° Delta-Wing Missile Configuration Having an All-Movable Tail, by Martin T. Moul and Hal T. Baber, Jr., *NACA RM* L53G29, October 1953, 43 pp. (Declassified from Confidential by authority of *NACA Res. Abs.* 118, p. 12, 8/16/57.)

A Pressure-Distribution Investigation of a Fineness-Ratio-12.2 Parabolic Body of Revolution (NACA RM-10) at M = 1.59 and Angles of Attack up to 36°, by Morton Cooper, John P. Gapcynski and Lowell E. Hasel, *NACA RM* L52G14a, Oct. 1952, 89 pp. (Declassified from Confidential by authority of *NACA Res. Abs.* 118, p. 11, 8/16/57.)

Investigation of Flow Around Simple Bodies in Hypersonic Flow, by Toshi Kubota, *Calif. Inst. Tech., Hypersonic Res. Project, Mem.* 40, June 25, 1957, 91 pp.

Bodies of Revolution Having Minimum Drag at High Supersonic Speeds, by A. J. Eggers, Jr., Meyer M. Resnikoff, and David H. Dennis, *NACA Rep.* 1306, 1957, 12 pp. (supersedes NACA TN 3666).

Performance Characteristics of Canard-Type Missile with Vertically Mounted Nacelle Engines at Mach Numbers 1.5 to 2.0, by Leonard J. Obery and Howard S. Krasnow, *NACA RM* E52H08, Sept. 1952, 25 pp. (Declassified from Confidential by authority of *NACA Res. Abs.* 119, p. 18, 8/16/57.)

Free-Flight Tests to Determine the Power-on and Power-off Pressure Distribution and Drag of the NACA RM-10 Research Vehicle at Large Reynolds Numbers between Mach Numbers 0.8 and 3.0, by Sherwood Hoffman, *NACA RM* L55H02, Sept. 1955, 55 pp. (Declassified from Confidential by authority of *NACA Res. Abs.* 119, p. 23, 8/16/57.)

A Theoretical Analysis of a Simple Aerodynamic Device to Improve the Longitudinal Damping of a Cruciform Missile Configuration at Supersonic Speeds, by James E. Clements, *NACA RM* L55H31, Oct. 1955, 36 pp. (Declassified from Confidential by authority of *NACA Res. Abs.* 119, p. 23, 8/16/57.)

Experimental Investigation of Thick, Axially Symmetric Boundary Layers on Cylinders at Subsonic and Hypersonic Speeds, by Ronald L. Richmond, *Calif. Inst. Tech., Hypersonic Res. Project, Mem.* 39, June 20, 1957, 66 pp.

Measurement of the Upwash Factor on a Cone-Cylinder Model, by Oscar C.

Holder, *Army Ballistic Missile Agency, Rep.* DA-R-11, June 20, 1957, 23 pp.

A Correlation of Free-flight Transition Measurements on Various Blunt Nose Shapes by Use of the Momentum-thickness Reynolds Number, by W. R. Witt, Jr., and J. Persh, (Aeroballistic Range Symposium, Proc., Jan., 1957), *Aberdeen Proving Ground, Ballistics Res. Lab., Rep.* 1005, Pt. 1, March 1957, pp. 23–43.

Jet and Rocket Propulsion Engines

Experimental Investigation of an Axial-Flow Supersonic Compressor Having Rounded Leading-Edge Blades with an 8-per cent Mean Thickness-Chord Ratio, by Theodore J. Goldberg, Emanuel Boxer and Peter T. Bernot, *NACA RM* L53G16, Dec. 1953, 43 pp. (Declassified from Confidential by authority of *NACA Res. Abs.* 118, p. 8, 8/16/57.)

Effects on the Weight-Flow Range and Efficiency of a Typical Axial-Flow Compressor Inlet Stage That Result from the Use of a Decreased Blade Camber or Decreased Guide-Vane Turning, by Robert J. Jackson, *NACA RM* E52G02, Sept. 1952, 41 pp. (Declassified from Confidential by authority of *NACA Res. Abs.* 18, p. 8, 8/16/57.)

Experimental Investigation of a 16-inch Impulse-Type Supersonic-Compressor Rotor, by Guy N. Ullman, Melvin J. Hartmann and Edward R. Tysl, *NACA RM* E51G19, Oct. 1951, 29 pp. (Declassified from Confidential by authority of *NACA Res. Abs.* 118, p. 7, 8/16/57.)

The 20,000-lb. s.t. de Havilland Gyron D.Gy.2, *Aeroplane,* vol. 93, Aug. 2, 1957, pp. 154–158.

A Theoretical Investigation of the Effects of Changes of Shape on the Operation of the R.P.I. Wave Engine, by R. S. Rainhill, *Rensselaer Polytech. Inst., Res. Inst.,* TR-AE-5703, June 1957, 33 pp., 24 fig., 3 tab.

A Method for Eliminating the Effects of Residual Nitric Acid in Rocket Engines and Related Equipment, by Edward L. Harris, *Wright Air Dev. Center, Tech. Rep.* 57-31 (*ASTIA AD* 1107327), Dec. 1956, 6 pp.

Screen-Type Noise Reduction Devices for Ground Running of Turbojet Engines, by Willard D. Coles and Warren J. North, *NACA TN* 4033, July 1957, 23 pp.

Foreign-Object Retention and Flow Characteristics of Retractable Engine-Inlet Screens, by Fred W. Steffen and Lewis A. Rodert, *NACA RM* E57A15, July 1957, 30 pp.

Modern Developments in Solid-Propellant Rocket Engineering, by Richard D. Geckler and Robert E. Davis, *Aeron. Engng. Rev.,* vol. 16, Aug. 1957, pp. 42–46, 51.

Progress in Air Force Rocketry, by Frederick I. Ordway III and Ronald C. Wakeford, *Missiles and Rockets,* vol. 2, July 1957, pp. 83–87.

Propulsion Progress, *Missiles and Rockets,* vol. 2, July 1957, pp. 81.

Investigation of Supersonic-Compressor Rotors Designed with External Compression, by Lawrence J. Jahnsen and Melvin J. Hartmann, *NACA RM* E54G27a, Sept. 1954, 41 pp. (Declassified from Confidential by authority of *NACA Res. Abs.* 118, p. 9, 8/16/57.)

Small Solid Rockets for Commercial Use, by G. E. Rice, *Missiles and Rockets,* vol. 2, Aug. 1957, pp. 80–81.

Solid Propellant Rocket Testing, by

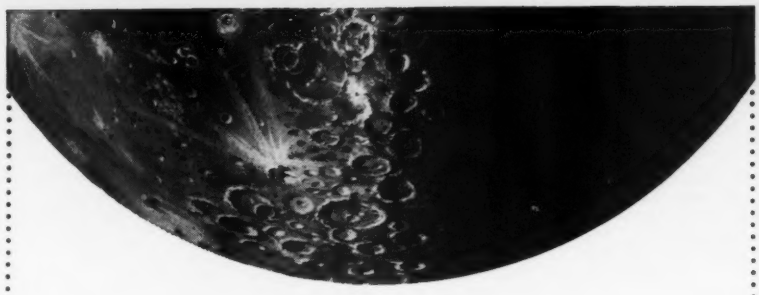

Men who know

TURBINES, PUMPS, COMPRESSORS

Get in on the development of the most advanced high-speed rotary equipment ever built

Here's your opportunity to step up to a new, higher level of turbo-machinery technology—the Large Rocket Engine.

Whatever type of rotating machinery you know best, your experience could be extremely valuable in the important developments now going on at Rocketdyne. The seasoned and ambitious man who has cut his teeth on jet engines, steam or gas turbines, or other elements of rotating machinery, is urgently needed to apply mechanical principles to meet the increasing demands of power plant performance.

The combination of high speed, light weight, heavy loadings and exceptional pressures required in rocket engine work is leading to an entirely new breed of high-performance rotating machinery... and a new breed of engineer. You can be one of this advance guard of the turbo-machinery field—if you have the desire to build your professional status by accepting new challenges.

Rocketdyne is building high-thrust rocket engines for the nation's major missiles. You'll work with the leading producer in the nation's fastest growing industry. You and your work will be recognized as a vital part of the overall achievements. Testing facilities are among the world's finest. The power produced is beyond anything ever before thought possible. If you would like to tackle new assignments working alongside some of the finest minds in turbo-engineering, write and tell us about your background: A. W. Jamieson, Rocketdyne Engineering Personnel Dept. R-3, 6633 Canoga Avenue, Canoga Park, California.

ROCKETDYNE

A DIVISION OF NORTH AMERICAN AVIATION, INC.

BUILDERS OF POWER FOR OUTER SPACE

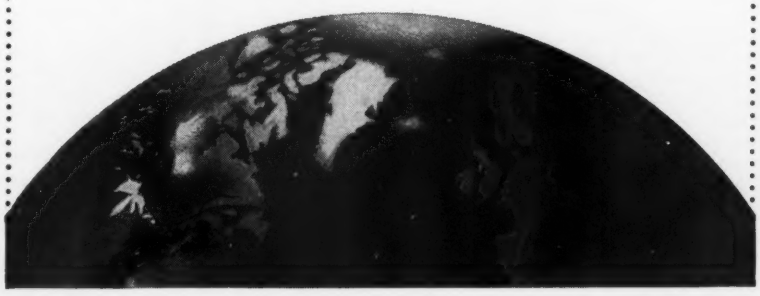

H. E. Westgate, *Missiles and Rockets*, vol. 2, Aug. 1957, pp. 87–90.

Determination of Surge and Stall Limits of an Axial-Flow Turbojet Engine for Control Applications, by Ross D. Schmidt, George Vasu, and Edward W. McGraw, *NACA TN* 3585, Sept. 1957, 29 pp. (supersedes RM E53B10).

Visualization of Rotor Tip Secondary Flows with Blade Tip Air Discharge and Suction in a Low-Speed Turbine, by Milton G. Kofskey and Hubert W. Allen, *NACA RM* E56E16, August 1956, 28 pp. (Declassified from Confidential by authority of *NACA Res. Abs.* 119, p. 20, 8/16/57.)

Aerodynamic Forces on a Vibrating Unstaggered Cascade (Luftkräfte an einem schwingenden Gitter), by H. Söhngen, *NACA TM* 1412, Aug. 1957, 16 pp. (translation from *ZAMM* vol. 35, March 1955, pp. 81–88).

Preliminary Investigation of Hollow-Bladed Turbines Having Closed and Open Blade Tips, by Gordon T. Smith and Robert O. Hickel, *NACA RM* E55F27a, Aug. 1955. 18 pp. (Declassified from Confidential by authority of *NACA Res. Abs.* 119, p. 20, 8/16/57.)

Performance of a Supersonic Mixed-Flow Rotor with a Swept Leading Edge and 0.52 Inlet Radius Ratio, by Arthur W. Goldstein and Ralph L. Schacht, *NACA RM* E53H27, Nov. 1953, 34 pp. (Declassified from Confidential by authority of *NACA Res. Abs.* 119, p. 19, 8/16/57.)

Performance of a Swept Leading Edge Rotor of the Supersonic Type with Mixed Flow, by Arthur W. Goldstein and Ralph L. Schacht, *NACA RM* E52K03, Jan. 1953, 34 pp. (Declassified from Confidential by authority of *NACA Res. Abs.* 119, p. 19, 8/16/57.)

Investigation of a 24-inch Shock-in-Rotor Type Supersonic Compressor Designed for Simple Radial Equilibrium behind Normal Shock, by Harold Lown and Melvin J. Hartmann, *NACA RM* E51H08, Dec. 1951, 25 pp. (Declassified from Confidential by authority of *NACA Res. Abs.* 119, p. 17, 8/16/57.)

Spectre—de Havilland's Latest Rocket Motor, *Flight*, vol. 72, Aug. 23, 1957, p. 245.

The Rocket Comes of Age, by W. von Braun, *Interavia*, vol. 12, Aug. 1957, pp. 789–790.

Rocket Propulsion Units, by Vernet-Lozet, *Interavia*, vol. 12, Aug. 1957, pp. 799–801.

Solid Propellant Rocketry, by J. K. Elder, *Interavia*, vol. 12, Aug. 1957, pp. 801–802.

Principles of Control of Aircraft Gas Turbines, by L. Beck, *Z. Flugwissenschaften*, vol. 5, July 1957, pp. 199–204.

Heat Transfer and Fluid Flow

One-dimensional and Two-dimensional Gas Dynamics Analogies, by R. A. A. Bryant, *Aust. J. Appl. Sci.*, vol. 7, no. 4, Dec. 1956, pp. 296–313.

Study of Stagnation Temperature and Pressure in a Free-Molecular Flow Regime by Means of the Revolving Arm Method, by F. M. Devienne. *Lab. Mediterranean de Rech., Thermodynamiques TR (AFOSR TR* 57-32), (*AD* 126495), March 1957, 102 pp.

Velocity, Temperature, and Heat-transfer Measurements in a Turbulent Boundary Layer Downstream of a Stepwise Discontinuity in Wall Temperature, by D. S. Johnson, *J. Appl. Mech.*, vol. 24, March 1957, pp. 2–8.

Effect of Adverse Pressure Gradients on Turbulent Boundary Layers, by J. M. Robertson and J. W. Holl, *J. Appl. Mech.*, vol. 24, June 1957, pp. 191–196.

Film Condensation of Vapor in Horizontal Tube, by J. G. Chaddock, *Refriger. Engng.*, vol. 65, April 1957, pp. 36–41, 90, 92–95.

Heat Transfer in Condensation of Steam Flowing in a Horizontal Group of Tubes, by S. N. Fuks, *Teploenergetika*, vol. 4, Jan. 1957, pp. 35–38 (in Russian).

Study of Boiling in Short Narrow Channels and Its Application to Design of Magnets Cooled by Liquid H_2 and N_2, by S. G. Sydoriak and T. R. Roberts, *J. Appl. Phys.*, vol. 28, Feb. 1957, pp. 143–148.

Heat Transfer Media, by P. M. Krishna and D. Venkateswarlu, *Chem. and Process Engng.*, vol. 37, Nov. 1956, pp. 382–388.

Production and Use of Very High Temperature, by W. Lochte-Holtgreven, (*VDI Zeitschrift*, No. 23, 1955, pp. 785–788), *Gr. Brit., RAE Lib. Transl.* 630, Jan. 1957.

Some Structural Penalties Associated with Thermal Flight, by J. W. Mar and L. A. Schmit, *Trans. ASME*, vol. 79, July 1957, pp. 990–1004.

Generation of High Temperatures (up to 55,000°) in the Laboratory, by O. Preining (*Ost. Chemiker-Zeit.*, no. 5/6, 1957, pp. 67–72), *Gt. Brit., RAE Lib. Transl.*, 629, Feb. 1957, 11 pp., 20 refs.

"MONOBALL"®
Self-Aligning Bearings

CHARACTERISTICS

	ANALYSIS	RECOMMENDED USE
1	Stainless Steel Ball and Race	For types operating under high temperature (800-1200 degrees F.).
2	Chrome Alloy Steel Ball and Race	For types operating under high radial ultimate loads (3000-893,000 lbs.).
3	Bronze Race and Chrome Steel Ball	For types operating under normal loads with minimum friction requirements.

Thousands in use. Backed by years of service life. Wide variety of Plain Types in bore sizes 3/16" to 6" Dia. Rod end types in similar size range with externally or internally threaded shanks. Our Engineers welcome an opportunity of studying individual requirements and prescribing a type or types which will serve under your demanding conditions. Southwest can design special types to fit individual specifications. As a result of thorough study of different operating conditions, various steel alloys have been used to meet specific needs. Write for revised Engineering Manual describing complete line. Dept. JP-58.

SOUTHWEST PRODUCTS CO.
1705 SO. MOUNTAIN AVE., MONROVIA, CALIFORNIA

Electro
ADVANCED DESIGN TRANSDUCERS

Powr-Mite #3040 $25.00 list

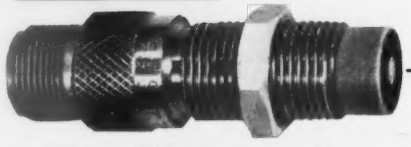

NEW Self-Powered Speed Sensing Pickup operates relays directly*

Ferrous metals passing pickup operate relay without amplifier

No tubes or transistors needed with the Powr-Mite #3040 *self* powered magnetic pickup.

Simply feed the Powr-Mite #3040 output into any relay having 100 milliwatts sensitivity.

You get extra dependability through circuit simplification, plus important savings in weight and space.

Ideal for use with over and under speed controls.

AMPLIFIER
RELAY
CONTROL UNIT

Write for new bulletin

*100 milliwatts of power at surface speeds of 250 in./sec.

Electro
TRANSDUCERS FOR COUNTING CONTROL AND MEASUREMENT

ELECTRO PRODUCTS LABORATORIES
4501-J North Ravenswood, Chicago 40
Canada: Atlas Radio Ltd., Toronto

Heat Transfer Rates for Gases, by F. L. Rubin, *Petroleum Refiner*, vol. 36, March 1957, pp. 226–228.

Mean-Temperature Difference in One, Two, and Three-Pass Crossflow Heat Exchangers, by R. A. Stevens, J. Fernandez and J. R. Woolf, *Trans. ASME*, vol. 79, Feb. 1957, pp. 287–297.

On the Heat Transfer Coefficients of Cylindrical Bodies, II, by T. Tsubouchi, S. Sato, and H. Usami, *Tohoku University, Rep. Inst. High Speed Mech.*, vol. 7, 1956, pp. 31–44.

A New Method to Measure Prandtl Number and Thermal Conductivity of Fluids, by E. R. G. Eckert and T. F. Irvine, Jr., *J. Appl. Mech.*, vol. 24, March 1957, pp. 25–38.

Predict Thermal Conductivity, II. How to Estimate Engineering Properties, by Wallace R. Gambill, *J. AIChE*, vol. 64, March 1957, pp. 271–276.

Heat Transfer to Turbine Blades, by S. J. Andrews and P. C. Bradley, *Gt. Brit., Aeron. Res. Council, Current Paper* 294, (formerly *ARC Tech. Rep.* 12078; *Natl. Gas Turbine Estab., Mem.* M37), 1957, 12 pp., 11 fig.

Investigation of Vanes Immersed in the Jet of a Solid-Fuel Rocket Motor, by Leo V. Giladett and Andrew R. Wineman, *NACA RM* L52F12, Sept. 1952, 30 pp. (Declassified from Confidential by authority of *NACA Res. Abs.* 116, p. 21, 7/5/57.)

A Theoretical Investigation of Shock Oscillations in One Dimensional Flows with and without Pressure Gradients, by Hans B. Schechter, *Wright Air Dev. Center, TN* 57-37, Feb. 1957, 30 pp.

On the Mixing Theory of Crocco and Lees and Its Application to the Interaction of Shock Waves and Laminar Boundary Layer, Part I: Generals and Formulations, by Sin I. Cheng and K. N. C. Bray, *Princeton Univ., Dept. Aeron. Engng., Rep.* 376 (*AFOSR-TN*-57-283; *ASTIA AD* 132354), May 1957, 46 pp., 19 fig.

Reflection and Refraction of Acoustic Waves by a Shock Wave, by J. Brillouin, *NACA TM* 1409, July 1957, 42 pp. (Translation from *Acustica*, vol. 5, no. 3, 1955, pp. 149–163.)

Study of Certain Problems of Liquid Gravity Waves, by Georges Brillouet, *France, Ministere de l'Air, Pub. Sci. Tech.* 329, 1957, 145 pp. (in French).

One Dimensional Treatment of Nonuniform Flow, by R. D. Tyler, *Gt. Brit. Aeron. Res. Council, Rep. and Mem.* 2991 (Formerly *ARC Tech. Rep.* 17186), 1957, 20 pp.

The Effect of Chemical Nature of Heating Surfaces on the Heat Transfer Coefficients of Pool Boiling Liquids, by George W. Preckshot, *Atomic Energy Comm., AECU*-3183, Dec. 1955, 61 pp.

Heat Transfer to Lead Bismuth in Turbulent Flow in an Annulus, by R. A. Seban and D. F. Casey, *Atomic Energy Comm., AECU*-3164, June 1956, 16 pp.

Heat Transfer to Liquid Metals in Concentrated Annuli, by Raymond V. Bailey, *Atomic Energy Comm., ORNL*-521, June 1950, 45 pp.

Heat Transfer; a Bibliography of Unclassified Report Literature, by James M. Jacobs and Gifford A. Young, *Atomic Energy Comm., TID* 3305, March 1957, 169 pp.

Analysis of Heat-driven Oscillations of Gas Flows, II: On the Mechanism of the Rijke-tube Phenomenon, by H. J. Merk, *Applied Sci. Res.*, vol., 6, Sect. A, no. 5–6, 1957, pp. 402–420.

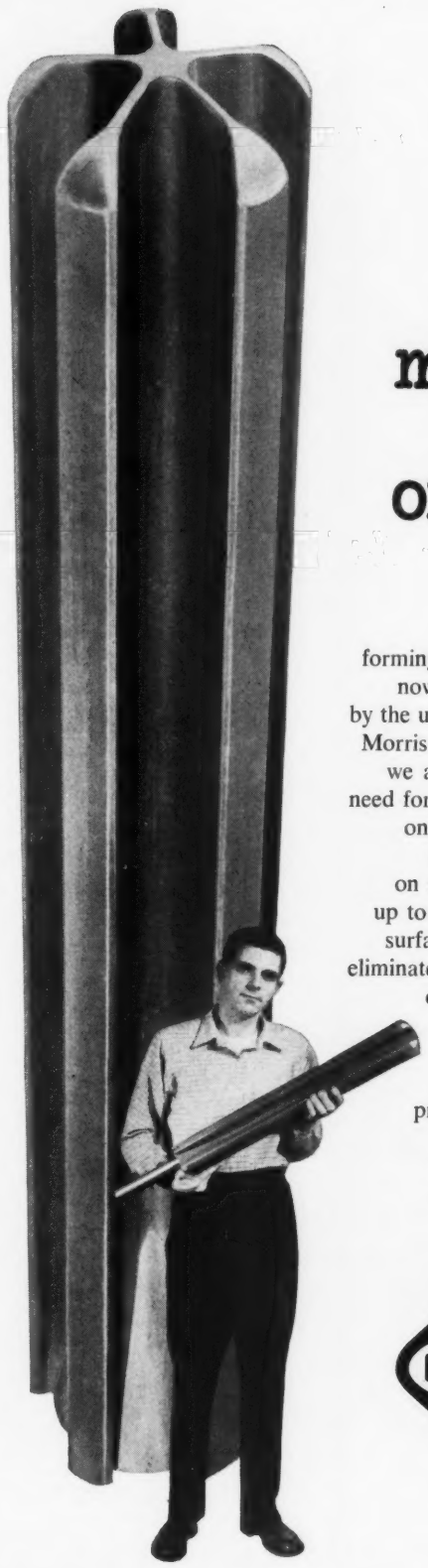

cast

mandrels

or cores?

Aluminum mandrels for forming solid fuel propellant are now being cast in production by the unusual foundry methods of Morris Bean & Company. While we assume there is no present need for a mandrel as large as the one on the left, it *can* be cast. Currently we are working on solid and hollow mandrels up to 8 feet long. Their smooth surfaces and accurate contours eliminate much difficult machining; cost is drastically reduced. In addition to large size, we would be happy to explore with you ways to produce intricate star-lobes. *Telephone or write.*

Morris Bean & Company, Yellow Springs 6, Ohio.

BEAN

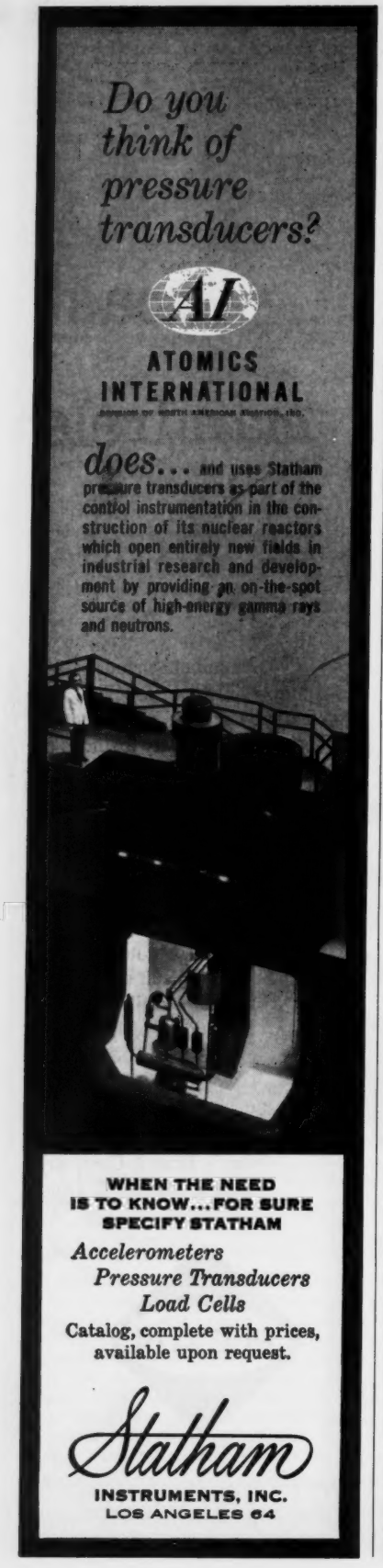
Do you think of pressure transducers?
AI
ATOMICS INTERNATIONAL
does... and uses Statham pressure transducers as part of the control instrumentation in the construction of its nuclear reactors which open entirely new fields in industrial research and development by providing an on-the-spot source of high-energy gamma rays and neutrons.
WHEN THE NEED IS TO KNOW... FOR SURE SPECIFY STATHAM
Accelerometers
Pressure Transducers
Load Cells
Catalog, complete with prices, available upon request.
Statham
INSTRUMENTS, INC.
LOS ANGELES 64

Index to Advertisers

AEROJET-GENERAL CORPORATION ..... Back Cover
D'Arcy Advertising Co., Los Angeles, Calif.

AMERICAN POTASH & CHEMICAL CORPORATION 149
The McCarty Company, Los Angeles, Calif.

APPLIED PHYSICS LABORATORY, THE JOHNS HOPKINS UNIVERSITY 200
M. Belmont ver Standig, Inc., Washington, D. C.

AVCO MANUFACTURING CORPORATION, RESEARCH AND ADVANCED DEVELOPMENT DIVISION 152
Benton & Bowles, Inc., New York, N. Y.

CONTINENTAL AVIATION & ENGINEERING CORPORATION 207
The Hopkins Agency, Detroit, Mich.

DIVERSEY ENGINEERING COMPANY ..... Third Cover
Roark & Colby Advertising, Chicago, Ill.

DOUGLAS AIRCRAFT COMPANY, INC 203
J. Walter Thompson Company, Los Angeles, Calif.

EASTMAN KODAK COMPANY 201
The Rumrill Company, Inc., Rochester, N. Y.

ELECTRO PRODUCTS LABORATORIES 210
Robertson, Buckley & Gotsch, Inc., Chicago, Ill.

FORD INSTRUMENT COMPANY, DIVISION OF SPERRY RAND CORPORATION 155
James Thomas Chirurg Co., New York, N. Y.

THE GARRETT CORPORATION, AIRESEARCH MANUFACTURING COMPANY 154
J. Walter Thompson Co., Los Angeles, Calif.

LOCKHEED AIRCRAFT COMPANY, MISSILE SYSTEMS DIVISION 151
Hal Stebbins, Inc., Los Angeles, Calif.

MORRIS BEAN & COMPANY 211
Odiorne Industrial Advertising, Inc.

NEWBROOK MACHINE CORPORATION 206
Melvin F. Hall Adv. Agency, Inc., Buffalo, N. Y.

OLDSMOBILE DIVISION, GENERAL MOTORS CORPORATION 153
D. P. Brother & Company, Detroit, Mich.

THE RAMO-WOOLDRIDGE CORPORATION 156
The McMarty Company, Los Angeles, Calif.

REACTION MOTORS, INC. ..... Second Cover
The Aitkin-Kynett Co., Philadelphia, Pa.

RHEEM MANUFACTURING COMPANY 204
Getz & Sandborg, Inc., Beverly Hills, Calif.

ROCKETDYNE, A DIVISION OF NORTH AMERICAN AVIATION, INC. 209
Batten, Barton, Durstine & Osborn, Inc., Los Angeles, Calif.

SEATON-WILSON MANUFACTURING COMPANY 202

SOUTHWEST PRODUCTS COMPANY 210
O. K. Fagan Advertising Agency, Los Angeles, Calif.

STATHAM INSTRUMENTS, INC. 212
Compton Advertising, Inc., Los Angeles, Calif.

Cover
149
200
152
207
over
203
201
210
155
154
151
211
206
153
156
over
204
209
202
210
212
ULSION